

Electronic Thesis and Dissertation Repository

8-31-2017 10:30 AM

Analysis of Framing Failures in Wood-Frame Residential Roofs Under Wind Load

Sarah A. Stevenson, *The University of Western Ontario*

Supervisor: Dr. Greg Kopp, *The University of Western Ontario*

Joint Supervisor: Dr. Ayman El Ansary, *The University of Western Ontario*

A thesis submitted in partial fulfillment of the requirements for the Master of Engineering Science degree in Civil and Environmental Engineering

© Sarah A. Stevenson 2017

Follow this and additional works at: <https://ir.lib.uwo.ca/etd>



Part of the [Structural Engineering Commons](#)

Recommended Citation

Stevenson, Sarah A., "Analysis of Framing Failures in Wood-Frame Residential Roofs Under Wind Load" (2017). *Electronic Thesis and Dissertation Repository*. 4851.
<https://ir.lib.uwo.ca/etd/4851>

This Dissertation/Thesis is brought to you for free and open access by Scholarship@Western. It has been accepted for inclusion in Electronic Thesis and Dissertation Repository by an authorized administrator of Scholarship@Western. For more information, please contact wlsadmin@uwo.ca.

Abstract

Wood-frame residential roof failures are among the most common and expensive types of tornado damage. Hip roofs are commonly understood to be more resilient during extreme wind in relation to gable roofs. However, inspection of damage survey data from recent tornadoes has revealed a previously unstudied failure mode in which hip roofs suffer partial failure of the framing structure. This research focuses on proving the concept of framing failures in hip roofs. Evidence of partial framing failures and statistics of their occurrence are explored and discussed, and common roof design and construction practice is reviewed. Two-dimensional finite element models are developed to estimate the element-level load effects on hip roof trusses and stick-frame components. Following model development to estimate the maximum demand on the framing elements, the elements' capacities are estimated. The likelihood of failure in each member is defined based on relative demand-to-capacity ratios. Trussed and stick-frame structures are compared to assess the relative performance of the two types of construction. The present analyses verify the common understanding that toe-nailed roof-to-wall connections are likely to be the most vulnerable elements in a wood-frame roof. However, the results also indicate that certain framing members and connections display significant vulnerability under the same wind uplift, and the possibility of framing failure is not to be discounted. Furthermore, in the case where the roof-to-wall connection uses hurricane straps, certain framing members and joints become the likely points of failure initiation. The analysis results and damage survey observations are used to expand the understanding of wood-frame residential roof failures, as they relate to the Enhanced Fujita Scale, and provide assessment of potential gaps in residential design codes.

Keywords

Wood-Frame Structures, Finite Element Modeling, Tornado Damage, Enhanced Fujita Scale, Hip Roofs, Metal Plate Connected Trusses, Prescriptive Design, National Building Code of Canada.

Acknowledgements

Foremost, I would like to express my sincere gratitude to my advisors, Dr. Greg Kopp and Dr. Ayman El Ansary. I am thankful to them for their continuous support, patience, and advice. Their complementary expertise has enabled this research, and I have grown personally from working with each of them. The insightful, constructive feedback and warm encouragement I have received from Dr. Kopp and Dr. El Ansary has inspired me to continue pursuing my goals and challenging myself, and they have set a tremendous example of collaboration which I feel very fortunate to continuously benefit and learn from.

I would also like to acknowledge Dr. David Prevatt, not only for providing the data to enable this work in the first place, but additionally for his encouragement and the engaging discussions we shared during our short time together at ACWE13. The technical assistance and advice of Dr. David Henderson and Dr. Rakesh Gupta, and the oversight of Mr. Gero Michel and Mr. Paul Kovacs is also gratefully acknowledged.

This work was funded by NSERC under the Collaborative Research and Development Grant titled, “Linking hazard, exposure and risk across multiple hazards,” as well as by the Ontario government through the Queen Elizabeth II Graduate Scholarships in Science and Technology. I would also like to offer my special thanks to the Canadian Wood Council for their financial support and recognition through the Catherine Lalonde Memorial Scholarship. I sincerely hope that I have honored Mrs. Lalonde’s outstanding legacy.

On a personal note, I would like to show my heartfelt appreciation for my friends and family. My “Western family”; Emilio, Rahul, Anant, Cheng, Matt W., and many others, have made my graduate experience to date as enjoyable as possible. Their continued friendship and enthusiasm has boosted me up several steep learning-curves.

To my partner, Matthew Lynch, I owe a very important debt for his enormous support and the countless hours spent talking through my research and reviewing my thesis, being my biggest/only fan at my volleyball games, and encouraging me through both good and bad days. I thank Matt, my parents Lori and Peter, and my sister Amy for their loving support over the years and for going to such great lengths to help me achieve my goals.

Contents

Abstract	i
Keywords	i
Acknowledgements	ii
Contents	iii
List of Tables	vi
List of Figures	viii
1 Introduction	1
1.1 Background	1
1.2 Observations from Tornado Damage Surveys	2
1.2.1 Tornado Intensity Estimation using the Enhanced Fujita Scale	2
1.2.2 Survey Data from Recent Tornadoes	5
1.3 Wood-Frame Residential Roofs	16
1.3.1 Trussed-Roof Construction	17
1.3.2 Stick-Frame Construction	19
1.3.3 Roof Shapes and Performance Under Wind Loads	20
1.4 Past Research on Residential Roof Performance	22
1.4.1 Experimental Studies	22
1.4.2 Finite Element Analysis of Wood Frame Residential Roofs	23
1.4.3 Experimental Data for Truss Model Validation	31
1.4.4 Finite Element Modeling of Stick-Frame Construction	33
1.5 Objectives	35
1.6 Research Approach	36
2 Development and Validation of a Numerical Truss Model	37
2.1 Development and Validation of Truss Model	38

2.1.1	Truss Validation Models.....	39
2.1.2	Truss Deflection Validation.....	41
2.1.3	Force Envelope Validation.....	46
2.2	Model of Truss Under Uplift.....	55
2.3	Conclusions.....	60
3	Demand-to-Capacity Model of Hip Roof Trusses under Wind Uplift.....	62
3.1	Element Capacity Calculations.....	63
3.1.1	Member Capacity.....	63
3.1.2	Connection Capacity.....	65
3.1.3	Commentary on Current Design Practice.....	67
3.2	Demand-Capacity Analysis.....	68
3.3	Conclusions.....	72
4	Demand-to-Capacity Analysis of Stick-Frame Roofs.....	74
4.1	Design of Stick-Frame Roofs.....	74
4.2	D/C Analysis of Stick Frame Members and Joints.....	76
4.2.1	Analysis of Demand on Stick-Frame Member.....	76
4.2.2	Capacity Estimation for Stick-Frame Elements.....	78
4.2.3	D/C Analysis of Jack Rafter.....	79
4.3	Additional Discussion of Observed Stick-Frame Failures.....	79
4.4	Conclusions.....	83
5	Conclusions and Recommendations.....	84
5.1	Key Findings of the Current Work.....	85
5.2	Recommendations for Future Work.....	89
	References.....	91
	Appendix A: Semi-Rigid Joint Stiffness Inputs.....	98

Appendix B: Initial and Adjusted Wind Load Calculations	99
Appendix C: Calculation of Orthotropic Moduli of Elasticity for Truss A2 Members..	102
Appendix D: Truss A2 Joint Demand under Initial and Updated Uplift	103
Appendix E: Truss Joint Capacity Calculations and Minimum Joint Capacities for Truss 2A.....	106
Appendix F: Results of D/C Analysis of Truss A2 with Initial Loading Applied.....	114
Appendix G: Design Notes for Stick-Frame Hip Roof.....	115
Appendix H: Nailed Connection Capacity Calculations	116
Curriculum Vitae	118

List of Tables

Table 1-1: DOD descriptions and wind speed estimates for the FR12 DI, as adopted by Environment Canada (2013).....	3
Table 1-2: Elastic Ratios for Longleaf Pine Lumber, Obtained from Chapter 4 of (Forest Products Laboratory, 1999)	31
Table 2-1: List of model analog combinations and naming convention. Insertion point analogs are named as per SAP2000 Insertion Point naming convention.....	39
Table 2-2: Deflection validation of trusses modelled according to experimental program in Wolfe et al. (1986) – results obtained from trusses which contained oversized plate connections	43
Table 2-3: Deflection validation of trusses modelled according to experimental program in Wolfe and LaBissoniere (1991) – results obtained from trusses of conventional design	44
Table 2-4: Comparison of connectivity analogs, based on joint force estimates, from the CL insertion point models of Truss 3H from FPL-1991.....	50
Table 2-5: Comparison of connectivity analogs, based on joint force estimates, from the BL insertion point models for Truss 6H from FPL-1991	51
Table 2-6: Comparison of insertion point joint force envelopes for the 3H truss from FPL-1991	52
Table 2-7: Validation of force envelope method by comparing the envelope models against FPL-1996 data. Note that Truss L3 includes inaccurate readings.....	53
Table 3-1: Material properties and calculated member strengths for truss members using SPF No. 2 sawn lumber	64
Table 3-2: Demand-Capacity ratios and governing failure mode for Truss A2 under 0.57 N/mm uplift.....	71
Table 4-1: Maximum member and joint demand on jack rafter under 0.38 N/mm uplift. Envelope of results using Pinned and Rigid support conditions.....	77

Table 4-2: Member and joint capacity estimates for jack rafter under uplift	78
Table 4-3: Member and joint D/C ratios for jack rafter under 0.38 N/mm uplift.....	79
Table A-1: Joint stiffness assignment for Semi-Rigid analog	98
Table A-2: External pressure coefficients from Table 27.4-1 in ASCE 7-10.....	100
Table A-3: Truss A2 joint demand under initial uplift loading	104
Table A-4: Truss A2 joint demand under adjusted uplift loading	105
Table A-5: Truss A2 minimum joint capacities.....	113
Table A-6: D/C results for Truss A2 under initial uplift loading	114

List of Figures

Figure 1-1: Example of roof sheathing failure, corresponding to DOD-4.....	4
Figure 1-2: Example of roof-to-wall connection failure, corresponding to DOD-6.....	4
Figure 1-3: Partial hip roof failure observed following EF2 tornado in Angus, Ontario, June 2014.	8
Figure 1-4: Hip roof failures in Moore, OK following the EF5 Tornado of May 21, 2013. a) Framing failure of similar, neighboring hip roofs b) Framing failure of steep, stick-frame hip roof c) Hip roof displaying material failure of the wood framing members	11
Figure 1-5: West end of tornado damage path following the May 22, 2011 tornado in Joplin, MO; two present study regions are shown by white outlines	13
Figure 1-6: Map of Region 1 neighborhood (Sunset Drive) with aerial photography showing the aftermath of the tornado in Joplin, MO.....	14
Figure 1-7: Example of typical hip roof configuration in Region 1, with an aerial photo showing the footprint of the partial failure on the right-hand side of the figure	15
Figure 1-8: Partial hip roof failure in Region 2	16
Figure 1-9: Illustration of MPC Truss with Components Labelled	18
Figure 1-10: Illustration of Stick-Frame Hip Roof with Components Labelled.....	20
Figure 1-11: Geometric analogs applied to a 3:12 slope Fink truss, using different chord member insertion points: a) Chord Centerline, b) Chord Bottom-Line.....	29
Figure 1-12: Illustration of Fink trusses used in 2-D model validation, based on the 6:12 slope and 3:12 slope truss configurations tested in FPL (1986, 1989, 1991, 1996).....	32
Figure 2-1: Overview of Fink Trusses used in 2-D Model Validation, based on the 6:12 (upper) and 3:12 (lower) Truss Configurations Tested by (Wolfe, et al., 1986) and (Wolfe & LaBissoniere, 1991)	40
Figure 2-2: Truss 3H joint and member naming convention.....	49

Figure 2-3: 6:12 slope trusses tested in FPL-1996, with members labeled and approximate locations of force data readings shown by location of member labels	54
Figure 2-4: Model rendering of full-scale hip roof tested by Henderson et al. (2013).....	56
Figure 2-5: Dimensioned drawing of hip roof Truss A2 from the full-scale house tested at the Insurance Research Lab for Better Homes	58
Figure 2-6: SAP2000 model of Truss A2, with numbered joint labels and lettered member labels	58
Figure 2-7: Sample of relative axial force results from the rigid SAP2000 model of Truss A2, under 1.22 N/mm uniform uplift. The blue positive results indicate tension and the red results indicate compression	59
Figure 2-8: Sample of relative member moments from the rigid SAP2000 model of Truss A2, under 1.22 N/mm uniform uplift.....	59
Figure 3-1: Half of modeled hip roof truss with MPC joints and members labeled according to truss manufacturer’s drawing package.....	66
Figure 3-2: Schematic of failure locations in Truss A2 based on estimated D/C ratios from Table 11	72
Figure 4-1: Plan-view, dimensioned stick-frame member layout drawings	75
Figure 4-2: SAP2000 model of jack rafter under 0.38 N/mm uniform uplift.....	77
Figure 4-3: Failure of stick-frame roof with irregular roof shapes	80
Figure 4-4: Partial stick-frame, hip roof failure with ceiling joists intact	81
Figure 4-5: Loss of the entire surface of a stick-frame hip roof with intact ceiling joists.	82
Figure A-1: Diagram of Truss A2 under uplift pressure	99
Figure A-2: Truss A2 Joint 3 diagram with member TC1 contact area shown	106
Figure A-3: Joint 3 with shear and tension lengths labeled	109

1 Introduction

1.1 Background

Wood-framed houses comprise the highest percentage of housing in North America (Amini & van de Lindt, 2014; Standohar-Alfano & van de Lindt, 2016). These structures are highly susceptible to damage from extreme wind events such as tornadoes and hurricanes due to their light weight and possible weak links in the vertical load path. Residential failures caused by tornadoes can cause catastrophic damage in densely populated areas, however current design practice does not include tornado-resistant design due to the low probability of occurrence for any one building. When these events do occur, they can result in significant losses (Graettinger, et al., 2014; Changnon, 2009). In fact, it has been reported that overall losses due to tornadoes are similar in magnitude to those from hurricanes in the United States (Simmons, et al., 2015). The resilience of houses during extreme wind events is essential to ensure safety of occupants and minimize damage to internal contents. Significant work has been completed to date to address commonly observed failure modes in residential structures, which are primarily related to the roof and wall cladding systems and the vertical load path between the structural components (van de Lindt, et al., 2013).

Roof cladding systems in North America commonly consist of plywood sheathing fastened to the roof structure using common wire nails, and topped with asphalt shingles (Canada Mortgage and Housing Corporation, 2014). These systems fail through pullout of the sheathing fasteners, resulting in loss of the cladding panels and introduction of these elements into the wind field as damaging debris (Reed, et al., 1997). The weak link in the vertical load path is commonly located at the connection between the roof structure and the top plate of the load-bearing walls. Pullout failure of nailed roof-to-wall connections can result in removal of the entire roof, leading to collapse of the walls which are left laterally unbraced. Research over the past few decades has resulted in the invention of hurricane straps and other methods for improving sheathing performance, holding the roof down, and strengthening the vertical load path. Observations from post-storm damage surveys discussed herein have suggested an additional failure mode in which the roof framing structure may suffer partial failure of the members or their connections. This failure mode

has not been studied in the available work to date, and the conditions under which it may govern are unknown.

1.2 Observations from Tornado Damage Surveys

Damage surveys following destructive wind events offer the opportunity to improve construction practice and understand the complexity of structural behaviour under turbulent winds. It is not feasible to directly measure wind speeds due to the sporadic, highly localized, and intense nature of tornadoes. For this reason, structures and vegetation are inspected for damage following an event and common failures are analyzed to estimate the bounds of probable wind speeds (Kopp, et al., 2012). This section reviews the literature pertaining to damage observations for wood-frame houses following tornadoes.

1.2.1 Tornado Intensity Estimation using the Enhanced Fujita Scale

Because it is not practically feasible to assess tornado intensity directly using wind speed measurements, tornadoes are classified according to the levels and types of damage they inflict upon buildings and vegetation. The first standardized method for measuring tornadoes in this way was proposed by Fujita (1971). The Fujita Scale was used widely for over 30 years before it received significant updates. Through its use, the Fujita scale was found to have many limitations leading to inconsistencies in its use and inaccurate wind speed estimates (Wind Science and Engineering Centre, 2006; Sills, et al., 2014).

In 2006, researchers from Texas Tech University brought together a forum of Fujita scale users to review and revise it. The Enhanced Fujita (EF) Scale was proposed as a result of these efforts (Wind Science and Engineering Centre, 2006). The major enhancements to the scale included improved wind speed estimates and a more comprehensive list of common structures which can be assessed following a tornado. In 2013, Environment Canada further modified the EF-Scale to better suit the Canadian context. The present study will refer to the Canadian version of the EF-Scale for assessment of residential structures. More information on the Canadian modifications to the scale can be found in (Sills, et al., 2014) or on Environment Canada's website (Environment Canada, 2013).

The current version of the EF-Scale provides refined wind speed estimates for 31 categories of common structures and vegetation, referred to as Damage Indicators (DIs). Under each DI, the EF-Scale utilizes the concept of Degrees of Damage (DOD). DODs describe the sequential modes of damage that have been observed to occur in a particular DI. Each DOD is associated with a minimum, maximum, and expected wind speed. These values represent the estimated wind speeds required to cause the specified damage. They can be related back to the EF-Scale wind speeds to estimate the intensity of a tornado, from EF0 to EF5. In the present study, the DI for one- and two-family residences (FR12) is of particular interest. DOD descriptions and wind speed estimates are shown for this DI in Table 1-1.

Table 1-1: DOD descriptions and wind speed estimates for the FR12 DI, as adopted by Environment Canada (2013)

DOD	Description of Damage	Wind Speed Estimates [km/h]		
		Lower Bound	Expected	Upper Bound
1	Threshold of visible damage	85	105	130
2	Loss of roof covering material (up to 20%), gutters and/or awning; loss of vinyl or metal siding	100	125	155
3	Broken glass in door and windows	125	155	185
4	Uplift of roof deck and loss of significant roof covering material (more than 20%); collapse of chimney; garage doors collapse inward; failure of porch or carport	130	155	185
5	Entire house shifts off foundation	165	195	225
6	Large sections of roof structure removed (more than 50%); most walls remain standing	165	195	230
7	Exterior walls collapsed	180	210	245
8	Most walls collapsed, except small interior rooms	205	245	285
9	All walls collapsed	230	274	320
10	Destruction of engineered and/or well-constructed residence; slab swept clean	265	320	355

The EF-Scale offers a systematic method of assessing tornado intensity, and it helps investigators discern what fails, or what should fail first, so that unexpected failures can be easily identified. The FR12 DI covers typical wood-frame houses constructed in Canada and the United States. In the present study, the DODs of interest are DOD-4 and DOD-6 for residential structures, corresponding to roof sheathing failure and loss of large sections of the roof structure, respectively. Most past research on roof damage focuses on sheathing and roof-to-wall connection (RTWC) failures, and it is apparent that the wind speed estimates for roof damage in the EF-Scale are based heavily on these well-understood

failure modes. Figure 1-1 shows an example of typical sheathing failure, and Figure 1-2 shows failure of the RTWC. The current understanding of DOD-6 is limited to research focused on RTWC failures.



Figure 1-1: Example of roof sheathing failure, corresponding to DOD-4 (Image provided by Dr. David Prevatt of University of Florida)



Figure 1-2: Example of roof-to-wall connection failure, corresponding to DOD-6 (Image provided by Dr. David Prevatt)

As seen in the shaded row of Table 1-1, DOD-6 describes failure of the RTWC and subsequent loss of large roof sections, which can occur at an expected wind speed of 195 km/h. This wind speed corresponds to relatively weak EF2 tornadoes (Environment Canada, 2013). DOD-4 occurs at lower wind speeds; however, loss of a single sheathing panel can allow for water ingress, which often results in loss of the entire house and its contents (Sparks, et al., 1994). As discussed in the following sections, gable roofs have been observed to perform poorly under these modes, especially DOD-6, relative to neighboring hip roofs of similar construction. In fact, the FR12 listing from the Canadian EF-Scale notes that for hip-roof homes, the upper-bound wind speeds for DODs 4 and 6 can be assumed. This is counter to the original EF-Scale documentation (Wind Science and Engineering Centre, 2006) which specifies that the lower bound of DOD-6 is due to inadequate construction or large overhangs while the upper bound is due to enhanced, construction such as the use of hurricane straps. The difference between the two versions of the EF-Scale is a significant point, which warrants further investigation.

1.2.2 Survey Data from Recent Tornadoes

Although the method of forensic investigation is the most appropriate method to date for assessing tornado intensity, it is limited in that the progression of failure cannot be observed. Survey data following a major event provides information about the end state of the components of a structure. Closer inspection of failed members can provide additional information about state of the structure leading up to the event. If the geographic location of the failed structure is known, online mapping tools such as Google Earth can also be used to gain an understanding of what the intact structure looked like. In research, the ability to make accurate assumptions regarding the initial structure is important for studying the most likely progression of failure. In experimental work such as that carried out by Henderson et al. (2013) and in numerical studies (Martin, 2010; Pfretzschner, 2012; Jacklin, 2013), proper construction is assumed and model structures are designed and constructed according to code and common practice. This method provides an indication of how the structure should behave, and may help to understand the conditions or discrepancies which make it behave unfavorably in reality.

Residential roof failures are among the most common and expensive types of tornado and hurricane damage and, thus, have been studied extensively. The density of houses relative to other structures in any populated area leads to high occurrence of residential failures during extreme winds and increased risk to neighboring structures due to blowing debris. The relative vulnerability of residential roofs is additionally important because loss of a single sheathing panel, which occurs at relatively low wind speeds, can allow for water ingress. This often leads to loss of the entire structure and its contents due to the heavy rainfall that accompanies extreme wind events. Sparks et al. (1994) compared insured losses to observed damage and gradient wind speeds from past hurricanes. Their analysis indicated a sudden rise in insured losses between 151 km/h and 172 km/h 10-meter mean wind speeds (64 m/s and 72 m/s 3-second gust speeds). Statistics from damage survey observations identified the cause of this rise to be failure of the building envelope through loss of roof sheathing panels and broken windows or doors.

The straight-line wind speeds from Sparks et al. (1994) can't be directly compared to the EF-Scale wind speed estimates for FR12, however an important finding of Sparks's study showed that over half of insured losses in a major hurricane are due to failure of the building envelopes of houses. Even though the walls don't often collapse, serious damage occurs once the seal provided by the roof or walls has been broken. Repetitive, similar failures are frequently observed across neighborhoods where a common design was implemented or the same party was responsible for construction of many houses. This is often the case in modern subdivisions. Identical failures of similar components suggest that widespread mitigation is possible; improved design approaches and innovative fasteners have been recommended to help mitigate the prevalent sheathing and RTWC failure modes in the work to date.

Damage survey observations have previously led to the identification of important failure trends in various building components. In particular, residential gable roofs have been the subject of a number of studies due to their tendency to lift off at the toe-nailed roof-to-wall connection during a tornado. Hip-roof structures are commonly considered more resilient due to reasons discussed in the following section. However, inspection of the available data

has revealed a previously unstudied failure mode in which hip roofs suffer partial framing failure, presumably initiated at member connections.

1.2.2.1 EF2 Tornado in Angus, Ontario

Following an EF2 tornado that damaged a residential neighborhood in Angus, Ontario on June 17, 2014, Kopp et al. (2016) evaluated damage to 101 houses and analyzed the observed failures. Repetitive failures of similar building components were observed across the study area. The statistics of these failures were presented in Kopp et al. (2016), followed by fragility analyses of comparable gable and hip roofs. The fragility analyses showed that for failure of the roof-to-wall connections in a hip roof, the required wind speeds fall above the range specified in the EF-Scale for DOD-6, i.e., about 50 km/h higher than the wind speeds required for that in a gable roof. This is greater than one category in the EF-Scale.

Kopp et al. (2016) concluded that when toe-nailed RTWCs are used on gable roofs, the RTWCs are more likely to fail than the sheathing panels. In hip roofs, depending on the length of the sheathing fasteners, sheathing loss may be more likely than failure of the RTWC. Both categories of failure occur at much lower wind speeds in gable roofs. Though this study confirmed that hip roofs are more resistant to the common failure modes for residential roofs, failure was still observed in hip roofs or in the hip portions of combination roofs.

An example of a partial hip roof failure from the Angus tornado is shown in Figure 1-3. This failure does not appear to have occurred simply as sheathing failure or failure of the RTWC. At the left corner of the damaged house there is an opening where it appears that a portion of the roof has been removed. Inside of the opening intact trusses are still visible. This suggests either that hip trusses near the edge of the roof have failed, or that smaller framing members making up the corner of the roof have been removed. In either scenario, partial failure of the roof frame has occurred, though it may have been initiated by failure of the RTWC at the corner. Several other observed failures which do not clearly fall into the sheathing or RTWC failure categories will be introduced in the following section, providing further background and justification for the current research.



Figure 1-3: Partial hip roof failure observed following EF2 tornado in Angus, Ontario, June 2014. (Image provided by Dr. Greg Kopp)

Framing failures in hip roofs may address a gap in the current DOD listing for residential roofs. Although DOD-6 allows for failures other than that of the RTWC, hip framing failures - and the wind speeds at which they are likely to occur - have not been studied in the literature to date. Further evidence for these possible failure modes is examined in the next section.

1.2.2.2 EF4 and EF5 Tornadoes in the Southern US

Additional data from recent events in the United States have been obtained for examination in the present research. These data were gathered following destructive tornadoes in the Southern US, including the Moore, Oklahoma tornado of 2013 (EF5) and the Tuscaloosa, Alabama (EF4) and Joplin, Missouri (EF5) tornadoes of 2011. They were provided to the author by Dr. David Prevatt of the University of Florida. A forensic assessment team of researchers, engineers, and students spent the days following these events surveying the affected areas and documenting observed damage. Their reports on these tornadoes can be found in (Prevatt, et al., 2011; Prevatt, et al., 2013; Graettinger, et al., 2014). The combined

database provides thousands of images of damage to houses, ranging from sheathing loss to total destruction.

The Moore, OK tornado was determined to be an EF5 event, with damage ranging from EF0 to EF5 observed across the path of the tornado. This event killed 24 people and was estimated to have caused \$3 billion of economic loss (Graettinger, et al., 2014). EF0 to EF2 winds typically comprise about 85% of the damage area of a strong EF4 or EF5 tornado, and so many stages of damage progression could be identified (Graettinger, et al., 2014). The survey performed following this event has informed subsequent research including identification of new methods for improved damage surveys, fragility analyses of house components, and the development of improved laboratory simulations for tornadoes (Graettinger, et al., 2014). It also led to changes in the Moore, OK building code such that wood-frame houses have new prescriptive requirements to mitigate up to DOD-6 damage.

The raw database of photos taken following the Moore, Tuscaloosa and Joplin tornadoes was used in the present study to examine the nature of hip roof failures. Many instances of partial hip roof failures were identified in the data. As with the findings of the fragility analyses in Kopp et al. (2016), the observed failures evoked additional questions regarding the likelihood and conditions under which partial hip roof failures may occur. Select examples of the observed failures from Moore are shown in Figure 1-4 and discussed below.

Figure 1-4(a) shows neighbouring hip-roofed homes that exhibit similar failures of the front face of the roof. The RTWC appears to be intact around the remaining perimeter of the roof and it is apparent that several members of the roof frame have failed or been removed, in addition to the sheathing covering this portion. At the right side of the photo the remaining part of the roof is sagging, which further indicates that the underlying frame has failed. The houses shown in Figure 1-4 (a) were located along Kyle Drive at the western edge of Moore, OK. Several houses along this short stretch had similar failures of hip roof framing. The houses in this area had similar structural configurations and were built around 2006 (Graettinger, et al., 2014). Inspection of the damage photos from this neighborhood indicated that, of houses experiencing DOD-4 or DOD-6 roof damage, 40% appeared to

have failed through similar partial failures. In these cases, it appears that the frame failed at the nailed connections between the members, as no broken lumber is visible. The following section will present additional statistics and observations from two selected neighborhoods following the Joplin, MO tornado.

Figure 1-4(b) shows a similar failure to that in 4(a) but of a much steeper roof. The RTWC appears to be intact, and a large open cavity is visible where both framing members and sheathing have been removed. Similar to 4(a), it is apparent that this roof did not exclusively suffer sheathing loss, although the smaller area of sheathing loss at the right side of the photo should be noted. The lack of visible internal members in the cavity, especially those supporting the intact opposite face of the roof, strongly suggest that this roof was built as a stick-frame structure as opposed to one containing prefabricated trusses. Many of the failed hip roofs in the available data appear to have used stick-framing. The trussed and stick-frame construction methods will be described in Section 1.3.

Figure 1-4 (c) shows a partial failure of a combined hip/gable roof. This failure is unique from those shown in Figures 1-4(a) and 1-4(b) because material failure of the wood members is apparent. The RTWC appears to be intact, with the lower part of the roof having lost only sheathing on the right side, and framing members in addition to sheathing on the left. Near the peak of the roof, the frame has failed on both faces. This structure appears to contain either trusses or stick-framing with robust connections. As indicated on the figure just above the RTWC, the members were connected or otherwise reinforced using nailed wooden plates.



Figure 1-4: Hip roof failures in Moore, OK following the EF5 Tornado of May 21, 2013. a) Framing failure of similar, neighboring hip roofs b) Framing failure of steep, stick-frame hip roof c) Hip roof displaying material failure of the wood framing members (Images provided by Dr. David Prevatt)

Upon inspection of the failures shown in Figure 1-4 and similar damage in the available photos, it becomes apparent that partial framing failures are another possible, repetitive mode of failure occurring in hip roofs. When comparing these hip roof failures to nearby structures from the data, it was determined that framing failures such as those shown in Figure 1-4 may govern in hip roofs at EF2 wind speeds, rather than RTWC failures or sheathing loss. It was also noted that the construction of the roof may be important. The observed stick-frame failures especially suggest that the performance of stick-frame roofs may need to be distinguished from that of trussed structures in analysis and design, as well as in the present research.

1.2.2.3 Statistics for Occurrence of Partial Roof Failure

For a complete analysis of the occurrence of partial roof failures, all observed damage within the DOD-4 and DOD-6 ranges must be categorized further to identify whether the observed failures are related to the sheathing, RTWCs, or the roof framing. Sorting the data by neighborhood offers additional information about trends across small regions, compared to the entire damage track of an event. As mentioned, the survey data provided by the University of Florida includes a database of photos. Some of these photos include geographical metadata, however many do not. Additional manipulation of the data, and the provided damage assessment spreadsheets, is required to allow for mapping of all photos and locations of rated damage. Preliminary work in this area has focused on the data from the Joplin, MO tornado of May 22, 2011.

The damage survey data provided from the Joplin tornado includes an Excel spreadsheet which lists every photo that was used for assessing the event in accordance with the EF-Scale. The longitude, latitude, and EF-Scale rating at each location was listed, along with the file and path name for each image. The EF-ratings were assigned by the damage survey team at the time of the investigation. Using this data to manually create source code for the .kml file type used by Google Earth, it is possible to map the photos, including those with no GPS metadata, and label them using color-coded pins to represent the EF-Scale ranking. A sample from the resulting map is shown in Figure 1-5. This map shows the two areas analyzed to obtain the preliminary statistics presented herein. These neighbourhoods are located at the West end of the damage path. Only the data corresponding to EF1, EF2, and

EF3 damage was analyzed because these rankings correspond to the DOD-4 and DOD-6 wind speeds for residential roofs. In the figure, EF1, EF2, and EF3 rankings are represented by yellow, orange, and red pins, respectively.



Figure 1-5: West end of tornado damage path following the May 22, 2011 tornado in Joplin, MO; two present study regions are shown by white outlines

Two study areas, outlined in white on Figure 1-5, were analyzed and the occurrence of different failure modes can be compared across them. The damage photos at the marked locations in each region were inspected and the perceived mode of failure was noted. This pass through the data marked each separate residence based on whether the damage appeared to be wall, RTWC, sheathing, or framing failure. Wall failures corresponding to DOD-7 were included because the expected wind speeds causing this failure mode falls under the same EF category as DOD-6. The study areas were selected based on the characteristics of the houses in each. Region 1, on the left side of Figure 1-5, was found to contain houses that appeared to be newer, most with steep-sloping hip roofs and large building footprints. The homes in Region 2 mostly appeared to be older, masonry homes with shallow wood-framed roofs.

The results of the present analysis found that in Region 1, 42% of the houses with relevant damage failed through partial framing failure, while 40% showed signs of failure of the RTWC. Figure 1-6 shows Region 1 at a smaller scale, including aerial imagery depicting the aftermath of the tornado. As can be seen, most of the damage in this neighborhood was limited to the EF2 range, aside from one location on Jessica Drive. Figure 1-7 shows an example of the steep-sloping hip roofs visible throughout this neighbourhood, with an aerial image showing how the surface area of the roof was affected by the failure. In many instances, the largest surfaces of the roof were removed, while parts of the structure enclosing smaller spaces remained in place. Many of these structures also appeared to be of stick-frame construction.



Figure 1-6: Map of Region 1 neighborhood (Sunset Drive) with aerial photography showing the aftermath of the tornado in Joplin, MO (Image provided by Dr. David Prevatt)



Figure 1-7: Example of typical hip roof configuration in Region 1, with an aerial photo showing the footprint of the partial failure on the right-hand side of the figure (Image provided by Dr. David Prevatt, Google Earth)

The distribution of failure types in Region 2 is different from that of Region 1; 15% showed partial failures, while 2%, 22%, and 18% suffered RTWC failure, sheathing failure, and wall collapse, respectively. This shift could have occurred due to a number of factors; however, it was noted that many of the houses in Region 2 appeared to be of older construction than those in Region 1, and had lower-sloping roofs. While this observation may suggest that roof slope contributes to the occurrence of framing failures, it is not apparent what other factors may have had an additional impact. For example, the lack of lateral restraint in older houses may have led to increased numbers of wall collapses, and aging structures may also be less resistant to debris damage. In the example shown in Figure 1-8, partial roof failure occurred. However, this failure may have occurred due to the tree debris visible on top of the failed roof. Other instances of partial failure in Region 2 were similarly ambiguous, and because Region 2 was downwind of Region 1, debris likely played a larger role. In both regions, partial failures were found to occur at least as often as other modes of roof failure. More work is required to obtain a complete set of statistics on these failures and better define the regional conditions that may contribute to their occurrence.



Figure 1-8: Partial hip roof failure in Region 2 (Image provided by Dr. David Prevatt).

1.3 Wood-Frame Residential Roofs

More than 90% of the residential building stock in North America consists of light-frame wood construction (van de Lindt & Dao, 2009). By far, wood-frame residential buildings are the most prevalent in any community, but they are also among the most susceptible to wind damage. Wood-frame construction in Canada and the US take similar approaches in that prescriptive or conventional designs are predominant (Canada Mortgage and Housing Corporation, 2014; van de Lindt, et al., 2007). For the roof structure, these approaches consist of following documents such as the International Residential Code or Part 9 of the National Building Code of Canada (NBCC) to determine member size, spacing and fastener requirements. In Canada, these requirements are taken from tabulated values based on the design snow loads.

Prescriptive design approaches include additional requirements for buildings located in regions of higher wind or earthquake risk, which occurs in about 50 locations across the country. These requirements include ties capable of resisting 3 kN of uplift at the RTWCs, improved lateral bracing of walls, and foundation anchorage, but they do not include

fortified roof structures. Buildings that fall within the “Extreme” exposure category must be fully engineered, however there is only one region in Canada (Resolution Island, Nunavut) which falls into this category for wind. Aside from this single region for wind, and three regions for earthquake exposure, all new houses in Canada may be constructed according to prescriptive approaches unless architectural choices lead to exceptions. Provincial adoptions of the NBCC may impose additional requirements, however most provinces have either fully or majorly adopted the same provisions as the NBCC in their provincial building codes (National Research Council of Canada, 2017).

Prescriptive design encompasses both stick-frame and trussed roofs, although the trusses themselves are required to be designed to handle regional snow loads, and come with site instructions for care, handling, and installation. Trusses are becoming the predominant form of new residential roof construction in Canada (Canada Mortgage and Housing Corporation, 2014), however stick-framing is still used and much of the aging housing stock consist of stick-frame construction. The two construction methods will be described in more detail in the following sections. Trussed and stick-frame structures both require consideration in the present study because both types of roof have been observed to fail in the available survey data. Ongoing research has identified a number of common design issues and construction errors that occur throughout North America, and it has become apparent that many factors must be considered and addressed to significantly mitigate roof failures. The factors contributing to wood-frame roof vulnerability at present include gaps in current design practice; these gaps may occur in different forms for trussed and stick-frame structures. It is also important to note that current design codes specify wind loads based on straight-line winds only.

1.3.1 Trussed-Roof Construction

Metal-Plate-Connected (MPC) trusses have been used in residential structures in North America as early as the 1950’s. Today, trussed roofs are constructed using prefabricated portions of the roof frame which are manufactured in a plant and shipped to site for assembly. Trusses consist of standard sizes of sawn lumber connected into a certain configuration. Metal plates with teeth punched out of the surface, and that protrude from one face of the plate, are pressed into the sawn lumber members to fasten them together.

MPC trusses are now implemented in many applications due to efficient production techniques, increased levels of quality control, ease of erection, and economy. As previously mentioned, trusses consist of two primary elements: sawn lumber members and the metal plates that join them.

Figure 1-9 illustrates the parts of a MPC truss and shows the nomenclature used in the present study. On site, trusses are placed on top of the wall top plate at equal spacing. Roof sheathing is fastened to the top of the top chords to enclose the roof, and ceiling drywall is typically fastened directly to the bottom faces of the bottom chord members. In gable roofs, all trusses in a roof may be identical in shape and configuration, while hip roofs require progressively taller trusses moving towards the centre of the roof, as well as short jack trusses placed perpendicular to the outermost full-length trusses to complete the roof slope at the eaves. For the reader's reference, Figure 2-4, later in this thesis shows a 3-dimensional model of an entire trussed hip roof, including full-length hip trusses and jack trusses.

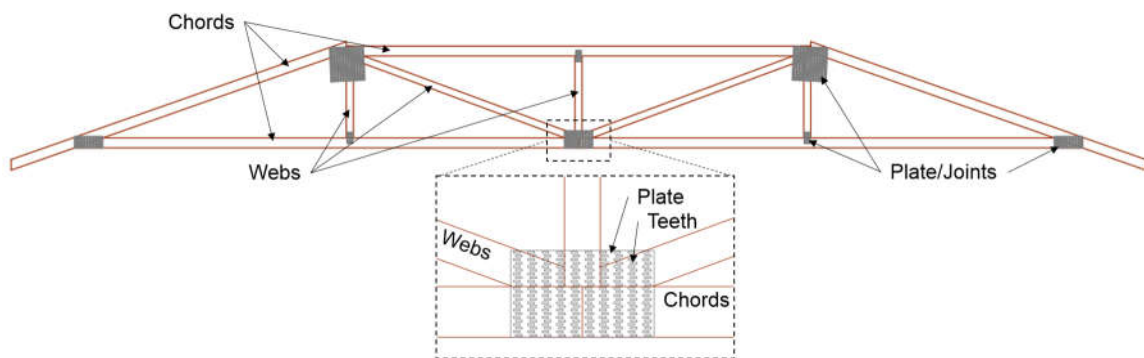


Figure 1-9: Illustration of MPC Truss with Components Labelled

MPC trusses are designed based on a tributary load distribution by companies who specialize in truss fabrication. Analysis for design is typically carried out using specialized computer software developed by these companies. Truss design software is commonly based on the Finite Element (FE) method. However, it is also usually proprietary software so model assumptions, simplifications to the design method, or any built in “rules-of-thumb” are not disclosed. The governing bodies for truss design publish procedures and guidelines to be followed in design of MPC trusses. The Truss Plate Institute (TPI) and the

Truss Plate Institute of Canada (TPIC) are responsible for publishing design and testing methodology in the US and Canada, respectively. The Wood Truss Council of America (2002) published a handbook to guide the use and design of MPC trusses. This resource provides a comprehensive guide and history of MPC trusses.

1.3.2 Stick-Frame Construction

Stick-frame roof structures consist primarily of repetitive, sloped rafters, nailed at the peak of the roof to the ridge board or hip rafter, and connected at the base of the roof to the wall top plate. Horizontal restraint that prevents the rafters from kicking outwards under gravity loads may be provided by the ceiling joists, which also rest on the wall top plate and are nailed to the rafters, or by horizontal collar ties which connect opposite rafters partway up the slope. Figure 1-10 shows a labelled illustration of a stick-frame hip roof structure with a square footprint. This design was prepared by the author, in accordance with Part 9 of the NBCC (2010). The Canada Mortgage and Housing Corporation (CMHC) (2014) published a general guide which describes common residential design in accordance with the same version of the NBCC. Additional explanation and figures describing recommended roof construction practices can be found in the CMHC document.

In stick-frame roofs such as that shown in Figure 1-10, the closely-spaced jack rafters are structural members, while the larger hip rafters simply provide a rigid, continuous member for the jack rafters to frame into. There is no requirement in the code to join the hip rafters together at the peak of the roof, and it is expected that the roof sheathing significantly contributes to load sharing throughout each face of the roof. The connections between the jack rafters and hip rafters along the ridge typically consist of nails going through the side of the hip rafter and into the end of the jack rafter, though they can alternatively be horizontal toe-nailed connections. It is well understood that both end-nailing and toe-nailing yield weak connections, and strength reduction factors must be applied to these values during capacity estimation (Canadian Wood Council/Canadian Standards Association, 2015). At the RTWC, the jack rafter is nailed to the ceiling joist using several nails perpendicular to the length of each member, and both the jack rafter and the ceiling joist are toe-nailed into the top plate.

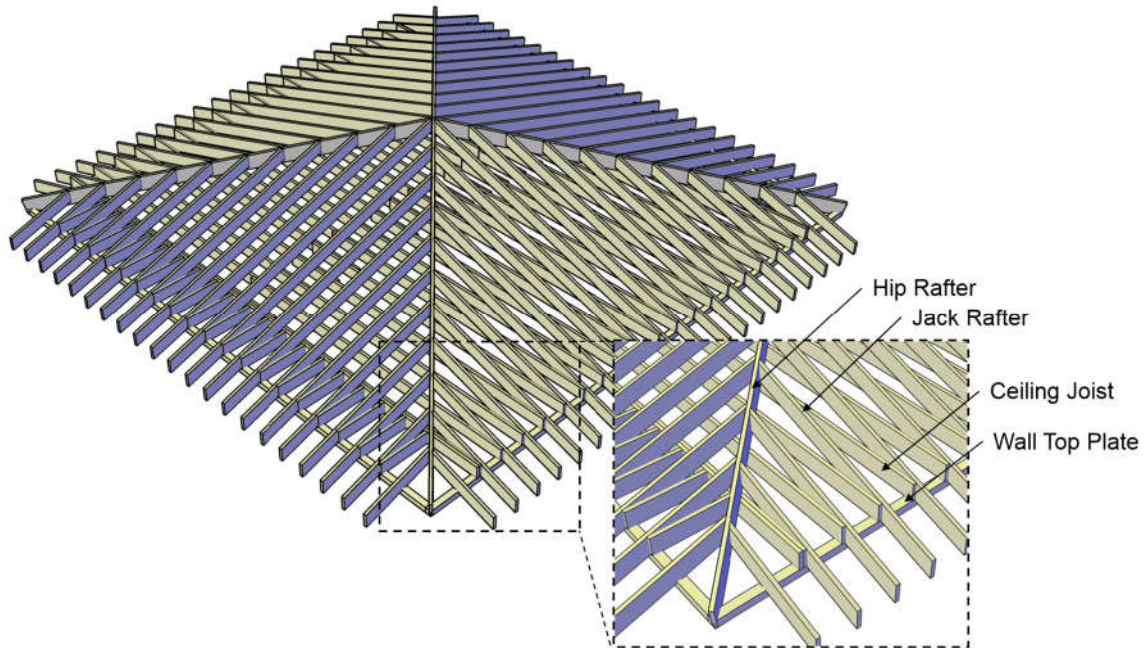


Figure 1-10: Illustration of Stick-Frame Hip Roof with Components Labelled

New housing construction in Canada largely consists of trussed structures (Canada Mortgage and Housing Corporation, 2014); however, stick-framing has prevailed historically so many existing structures in Canada and the US are still of stick-frame construction. The significant difference between trussed structures and stick-framing is the use of engineered trusses versus an entirely prescriptive approach, which is commonly the case for stick-built homes. In addition, truss framing members are joined by toothed metal plates, while stick-frame members are connected by nails in specified patterns. In a recent study, Weston and Zhang (2017) recognized that the use of nailed connections and aging of structures results in connections that are weaker than the framing members that they join.

1.3.3 Roof Shapes and Performance Under Wind Loads

Residential roofs can be constructed using a range of shapes and slopes. Many include dormers or other discontinuities to cover irregular shaped houses. Out of the various roof shapes possible in wood-frame construction, the most common in North America are gable and hip roofs (or their composite). Hip roofs, which are the focus of this thesis, are those

with sloping faces on all sides of the roof, as opposed to two sloped faces in the gable roof shape. Samples of standard hip roof designs are shown in Figure 1-10 and Figure 2-4.

Wind engineering research for residential roofs has historically focused on gable roofs. They have been observed to fail frequently, and under two predominant modes during relatively weak tornadoes. Damage surveys following wind storms, and subsequent research, has frequently identified a disparity in damage between the different geometric forms of residential roofs (Meecham, 1992). Hip roofs are generally known to perform better than other roof shapes. Recent work at the University of Western Ontario (Gavanski & Kopp, 2017) has even suggested that a single DI for residential structures in the EF-Scale may be inadequate due to significant variations in the estimated failure wind speeds for different roof shapes, although this has not been quantified in damage surveys.

Several past studies have investigated the superior performance of hip roof homes (Meecham, et al., 1991; Meecham, 1992), with some more recent works directly investigating hip roof behaviour with regard to roof sheathing (DOD-4) and RTWC (DOD-6) performance (Kopp, et al., 2016; Henderson, et al., 2013). In 1991, Meecham et al. (1991) performed wind tunnel testing to further the technical understanding of hip roof performance and found that there is an important relationship between pressure distribution and underlying framing configuration in wood-frame roofs. Despite significant differences between the pressure distributions recorded for the gable and hip roof models, the overall roof uplift and overturning moments were found to be quite similar. This verified that preferable aerodynamic geometry is not the only reason for improved performance of hip roofs.

Meecham's (1991) results indicated that the orientation of framing members in a hip roof, relative to the distribution of uplift, provides additional resilience. In contrast, the shape of the gable roof causes higher localized peak pressures and the orientation of framing members result in unfavorable load sharing. In addition to this, hip roofs have RTWCs around their entire perimeters, while gable roofs are only connected to the wall framing along two opposite walls. In combination with improved load sharing within trussed hip

roofs, these factors are generally believed to make hip roofs significantly more resistant to wind uplift.

1.4 Past Research on Residential Roof Performance

Past research on tornado damage to residential structures is largely limited to interpreting data from field observations. Experimental work to study the progression of failure is not generally feasible due to the destructive nature of these tests and the risk of debris damage to test facilities. Computer modelling of tornado failures may be possible, however finite element modeling for entire houses has been limited to straight-line wind assessments and the general flexibility response and system effects of the roof structure (Pfretzschner, 2012; Martin, 2010; Jacklin, 2013). It is valuable to understand the body of existing knowledge from both experimental and numerical studies to aid model development and validation in the present research.

1.4.1 Experimental Studies

In practice, residential structures are designed to withstand idealized uniform positive and negative pressures, yielding equivalent static load effects on the members and components within prescribed roof zones (Kopp, et al., 2012; Henderson, et al., 2013). However, the true wind field within a tornado or other extreme wind events is a highly turbulent environment, affected by many factors including building shape, size, and terrain roughness conditions. These factors cause the wind loading to vary both in space and time over the surface of a roof. The simplifications involved in building code designs and standardized product tests often result in load envelopes that neglect the effects of the complex wind behaviour. Numerous new facilities and test methods have emerged recently to assist in assessing the full-scale behaviour of residential structures under realistic wind loads. These methods also improve the evaluation of damage survey observations by attempting to replicate observed failures through experiments. Kopp et al. (2012) provides an overview of current methods and facilities employed to assess the true effects of spatial and temporal variations in wind loading on low-rise structures.

In addition to emerging full-scale tests and the ability to obtain realistic loading from wind tunnel testing and tornado simulators, experimental studies also provide component-level

stiffness and resistance data. Shanmugam, et al. (2009) tested four existing residential structures in the field to determine the uplift capacities of RTWCs and sheathing units. Fragility analyses were carried out and the distribution of capacities was identified. From these results, an analytical model to approximate RTWC behaviour was developed. Other component-level test results provide validation data for modeling the nonlinear behaviour of sheathing fasteners (Dao & van de Lindt, 2008) and RTWCs (Morrison & Kopp, 2011), as well as the overall deflection of entire trusses (Wolfe, et al., 1986). The present research uses some of the available data for validation of the truss models. It also requires an in-depth review of past modeling studies to identify appropriate methods for the present analysis.

1.4.2 Finite Element Analysis of Wood Frame Residential Roofs

To construct an analytical model of any structural system, approximations must be made carefully to ensure that the numerical model can accurately predict the behaviour of the structure. The approximation of a structural member in modeling is commonly referred to as the ‘analog’. In wood-frame structures, the most important analog decisions are concerned with accurately modeling the size, shape, and location of structural members, and the behaviour of the connections between members. These analogs have been found to vary throughout the literature. Other approximations which must be defined in models of wood-frame houses include support conditions, the behaviour and connection of the roof sheathing, and the anisotropic material properties of wood. This section presents a review of the published literature related to the development of finite element models for wood-framed roofs. The primary focus will be on identifying appropriate methods of modelling roofs containing MPC trusses, as these structures contain complex elements and connections relative to that of the stick-frame structure.

Past research has included analytical evaluation of MPC wood joints with varying degrees of finite element model intricacy. Mackerle (2005) prepared a literature review of past studies involving finite element analysis in wood research. This review provides 300 references to Finite Element Modeling (FEM) studies related to wood materials, fasteners, and structures including trusses and frames. The summary of the listed studies provides a comprehensive view of the work that has been done in this area. Several studies discussed

by Mackerle, in addition to several more recent publications, were of importance to the present work for demonstrating the current state of FEM methods for wood trusses and providing additional justification for the approaches taken herein.

Many past finite element analyses and experimental studies have focused narrowly on the detailed sheathing or RTWC behaviour, or on the general flexibility behaviour of the roof components or the wood-frame house as a system. The present analysis requires element-level estimates of forces, moments, and capacities within the framing that comprises the residential roof. Since no other study has modelled wood-framed roofs in this context, a detailed study of all relevant truss model analogs is carried out to identify the modeling methods that may be suitable for the present purpose. Several modeling techniques, applied in the literature for other purposes, are reviewed and the most practical analogs are identified, validated, and compared, as presented in Chapter 3.

As mentioned, review of past truss and roof modeling studies has suggested that there are two predominant analog categories to be considered. First, joint connectivity assumptions define the way that connected members interact with one another at the joints. The methods employed have varied across the published research and have been found to influence the flexibility of the truss. The second important analog category is that of member insertion points. These assumptions reflect the concentric or eccentric behaviour of the framing members. These categories will be explained further and their use will be discussed in the following sections, followed by material property considerations and a review of experimental work on trusses and analytical work on stick-frame structures.

1.4.2.1 Joint Connectivity

Traditionally, MPC trusses are modelled either as trusses having pinned connections with rotational freedom, or as frames with rigid joints. However, reality most often occurs between or beyond these two conditions due to semi-rigid joint behavior (Riley, 1998). Metal truss plates deform and interact with the surface of the connected wood members in ways that allow local axial, shear, and rotational deformation to occur before failure. These actions may be represented by load-displacement curves or simplified by linear joint

stiffness parameters (in units of force/distance), which can be modelled using partial end releases or spring elements in most finite element modeling software.

If semi-rigidity is to be incorporated in a model, experimental data or analytical tools that estimate the material behaviour of the joint elements must be used to determine joint stiffness in its nonlinear form, or simplified as a linear value. Joint strength and stiffness parameters depend on many factors including wood species and grade, plate type, orientation of plate, orientation of loading, and geometry of the plate-to-wood contact. Stiffness values for modeling are difficult to estimate due to the complexity of joint behaviour. Furthermore, experimental data can only be considered accurate for truss models in which the joint parameters closely resemble those that were tested.

In past studies, experimental stiffness values have been obtained as needed for validation; however, these studies are limited and often focus on specific joints (Vatovec, 1996) or behaviour such as out-of-plane bending (Liu, 2013). In the absence of experimental joint stiffness data or appropriate estimates for all configurations, MPC trusses are statically indeterminate structures and must be modelled with idealized pinned or rigid connections, or a combination thereof.

Several studies have attempted to estimate the semi-rigid behaviour of MPC truss joints through theoretical models. These models attempt to predict the load-deformation curve of the MPC joint, as a function of the geometry of the plate-to-wood interface and the material properties. One of the first and most widely referenced of such was developed by Foschi (1977). Foschi developed a joint model based on the assumption that the tooth-wood interaction in a MPC joint was responsible for all deformation, while the wood and plate were each assumed to remain rigid within the contact area. A three-parameter equation was developed to represent the nonlinear load-slip behaviour at the plate-wood interface. This model was used and evaluated in many subsequent studies (Li, 1996; Riley, 1998; Liu, 2013).

It was found that Foschi's (1977) model provides a reasonably accurate prediction of joint stiffness in the linear range (Liu, 2013). However, use of this model requires experimental data for calibration of all new joints. Other theoretical models following from or

contrasting Foschi's work also involved complex joint models in addition to experimental data for the material behaviour.

Riley (1998) developed a simpler model to predict the axial and rotational stiffness of MPC residential wood truss joints. This study included testing of 36 tension splice joints and heel joints to validate the analytical results. Three different joint behaviour assumptions were applied and compared in this work. The semi-rigid joint method made use of fictitious elements representing the stiffness parameters of the joints, which were calculated using joint and tooth geometry and material properties. Member forces and truss deflections from this analog were compared to those from analyses assuming pinned or fully fixed MPC joints. As was hypothesized, the pinned and rigid assumptions provided the outer bounds of maximum truss deflection results. The results of Riley's semi-rigid analysis fell in-between these sets of results.

When compared to experimental results, the semi-rigid stiffness values obtained from Riley's (1998) model fell within 10%, without being consistently larger or smaller. A comparison of absolute moment and axial force in the top and bottom chords was also carried out and showed that both the pinned and rigid joint models generally overestimate the results of the semi-rigid model. Riley's (1998) method was concluded to be valid for joints made from softwood lumber and light gauge steel plates, and can be applied where specific gravity and moisture content of wood, as well as plate geometry are known and well-defined.

In more recent studies, it has been identified that complex joint models, when used as part of larger models studying truss or whole roof behaviour, may be unnecessarily complicated (Martin, 2010). Despite the potential for improved accuracy, complex joint models were deemed inappropriate for the present study due to the time- and labor- intensive nature of their employment. Additionally, since this study focuses on hypothetical structures, many assumptions must be made. To employ a three-dimensional and/or nonlinear joint model, too many parameters would be assumed, and without experimental data there is no practical means of verifying the assumptions. As discussed in the following chapter, the modeling method is selected to represent the worst probable cases of truss loading. The outer bounds

of the possible truss behaviour can be estimated more certainly and can be used to identify all possible vulnerabilities. The semi-rigid behaviour of joints will be considered, where required, by applying linear experimental stiffness data.

In contrast to the complexity of joint models developed in some of the past research, other available literature describing finite element models of entire roofs was found to lack the level of detail required by the present study. In past MPC roof studies, truss modeling was primarily concerned with validating the deflection behavior of a single model analog so that the load sharing behavior of entire roofs could be captured (Jacklin, 2013; Pfretzschner, 2012; Martin, 2010; Limkatanyoo, 2003). In these studies, the researchers selected a truss analog and validated it to an acceptable level of agreement with experimental deflection values. Few studies have addressed truss member forces (Li, 1996; Vatovec, 1996), and experimental data on element-level behavior was found to be limited to two studies (King & Wheat, 1987; Wolfe, et al., 1996).

Li (1996) evaluated the member axial force and moment results of a semi-rigid joint analog of parallel-chord rectangular trusses tested by King & Wheat (1987). This analysis found good agreement between modeled and experimental axial forces, but could not validate the model with the member moments. Although intensive calculations were carried out to estimate joint stiffness values for Li's (1996) semi-rigid joint model, good overall agreement of moment results could not be achieved. In models where member moments compared closely to experimental data for certain members, there would be significant differences for other members. King & Wheat (1987) reported, based on their experimental results, that bending moments in truss members were highly sensitive to connection stiffness. These findings suggest that great caution should be used in applying a semi-rigid joint analog to any MPC structure unless sufficient experimental stiffness data is available for comparable joints to those being modeled.

In addition to the pinned, rigid, and semi-rigid joint analogs previously mentioned, (Li, et al., 1998) used a combination of semi-rigid and pinned connections; semi-rigid heel joints and bottom chord splices with moment releases at the crown joint and web member ends. At the time of publication of Li et al. (1998), experimental stiffness data was only available

for the heel and compression splice joints. Pfretzschner (2012) proposed a similar model; however, this work only combined rigid and pinned connections. By modeling the trusses of a gable roof using rigid heel joints, continuous members, and pinned crown and web member joints, Pfretzschner (2012) obtained satisfactory deflection validation for a series of single trusses, and applied this analog to study the vertical load path and system behaviour in an entire wood-framed house. Vatovec (1996) compared two-dimensional models using pinned connections, rigid connections, and semi-rigid connections at all joints using experimentally obtained stiffness values, and found that deflection results at mid-span from all analogs fell within 10% of experimental results.

Based on the body of published literature, truss deflections may be less sensitive, and therefore easier to predict, than those of the member forces or moments. Given that the pinned and rigid methods model the two possible extremes of joint rotational stiffness, it can be assumed that the actual deformation of any joint will fall within the range provided by models of each idealization. Joint translational semi-rigidity, however, poses simplification challenges. Initial modelling completed in the present work aims to calibrate a truss model that is both sufficiently accurate and efficient to implement. The connectivity analogs tested in this thesis includes all linear analogs deemed suitable by past studies, with the exceptions explained below:

- The Truss Plate Institute of Canada (2014) specification for modeling trusses recommends making use of a fictitious rigid element at the heel joint of the truss. This method was not tested because it was deemed unnecessary; the resulting load effects would be sufficiently encompassed by the other cases that make use of a rigid heel joint.
- The truss analog used by Li et al. (1998) was also neglected because the assumption of bottom chord joint stiffness would not be appropriate beyond the truss validation step. This is because under wind uplift, the bottom chord of each truss is expected to go into compression, and so deformation at the joints would be limited by the contact between the joined members. It was deemed more appropriate to evaluate the semi-rigid case where all significant joint stiffness values are modeled, such as the semi-rigid case in Vatovec (1996).

1.4.2.2 Member Insertion Point

Commonly, truss members are modeled along the centroid of their cross-section, as shown in Figure 1-11 (a). This assumption was used and validated with deflection data in many past studies (Li, 1996; Pfretzschner, 2012; Jacklin, 2013), and is the method most often used in conventional design and analysis. The Chord Centerline (CL) analog, as it will be referred to herein, assumes that the MPC truss behaves as an ideal truss, with member actions acting through concentric points at each connection. In reality, eccentricity occurs at most MPC joints due to member geometry and joint cut tolerances. Previous standards have recommended accounting for these eccentricities by using analog lines along the bottom edges of chord members (Limkatanyoo, 2003), as shown in Figure 1-11 (b).

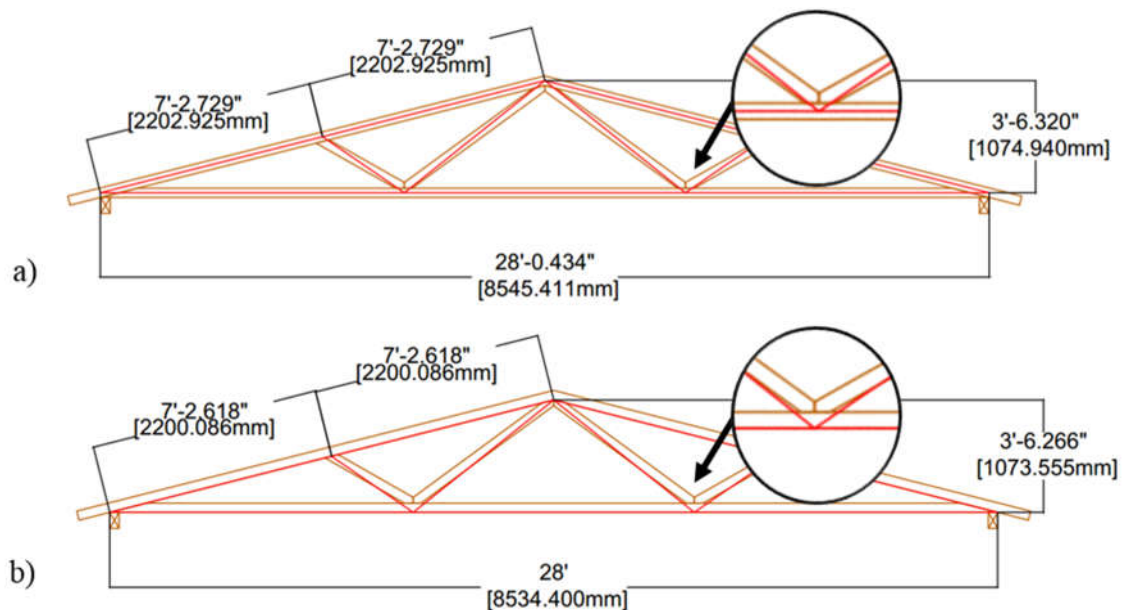


Figure 1-11: Geometric analogs applied to a 3:12 slope Fink truss, using different chord member insertion points: a) Chord Centerline, b) Chord Bottom-Line

Martin (2010) validated similar Fink trusses using the Chord Bottom-Line (BL) convention. In this analog, the top and bottom chords of the trusses are modelled along the center of the bottom face of the actual members. This results in an offset between the joint nodes and the neutral axes of the chord members equal to half of the height of a member.

The web members are modeled along their centerlines in both analogs, meeting the chord members at the appropriate horizontal dimensions.

1.4.2.3 Wood Material Properties

Because wood is a natural material subjected to many different, constantly changing conditions during formation, its properties vary considerably across species and the time and location of growth (Forest Products Laboratory, 1999). The mechanical properties of a single piece of sawn lumber are complex because they vary with time, temperature, moisture content, and direction and rate of loading (Mackerle, 2005). Wood is technically an anisotropic material because it has significantly different and independent mechanical properties in each of its three dimensions. However, it is commonly considered to be orthotropic in analysis and empirical ratios for relating the directional properties have been widely published (Forest Products Laboratory, 1999).

With respect to the growth rings of a tree, the principal axes of wood include the radial axis normal to the growth rings, the tangential axis, and the longitudinal axis parallel to the grains. These axes correspond to the z, y, and x-axes in a rectangular piece of sawn lumber, respectively, where the x-axis runs the length of the member and the y- and z-axes represent the cross-section. To represent the 3-dimensional elastic properties of wood in modeling, twelve different constants must be estimated; three moduli of elasticity (MOE), three moduli of rigidity (G), and six Poisson's ratios (μ). In SAP2000, orthotropic materials are defined by applying the relevant directional properties of wood in a table. Only three values of the Poisson's ratio are required by the software because the other three are dependent and can be calculated using the given MOE and μ values.

The handbook developed by the US Department of Agriculture (Forest Products Laboratory, 1999) provides experimental values for the required parameters as well as empirical factors, where possible, for relating longitudinal MOE values to the other directional mechanical properties. These factors, called elastic ratios, were obtained experimentally for many common species of wood and allow the anisotropy of wood to be idealized as orthotropic behaviour with dependent directional properties. The handbook reference provides these factors for many species of wood, which can then be applied to

specific batches of wood with known longitudinal stiffness. These ratios are used in the present study, along with strength and stiffness values published by (Canadian Wood Council/Canadian Standards Association, 2015) for the relevant species of wood. Table 1-2 shows the elastic ratios used in the present study, taken as the values for Longleaf Pine lumber, as this species provides average values among all Pine species. The subscripts T, L, and R refer to the tangential, longitudinal, and radial directions, respectively. These ratios are multiplied by E_L values obtained from member stiffness tests, or tabulated values for specified grades of lumber, to obtain the directional properties.

Table 1-2: Elastic Ratios for Longleaf Pine Lumber, Obtained from Chapter 4 of (Forest Products Laboratory, 1999)

Directionality of Ratio	Elastic Ratio
E_T/E_L	0.055
E_R/E_L	0.102
G_{LR}/E_L	0.071
G_{LT}/E_L	0.06
G_{RT}/E_L	0.012

1.4.3 Experimental Data for Truss Model Validation

In the published literature, experimental data for entire MPC trusses is scarce. The only studies which provide data for a large number of trusses were carried out as a series of experimental programs at the Forest Products Laboratory (FPL) in Madison, Wisconsin (Wolfe, et al., 1986; Wolfe & McCarthy, 1989; Wolfe & LaBissoniere, 1991; Wolfe, et al., 1996). Due to similar citations across all four studies, each one will be referred to herein by the abbreviation “FPL-” followed by the year of publication.

The FPL studies included tests performed on geometrically-similar trusses with slight differences in the truss design or test setup, depending on the scope of each study. In all reports, 28-foot-long, 3:12 slope and 6:12 slope Fink trusses were initially designed according to conventional design procedures. All trusses consisted of No. 2 Southern Pine sawn lumber with nominal cross-sectional dimensions of 38 by 89 mm (Standard 2x4 lumber). Figure 1-12 provides an illustration of the Fink trusses tested in the FPL studies.

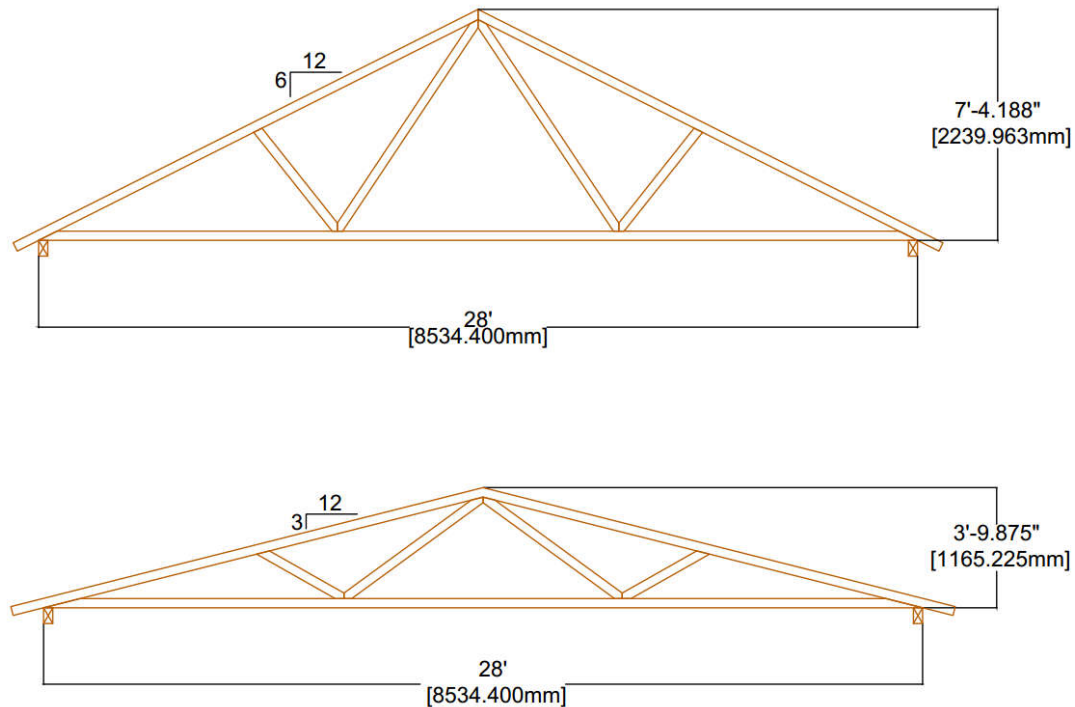


Figure 1-12: Illustration of Fink trusses used in 2-D model validation, based on the 6:12 slope and 3:12 slope truss configurations tested in FPL (1986, 1989, 1991, 1996)

In the FPL-1986 study (Wolfe, et al., 1986), 42 full-size trusses were tested; 24 to failure and the remaining 18 to 125% of the design load to determine stiffness characteristics. Half of the trusses tested were of each slope category. For the FPL-1986 study, the metal plate connections were intentionally oversized, using plates that were either thicker or larger in area, to force failure to occur in the wood truss members. In conventional design, the strength of the wood members is reduced for long-term loading, but the same load-duration factor is not applied to the design of the steel plates. For this reason, it was expected that a short-term test of conventional trusses would yield an unrepresentative proportion of connection failures. The “over-plated” trusses were designed to counteract the bias towards steel failure and provide data to assist in prediction in the probability of wood failure. The intact trusses and their stiffness results, were also used in a later study, FPL-1989, (Wolfe & McCarthy, 1989) to assess how relative truss stiffness affects load distribution within an entire roof system. The lumber used to fabricate these trusses were sorted by modulus of elasticity and used to build trusses of low, medium, and high stiffness.

In FPL-1991 (Wolfe & LaBissoniere, 1991), the authors tested Fink trusses of the same two slope categories and geometries as in the former study, but the plated connections were of conventional design. This provides the opportunity for direct comparison between conventional trusses and the previously “over-plated” design. In the present study, this contrast allows for assessment of the joint and geometric model analogs in comparison to two real joint stiffness cases. The conventional trusses tested in FPL-1991 are expected to behave similarly to the models with semi-rigid joints, while those tested in FPL-1986 should exhibit more rigid joint behaviour.

Finally, FPL-1996 (Wolfe, et al., 1996) presents the deflection and member force results from 6:12 slope Fink trusses. These truss specimens were tested under ramping loads to assess the effect of different web joint configurations. The study included three trusses of the conventional “fitted web” joint design, which was the same as the joints used in all previous FPL studies. Strain measurements taken during the FPL-1996 experiments were converted to stress values, which could then be used to estimate the axial forces and moments in the top chord and the compression web members during testing. The results of this study provide an important opportunity to extend the present model validation beyond the limits of past modeling studies, which validated the deflection results only. By comparing the member force results of the selected truss analog to experimental values, the analog behaviour could be better understood while refining the modeling method.

1.4.4 Finite Element Modeling of Stick-Frame Construction

As discussed in Section 1.3.2, Part 9 of the NBCC (2010) provides prescriptive design requirements for housing and small buildings. Section 9.23 covers wood-frame construction, including stick-frame roofs. The size and spacing of rafters, joists, and collar ties and the number and length of fasteners required are specified in the clauses and tables of this section, alleviating the need for analysis or design of residential structures that meet the conditions of Part 9. Due to these provisions, stick-frame structures are not analyzed in practice, and the literature indicates that stick-frame structures are not commonly considered in research either.

In the available literature, modeling of stick-frame roofs has not been specifically addressed; however, the behaviour of nailed connections in general has been described in several handbooks and explored in detail in the available literature. Other structural systems and building envelope components present in residential structures, such as wall and floor diaphragms and roof and wall cladding, make use of several configurations of nailed connections. Pan et al. (2014) reported that there are over 30 typical types of nailed connection employed in typical house construction. Several of these connections have been modeled in past studies.

Pan et al. (2014) developed a three-dimensional model of a gable roof wood-framed house to study the nailed connection-level behaviour under high wind loads. This study considered both the frame-to-frame connections and the sheathing-to-frame connections, however the frame-to-frame connections were limited to the wall diaphragm members because the roof of the model structure consisted of trusses. For all nailed connections, this study made use of the zero-mass nonlinear spring element in ANSYS. The load-displacement relationships of the connections were taken from previous test data. This study was able to accurately model some of the commonly observed failure modes following recent hurricanes; however, as previously mentioned, these failures may only be relevant to trussed, gable-roof structures.

Nonlinear spring elements are most commonly employed to represent the behaviour of a nail or a group of nails in a light-frame wood connection (Dao & van de Lindt, 2008; Kumar, et al., 2012). Much of the research using this method is concerned with the behaviour of sheathing fastener models rather than nailed connections between framing members. In a recent study, Weston and Zhang (2017) proposed a new method for modeling the behaviour of nailed connections in which spring elements are replaced by a single equivalent beam at each connection. This work found that the equivalent beam method reduces the number of spring elements required at each connection and is capable of including joint eccentricities, resulting in more conservative stress estimates in the nonlinear range of behaviour. The linear range of connection behaviour was accurately estimated by both connection models.

For the purposes of the present study, the published literature does not provide explicit guidance on modelling stick-frame roofs. However, observations of common practices were noted to guide modeling of the constituents of the stick-frame models. In most studies, framing and sheathing members were each modeled using similar elements across various software. In SAP2000, the framing members would be modeled using frame elements, and sheathing would use shell element; however, sheathing was not modelled in this thesis. Information is provided by the literature on modeling nailed sheathing connections, however these are not of primary concern in the present study. Other nailed connections are briefly addressed but no study to estimate failures, or member and joint forces, within the framing structure has been carried out.

Based on the available information on all types of nailed connection, nonlinear spring elements provide adequate estimates of the response of nailed connections. However, it is important to note that although substantial experimental load-displacement data is published for nailed connections, each set is specific to the tested combination of fastener and lumber properties. Changes to the type of wood, thickness of lumber, or type and length of nail will affect the displacement behaviour and strength. Care must be taken if the nonlinear response is to be modeled to ensure that appropriate model inputs are supplied. In the present research, trusses will be modelled considering linear behaviour, and the stick-frame analog will use a comparable level of model detail to provide similar analyses and interpretation of results.

1.5 Objectives

Based on the review of the available literature and damage survey observations presented above, it has become clear that modes of roof failure other than sheathing loss or RTWC failure are possible. This study aims to examine the conditions required for such failure modes to occur. The objective of this thesis is to define a method for assessing the wind-induced failure of the framing members in an entire hip roof, starting with the two-dimensional case of a single truss. Finite element modeling will be used in lieu of an experimental program so that multiple roof configurations, framing types, and individual trusses can be assessed in a time- and resource-efficient manner.

1.6 Research Approach

To prove the concept of partial failures within a hip roof frame, a numerical modeling method must be developed and validated to analyze the internal load effects and strength behaviour of the components of a wood-frame roof under wind uplift. Two-dimensional truss models are developed and validated to define the modeling method. Following model development to obtain member forces, the element capacities are calculated. This allows for performance, in terms of relative demand-to-capacity (D/C) ratios, of the structural components to be compared across a portion of a roof and the locations of vulnerability to be identified. In future work, similar three-dimensional analyses can be conducted and the locations of weak joints can also be compared to the distribution of uplift forces during extreme wind events.

Differences between roof construction methods, such as truss- and stick-framing, are assessed to determine the relative likelihood of framing failure in each type. The capacities of the roof framing elements are also compared to that of the roof-to-wall connections in order to provide a point of reference for relating the present results to commonly observed failure modes with well-established wind speeds. Assuming proper construction in the analyses allows for identification of gaps in current design, if failure is found to be likely. Otherwise, the findings will confirm improper construction.

2 Development and Validation of a Numerical Truss Model

To understand the possibility of member or connection failure in a hip roof frame, the load effects due to wind uplift on the framing elements must be determined and compared to the elements' capacities to resist those effects. Accurate analysis of wood structures must account for the anisotropic properties of wood, the complex behaviour of the connections, and numerous possible failure modes. The published literature provides detailed information on modeling nonlinear behaviour and establishing failure criteria for certain roof components, but there is very limited information available on other elements and stick-frame construction. To obtain comparable results and use consistent methods across different construction types, the analysis of all structures for the present proof-of-concept study is limited to the linear range of material behaviour. Elements likely to fail first are identified based on relative, linear demand-to-capacity ratios.

To observe the linear load effects on the members and connections of a roof system, internal forces are obtained through finite element modeling using SAP2000. Individual trusses and components of stick-frame roofs are modeled, and resulting axial forces and moments are used to assess the demand on each element. In the present work, the term “element” refers to both the lumber framing members and the connections between them. Both types of elements comprise links in the vertical load path and potential failures may originate in either one.

The present chapter discusses the development and validation of a suitable model analog for obtaining member and joint forces for a single MPC truss in SAP2000. The following chapter will then present the method for estimating the capacity of the truss components, then combine the demand and capacity analyses into a form for comparing the relative D/C ratios across the MPC truss. The locations that are likely to fail first when the truss is subjected to uniform uplift will be identified by this procedure. The analysis method is discussed in detail for a single truss that was tested as part of a hip roof in a previous study (Henderson, et al., 2013). Once the truss analysis method is established in Chapter 3 and the demand-to-capacity ratios are determined in Chapter 4, the analysis method can be extended for an entire trussed roof and adapted to model a geometrically-equivalent stick-

frame roof. Significant effort is put into developing the analysis method for the plane truss case to ensure its accuracy and efficiency prior to modeling the stick-frame case.

2.1 Development and Validation of Truss Model

To develop an accurate finite element model of any structural system, its components must be appropriately idealized using the model elements available in the selected software. This section presents the development and evaluation of several different two-dimensional truss models in SAP2000. These analogs make use of the Frame element in SAP2000. Frame member end releases and insertion point settings are altered to represent different connectivity and geometric analogs, respectively.

The ideal model analog is the most realistic representation of the actual truss behavior, which, in the present research, means the model that produces the most accurate member and joint forces. Given the complexity of the problem and number of trusses to be analyzed, computational efficiency is also to be considered. Detailed joint models are deemed unnecessary based on the literature. As discussed in the following sections, four simplified connectivity analogs are combined with two member geometry analogs, based on the information presented in Chapter 2, to find the most effective pairing. Considering the general scope of past research, a single truss analog could not be selected for the present analysis based solely on the findings of the literature review. For this reason, the validation process becomes more complex than in past roof modeling studies.

The model development and validation procedure is as follows:

- Information on common modeling methods for MPC trusses is gathered from the literature. This results in the identification of eight different sets of assumptions to be tested independently, as listed in Table 2-1. Details of the analog cases are provided in Section 2.1.1.

Table 2-1: List of model analog combinations and naming convention. Insertion point analogs are named as per SAP2000 Insertion Point naming convention

Connectivity Analog	Member Insertion Point	
	Centroid (CL)	Bottom-Centre Line (BL)
Pinned (P)	P-CL	P-BL
Rigid (R)	R-CL	R-BL
Semi-Rigid (S)	S-CL	S-BL
Combined (C)	C-CL	C-BL

- The experimental member property and deflection data from the FPL studies (Wolfe & LaBissoniere, 1991; Wolfe & McCarthy, 1989; Wolfe, et al., 1996; Wolfe, et al., 1986) are also gathered and sorted. The deflection data made available by these studies provides the opportunity for deflection validation and comparison of all eight model analogs.
- The 3:12 and 6:12 slope Fink trusses from the FPL studies are modeled; each tested truss is modeled eight times according to the analog cases shown in Table 2-1, and the deflection results of each truss model are compared to the test data to inspect the flexibility behaviour of each analog method and identify the most accurate model for deflection.
- The models previously developed for the deflection validation are then compared based on their joint and member force results. This comparison revealed that a clear majority of the maximum force and moment results across each truss are produced by two of the eight analog cases; the P-BL and R-BL analogs. The reasons for pursuing the maximum force results, rather than direct validation to simulate the test results, will be discussed in Section 2.1.3.
- Final validation of the selected analog cases is completed using the member force data from FPL-1996.

2.1.1 Truss Validation Models

The discussed analog assumptions are applied to the same experimental truss configurations and compared during the deflection validation phase. Based on the literature, connectivity and member geometry assumptions comprise the two important

analog decisions for MPC trusses. Four connectivity analogs and two insertion points are applied in all permutations to reveal the most accurate internal force modeling method. The truss members are modeled using SAP2000 frame elements, arranged according to the dimensions of the trusses tested in the FPL reports (Wolfe & LaBissoniere, 1991), as diagrammed in Figure 2-1 below. Details of the experimental programs are provided in Section 1.4.3.

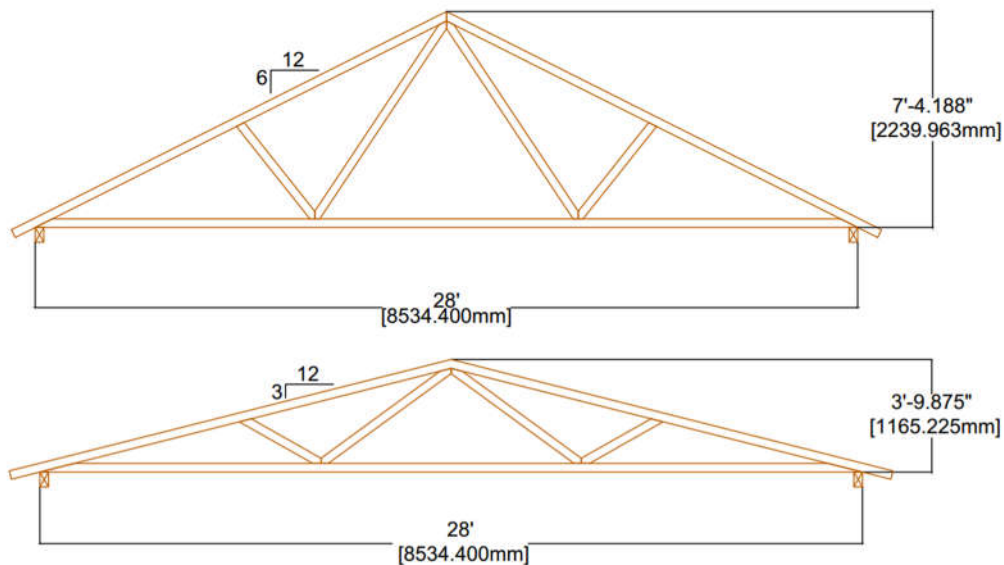


Figure 2-1: Overview of Fink Trusses used in 2-D Model Validation, based on the 6:12 (upper) and 3:12 (lower) Truss Configurations Tested in FPL-1986 and FPL-1991

The CL and BL analogs, introduced in Section 1.4.2.2, are modeled as follows. For the CL analog, the frame members are drawn with no insertion point specified, meaning that the default centroid point is used. In the BL analog, the insertion points for the sloped top chord members and the horizontal bottom chord members are set to the Bottom-Centre option. In both geometric analogs, the location of the web member connection along the top chord is assumed to be at the mid-span of the top chord, as this dimension is not provided in the referenced studies.

The validation models developed for this study make use of the connectivity assumptions from several past studies. A similar comparative study was completed as part of the Doctoral research of Vatovec (1996), including the semi-rigid case. Joint stiffness values

obtained from all available literature (Maraghechi & Itani, 1982; Vatovec, 1996; Liu, 2013) are used in the present study; however, the quantity of such data is limited. The four connectivity assumptions tested are as follows:

- Pinned (P): Rotational end releases are applied to all members. Continuous members are not released across joints.
- Rigid (R): No end releases are applied to any member
- Semi-Rigid (S): Available joint stiffness values are applied to the applicable members as partial axial and rotational end releases. An example showing the joint stiffness inputs for a single truss is shown in Appendix A.
- Combined (C): The web member ends and the top chord at the peak of the truss are assigned end moment releases (ie. pinned joints), the heel joints are modeled as rigid joints, and the top and bottom chords are assumed to be continuous.

SAP2000 contains many built-in material and section properties; however, wood is seldom included in any commercial design software. For this reason, the wood material properties must be defined manually as an orthotropic material. The FPL reports used for model validation provide the longitudinal MOE for every member of every tested truss in appendix tables. This data is included in the truss models, and the elastic ratios from FPL (1999) are used to calculate the other directional properties of the member materials. Incorporating the orthotropic behaviour of the truss members will not affect the results of the two-dimensional truss analysis in the validation phase. It is included here to prove the entire modeling method as best as possible and to avoid major methodology changes during the transition into three-dimensional models in subsequent work.

2.1.2 Truss Deflection Validation

The experimental data sets from FPL-1986 and FPL-1991 provide sufficient deflection data for validation. Each study tested twenty-four Fink trusses; twelve each of the 3:12 slope and 6:12 slope designs. The difference between the over-designed joints tested in FPL-1986 and the conventional design used in FPL-1991 provide the opportunity to compare the model results to an additional joint stiffness case and assess the sensitivity of truss deflection to the MPC joint properties. To streamline the validation phase, each group of twelve trusses is sorted and condensed into three groups according to their average top

chord deflection at the design load. The trusses with the lowest average deflection can be considered to have the highest stiffness. Accordingly, the groups are named based on their relative stiffness; “High”, “Medium”, and “Low”. The average, member-by-member MOE values are applied to the frame members in SAP2000, such that a single truss model can be assumed to represent the average behaviour of the relevant stiffness group.

The deflection results of the truss models developed using SAP2000 are compared to the average of the measurements taken from the four trusses tested in each group. In FPL-1986, vertical displacements were measured at each of the five chord joints and averaged, while FPL-1991 averaged the displacement of the three top chord joints. The model deflection results are taken according to the convention used in each FPL study. Table 2-2 and Table 2-3 provide an overview of the comparison between model and experimental deflection results for each study. The truss analogs are labelled according to the slope of the truss (“3” and “6”), followed by the stiffness category (“L”, “M”, and “H”), with an additional “BL” and “CL” suffix representing the models where the bottom-line and centerline member analogs are used, respectively. Table 2-2 and Table 2-3 show the deflection results of the models, compared to the experimental results of FPL-1986 and FPL-1991, respectively.

As can be seen in the tables, no analog consistently estimates the deflection results within $\pm 10\%$ of the experimental values. Discussion of the observed disparities for each analog case allows for comparison between the models; however, it must be clarified that it was not deemed necessary in this study to bound the deflection results within $\pm 10\%$ of the experimental data, as is commonly done in model validation studies. The range of stiffness and member eccentricity properties applied across all eight analogs is expected to lead to a wide range of truss deformation results. In terms of verifying the initial deflection models, the calculated error confirmed that all cases provided results within the correct order of magnitude. The Rigid and Semi-Rigid connectivity cases are representative of the actual truss behaviour where expected and as discussed below. Therefore, the range of deflection results presented herein can be concluded to be realistic, although not necessarily fully representative of the tested trusses. The percent error values are used to compare the behaviour of the analogs to one another.

Table 2-2: Deflection validation of trusses modelled according to experimental program in Wolfe et al. (1986) – results obtained from trusses which contained oversized plate connections

Wolfe 1986		Connection Analog	Rigid		Pinned		Semi-Rigid		Combined	
Truss	Experimental Δ [mm]	Member Analog	Δ_{FE} [mm]	% error	Δ_{FE} [mm]	% error	Δ_{FE} [mm]	% error	Δ_{FE} [mm]	% error
3H	6.78	CL	7.22	6	9.19	36	11.17	65	6.66	-2
		BL	7.30	8	10.38	53	11.50	70	8.05	19
3M	8.10	CL	9.05	12	11.47	42	12.99	60	8.39	4
		BL	9.16	13	13.04	61	13.38	65	10.41	28
3L	11.58	CL	12.92	12	15.60	35	16.85	46	11.96	3
		BL	13.07	13	18.08	56	12.39	7	14.36	24
6H	2.59	CL	2.15	-17	4.44	71	3.48	34	3.32	28
		BL	2.26	-13	5.01	93	3.68	42	3.31	28
6M	3.15	CL	2.68	-15	5.69	81	3.99	27	4.02	28
		BL	2.83	-10	6.60	109	4.25	35	4.05	29
6L	4.72	CL	3.94	-17	8.01	69	5.25	11	6.13	30
		BL	4.15	-12	8.94	89	5.58	18	6.06	28
Average Error		CL	-3		56		40		15	
		BL	0		77		39		26	
Absolute Average Error		CL	13		56		40		16	
		BL	11		77		39		26	

Table 2-3: Deflection validation of trusses modelled according to experimental program in Wolfe and LaBissoniere (1991) – results obtained from trusses of conventional design

Wolfe 1991		Connection Analog	Rigid		Pinned		Semi-Rigid		Combined	
Truss	Experimental Δ [mm]	Member Analog	Δ_{FE} [mm]	% error	Δ_{FE} [mm]	% error	Δ_{FE} [mm]	% error	Δ_{FE} [mm]	% error
3H	12.32	CL	8.83	-28	10.78	-12	13.59	10	9.85	-20
		BL	9.02	-27	12.04	-2	13.38	9	8.69	-29
3M	13.90	CL	9.71	-30	11.92	-14	14.47	4	10.85	-22
		BL	8.62	-38	12.54	-10	13.73	-1	9.05	-35
3L	15.73	CL	10.72	-32	13.09	-17	15.46	-2	11.96	-24
		BL	11.18	-29	16.26	3	16.37	4	11.74	-25
6H	4.80	CL	3.08	-36	6.16	28	4.74	-1	4.75	-1
		BL	3.59	-30	7.95	55	5.40	5	4.81	0
6M	5.13	CL	3.29	-45	6.30	23	4.94	-18	5.01	-2
		BL	3.66	-24	8.11	69	5.47	14	4.91	-4
6L	6.00	CL	3.40	-43	6.82	14	5.05	-16	5.26	-12
		BL	3.54	-41	7.84	31	5.34	-11	4.75	-21
Average Error		CL	-36		4		-4		-14	
		BL	-31		24		3		-19	
Absolute Average Error		CL	36		18		8		14	
		BL	31		28		7		19	

The effect of the insertion point analog on the deflection results must be discussed, in addition to that of the connectivity assumptions. Upon inspection, neither of the member offset cases result in consistently higher or lower displacement values. However, a few relationships can be discussed based on the nature of each model. Most notably, as surmised in the previous section, the bottom chord analog results in imposed eccentricity and increased joint deformation. In rigid joints, this eccentricity simply leads to higher internal moments taken by the joints. In models containing pinned joints along the chord members, these additional moments either exaggerate or counteract the rotation at the joints due to loading. This effect is verified upon inspection of the results. In all Pinned trusses, the bottom-line models calculated higher deflection values than did the centerline models. The effects of this behavior on the force results will be discussed in Section 2.1.3.

Another possible source of error in models using the bottom-line analog is the slight alteration to the overall truss dimensions, as well as changes in the slopes of the web members due to vertical shifts in the joint locations. This effect is not of concern to the analyses in this study because beyond the initial validation structure, the geometry of all studied roof frames is approximate, based on common roof design practice. There is no exact geometry to replicate, therefore, geometrical assumptions of small consequence will have no effect on the conceptual findings. This effect is mentioned here to provide commentary on the overall method validation.

A final point of discussion is that of the relative stiffness of each joint analog, as well as their relative accuracy in modeling the behavior of the over-plated and conventional trusses. The results also show that the Rigid and Combined connectivity cases estimate lower deflections than the Pinned and Semi-Rigid cases. As expected, the rigid joint analog shows the best agreement in estimating the deflection of the trusses tested in FPL-1986. This is the case because the over-plating of the tested truss connections forced failure, and most of the deformation, to occur in the wood members. The connections are constructed to behave rigidly. Furthermore, the results of FPL-1991 are most closely validated by the Semi-Rigid case. This is expected because the translational and rotational stiffness applied to the model joints most closely simulates the actual behaviour of a conventionally

designed truss. It is interesting to note that applying translational stiffness, even using inexact values, results in the closest validation of numerical results to the experimental data out of all of the analog combinations. The other connectivity analogs only adjust the rotational joint behaviour, and the translational properties remain rigid. This observation supports the need for a larger published database of experimental joint behaviour to improve modeling and design software for MPC trusses across industry.

In general, the Rigid joint models provide the lowest deflection estimates, followed by the Combined, then the Semi-Rigid and Pinned joint analogs. The Combined model has the second highest proportion of rigid joints so this is another expected result. On the other hand, the relative stiffness of the Semi-Rigid and Pinned models cannot be assumed upon inspection prior to analysis. The deformation behaviour of the Semi-Rigid models can be altered significantly by adjusting the assigned joint stiffness values. Following confirmation of the modeling method and analog stiffness behaviour through deflection comparison, the analog cases are also compared in terms of the axial force and moment estimates they produce. The sensitivity of the joint and member force results to the connectivity and insertion point assumptions will be discussed in the following section, and a method for modeling the truss member forces for the present research is proposed.

2.1.3 Force Envelope Validation

The deflection validation of the FPL-1986 and FPL-1991 truss models in Section 2.1.2 allowed for refinement of the modeling method to an acceptable order of accuracy, and provided an initial indication of the behavioral differences between the member and connection analogs tested. In this section, the model assumptions are further examined to determine the most efficient and accurate method for assessing the element-level demand through modeling. The truss models themselves provide joint and member force data for comparison across the analog cases, and the FPL-1996 study provides some data for experimental validation.

The relevant force results from FPL-1996 are limited to three tested trusses, and provide force and moment readings for only two members per truss. Due to the data limitations, the most suitable analog for assessing both joint and member forces cannot be identified

through direct validation. Several force readings per truss element would be required to accomplish direct validation, and accurate joint stiffness data would need to be applied due to the sensitivity of member moments to these parameters. As noted in the literature review, Li (1996) encountered similar limitations while attempting to validate their truss moment results.

It was deemed practically impossible to identify a single analog, out of the eight tested, that would provide the most accurate results for all elements of a truss, especially if all load effects within a roof's load path are to be considered. Instead, the strategy is adjusted to assess whether more than one model analog can be used in combination to obtain the maximum possible load effects on every element. This envelope approach is considered appropriate for the present proof-of-concept because by comparing the capacity of every element to its worst possible scenario of loading, all vulnerable elements can still be identified. Another benefit of using the maximum forces is that it may reveal critical conditions that are possible but may not have been considered previously.

To determine which analog produces the force and moment envelope for each element, the joint force results are extracted from every truss model used in the deflection validation and compared across the connectivity and geometric analogs. Table 2-4, Table 2-5, and Table 2-6 on the following pages are used to explain the force envelope analysis. The data in these tables show the values and logical checks used to compare all eight analog cases for a single truss. The trusses assessed in Table 2-4 and Table 2-5 were chosen arbitrarily, out of the twelve models from the deflection validation, as an example of the comparison of the connectivity cases. Table 2-6 then shows the insertion point comparison for the truss from Table 2-4. As mentioned, all twelve trusses are each modeled eight times; once under each analog combination. The present force envelope analysis is done on all twelve sets of data. Discussion of the general results and observations from all truss models, including mention of observed outliers, are provided later in this section.

The data in Table 2-4 show the joint forces and moments for the Truss 3H from FPL-1991, and Figure 2-2 shows the naming convention used to designate the chord members and joints in this truss. The joints are designated using a "joint-member" naming convention;

the joint label is shown, followed by the joined member, separated by a hyphen. The axial force, acting on the joint along the length of the specified member, is taken as the resultant of the horizontal and vertical components of the local joint forces, labelled F1 and F3 respectively. Note that the splice joint in the bottom chord, labelled “SJ”, is not considered in this modeling. It is modelled as a rigid joint and its force results are neglected because under uplift, the joined members in the bottom chord would go into compression and this connection would not be subjected to significant demand due to compressive contact between the members.

The results from all four connectivity analogs are shown in blocks across Table 2-4, with the maximum values for each joint shown on the right side. The governing analog; that is, the connectivity analog producing the maximum axial force and moment values is also shown. Conditional formatting is applied to the maximum axial force and moment values to provide visualization of the governing connectivity analogs. As can be seen in Table 2-4, the Rigid and Pinned joint analogs govern in all joints for both moment and axial forces. Connectivity assumptions other than the Rigid and Pinned cases govern in few joints throughout the models. In cases where the Semi-Rigid or Combined analogs are found to govern, such as in Joints CJ-W and W-BC in Table 2-5, the difference between the governing analog and the other cases is marginal.

From the connectivity comparisons, it is shown that the axial force results are not sensitive to changes in joint stiffness. When the blocks of maximum force results from the CL and BL insertion points are then compared for each truss in the following step, it can be concluded that the axial force results are not sensitive to vertical member offsets or joint stiffness. As shown in Table 2-6, the percent differences between the maximum axial forces from the two analogs is consistently less than 1%. The joint moments are somewhat sensitive, however, with the BL analog consistently providing the maximum moments for all joints other than a few select web member joints. Certain web members consistently produce lower end moments in the BL analog than in the CL analog. It is not apparent which analog estimates the behaviour of the web joints more accurately, however these members are not expected to be critical. The interior web members which show this discrepancy are found to go into compression when the truss is subjected to uplift, and the

moments in these members' joints are still an order of magnitude lower than those present in the chord member joints. The discrepancy is accepted for these reasons.

An important consequence of the BL insertion point is that the member force results and joint force results no longer act through the same nodes at the joints. The member forces returned by the SAP2000 model always reflect the actions about the neutral axis of the member, while the joint forces are resolved about the insertion points of the joined members. This means that in the BL analog, the joint moments include an additional force due to the eccentricity between the axial force at the end of the chord members and the location of the joint. In the BL analog, this eccentricity is equal to half of the height of the chord member. It may appear as though this results in exaggerated moment estimated from the BL analog, however in reality no MPC joint is perfectly concentric. Taking these member eccentricities into account in this fashion is justified for the present study because it provides an appropriately conservative result compared to the idealized, CL analog.

The observed relationships between the connection analogs and insertion points, and their resulting effects on the modeled forces and moments, could be discussed in greater depth and may be of interest for further study. For the purposes of the present work, the appropriate force modeling method was determined to a sufficient degree of certainty so further refinement is not attempted. By a clear majority, it is concluded that the Pinned and Rigid joint analogs should be used with the BL insertion point to yield the extreme possible joint force results.

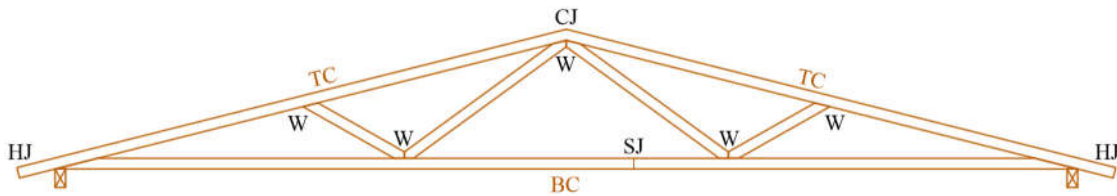


Figure 2-2: Truss 3H joint and member naming convention

Table 2-4: Comparison of connectivity analogs, based on joint force estimates, from the CL insertion point models of Truss 3H from FPL-1991

Joint	CL Analog - Truss 3H (FPL-1991)																			
	Rigid				Pinned				Semi-Rigid				Combined				Maximum			
	F1 [N]	F3 [N]	Moment [N-mm]	Axial Force [N]	F1 [N]	F3 [N]	Moment [N-mm]	Axial Force [N]	F1 [N]	F3 [N]	Moment [N-mm]	Axial Force [N]	F1 [N]	F3 [N]	Moment [N-mm]	Axial Force [N]	Moment [N-mm]	Governing Analog	Axial Force [N]	Governing Analog
CJ-TC	-12675	-1925	385081	12821	-12596	-1918	0	12742	-12668	-1923	342148	12813	-12424	-1915	0	12570	385081	Rigid	12821	Rigid
CJ-TC	12677	-1925	-391000	12822	12597	-1918	0	12742	12670	-1924	-342148	12815	12404	-1910	0	12551	391000	Rigid	12822	Rigid
CJ-W	2402	1924	-46995	3078	2395	1918	0	3069	2401	1923	0	3076	2398	1920	0	3072	46995	Rigid	3078	Rigid
CJ-W	-2404	1926	52913	3080	-2396	1918	0	3069	-2403	1924	0	3079	-2379	1905	0	3047	52913	Rigid	3080	Rigid
HJ-BC	15381	16	-89952	15381	15326	39	255129	15327	15377	17	-78023	15377	15128	43	73819	15128	255129	Pinned	15381	Rigid
HJ-BC	-15379	17	76886	15379	-15325	39	-255127	15326	-15374	18	75490	15374	-15147	38	-71888	15147	255127	Pinned	15379	Rigid
HJ-TC	15379	5128	-333090	16212	15325	5107	0	16154	15374	5127	-331642	16206	15147	5107	-183272	15985	333090	Rigid	16212	Rigid
HJ-TC	-15381	5129	346187	16213	-15326	5107	0	16155	-15377	5128	334225	16209	-15128	5102	181067	15965	346187	Rigid	16213	Rigid
SJ-BC	10273	9	-68553	10273	10201	8	191407	10201	10267	9	-80104	10267	10026	3	0	10026	191407	Pinned	10273	Rigid
SJ-BC	-10273	-9	68553	10273	-10201	-8	-191407	10201	-10267	-9	80104	10267	-10026	-3	0	10026	191407	Pinned	10273	Rigid
W-BC	-2704	1860	-39428	3281	-2729	1874	0	3311	-2706	1858	0	3283	-2723	1870	0	3304	39428	Rigid	3311	Pinned
W-BC	-2402	-1901	48694	3063	-2395	-1894	0	3054	-2401	-1899	0	3061	-2398	-1896	0	3057	48694	Rigid	3063	Rigid
W-BC	2404	-1902	-54917	3065	2396	-1895	0	3054	2403	-1900	0	3064	2379	-1881	0	3032	54917	Rigid	3065	Rigid
W-BC	2704	1859	33056	3281	2729	1874	0	3311	2707	1859	0	3283	2724	1871	0	3304	33056	Rigid	3311	Pinned
W-TC	2704	-1846	41563	3274	2729	-1861	0	3303	2706	-1845	0	3275	2723	-1857	0	3296	41563	Rigid	3303	Pinned
W-TC	-2704	-1846	-35097	3274	-2729	-1861	0	3304	-2707	-1846	0	3276	-2724	-1857	0	3297	35097	Rigid	3304	Pinned

Table 2-5: Comparison of connectivity analogs, based on joint force estimates, from the BL insertion point models for Truss 6H from FPL-1991

Joint	BL Analog - Truss 6H (FPL-1991)																			
	Rigid				Pinned				Semi-Rigid				Combined				Maximum			
	F1 [N]	F3 [N]	Moment [N-mm]	Axial Force [N]	F1 [N]	F3 [N]	Moment [N-mm]	Axial Force [N]	F1 [N]	F3 [N]	Moment [N-mm]	Axial Force [N]	F1 [N]	F3 [N]	Moment [N-mm]	Axial Force [N]	Moment [N-mm]	Governing Analog	Axial Force [N]	Governing Analog
CJ-TC	-7956	-2414	155663	8314	-7910	-2406	-362614	8267	-7953	-2412	106546	8311	-7830	-2415	-359646	8194	362614	Pinned	8314	Rigid
CJ-TC	7956	-2414	-155663	8314	7910	-2406	362614	8267	7953	-2412	-106546	8311	7830	-2415	359646	8194	362614	Pinned	8314	Rigid
CJ-W	1530	2414	-2580	2858	1525	2406	0	2848	1529	2413	0	2856	1531	2415	0	2859	2580	Rigid	2859	Combined
CJ-W	-1530	2414	2580	2858	-1525	2406	0	2848	-1529	2412	0	2856	-1531	2415	0	2859	2580	Rigid	2859	Combined
HJ-BC	9622	16	329166	9622	9594	49	791552	9594	9621	18	318816	9621	9511	34	563940	9511	791552	Pinned	9622	Rigid
HJ-BC	-9622	16	-329166	9622	-9594	49	-791552	9594	-9621	18	-318858	9621	-9511	34	-563940	9511	791552	Pinned	9622	Rigid
HJ-TC	9622	6397	44802	11555	9594	6365	508623	11514	9621	6396	34563	11553	9511	6380	280357	11453	508623	Pinned	11555	Rigid
HJ-TC	-9622	6397	-44802	11555	-9594	6365	-508623	11514	-9621	6396	-34522	11553	-9511	6380	-280357	11453	508623	Pinned	11555	Rigid
SJ-BC	6426	8	271547	6426	6385	8	698796	6385	6424	8	313746	6424	6299	8	513172	6299	698796	Pinned	6426	Rigid
SJ-BC	-6426	-8	-271547	6426	-6385	-8	-698796	6385	-6424	-8	-313746	6424	-6299	-8	-513172	6299	698796	Pinned	6426	Rigid
W-BC	-1666	2337	-60063	2870	-1685	2361	0	2900	-1668	2337	0	2871	-1681	2355	0	2893	60063	Rigid	2900	Pinned
W-BC	-1530	-2379	3037	2828	-1525	-2370	0	2819	-1529	-2377	0	2827	-1531	-2380	0	2830	3037	Rigid	2830	Combined
W-BC	1530	-2379	-3037	2828	1525	-2370	0	2819	1529	-2377	0	2827	1531	-2380	0	2830	3037	Rigid	2830	Combined
W-BC	1666	2337	60063	2870	1685	2361	0	2900	1668	2337	0	2871	1681	2355	0	2893	60063	Rigid	2900	Pinned
W-TC	1666	-2318	61686	2855	1685	-2342	0	2885	1668	-2318	0	2856	1681	-2337	0	2879	61686	Rigid	2885	Pinned
W-TC	-1666	-2318	-61686	2855	-1685	-2342	0	2885	-1668	-2318	0	2856	-1681	-2337	0	2879	61686	Rigid	2885	Pinned

Table 2-6: Comparison of insertion point joint force envelopes for the 3H truss from FPL-1991

Joint	Truss 3H (FPL-1991)					
	CL Analog		BL Analog		Moment % Difference (BL - CL)	Axial Force % Difference (BL - CL)
	Max. Moment [N-mm]	Max. Axial Force [N]	Max. Moment [N-mm]	Max. Axial Force [N]		
CJ-TC	385081	12821	566887	12809	32	-0.09
CJ-TC	391000	12822	566887	12809	31	-0.11
CJ-W	46995	3078	1785	3083	-2532	0.18
CJ-W	52913	3080	1785	3083	-2864	0.11
HJ-BC	255129	15381	945823	15382	73	0.01
HJ-BC	255127	15379	945822	15382	73	0.02
HJ-TC	333090	16212	719176	16205	54	-0.04
HJ-TC	346187	16213	719177	16205	52	-0.05
SJ-BC	191407	10273	860233	10264	78	-0.09
SJ-BC	191407	10273	860233	10264	78	-0.09
W-BC	39428	3311	123055	3311	68	0.00
W-BC	48694	3063	2031	3068	-2297	0.18
W-BC	54917	3065	2031	3068	-2604	0.11
W-BC	33056	3311	123055	3311	73	-0.02
W-TC	41563	3303	123884	3303	66	0.00
W-TC	35097	3304	123885	3303	72	-0.02

Table 2-7: Validation of force envelope method by comparing the envelope models against FPL-1996 data. Note that Truss L3 includes inaccurate readings

Experimental Readings	Deflection	Axial Force (N)				Member Moment (N-mm)				
Truss	(mm)	NC	SC	NW	SW	NC	SC	NW	SW	
L1	3.71	9475	10364	2491	3603	180776	203373	7909	38415	
L2	4.88	13167	8407	5783	3692	248566	248566	18078	15818	
L3	5.38	7695	14635	1868	8585	6779	6779	0	7909	
BL Insertion Point Analog										
Pinned Joints	Deflection	Axial Force (N)				Member Moment (N-mm)				
Truss	(mm)	NC	SC	NW	SW	NC	SC	NW	SW	
L1	4.36	7899	7899	2561	2561	710394	708379	1750	1750	
	<i>% error</i>	<i>17.6</i>	<i>-16.6</i>	<i>-23.8</i>	<i>2.8</i>	<i>-28.9</i>	<i>293.0</i>	<i>248.3</i>	<i>-77.9</i>	<i>-95.4</i>
L2	5.50	7899	7899	2561	2561	709398	708918	1750	1750	
	<i>% error</i>	<i>12.6</i>	<i>-40.0</i>	<i>-6.0</i>	<i>-55.7</i>	<i>-30.6</i>	<i>185.4</i>	<i>185.2</i>	<i>-90.3</i>	<i>-88.9</i>
L3	8.11	7970	7970	2566	2566	750940	750835	1750	1750	
	<i>% error</i>	<i>50.8</i>	<i>3.6</i>	<i>-45.5</i>	<i>37.3</i>	<i>-70.1</i>	<i>NA</i>	<i>NA</i>	<i>NA</i>	<i>-77.9</i>
Rigid Joints	Deflection	Axial Force (N)				Member Moment (N-mm)				
Truss	(mm)	NC	SC	NW	SW	NC	SC	NW	SW	
L1	3.27	7957	7956	2536	2536	250694	248577	43231	41315	
	<i>% error</i>	<i>-11.8</i>	<i>-16.0</i>	<i>-23.2</i>	<i>1.8</i>	<i>-29.6</i>	<i>38.7</i>	<i>22.2</i>	<i>446.6</i>	<i>7.6</i>
L2	4.09	7957	7957	2536	2536	249494	249026	42536	42034	
	<i>% error</i>	<i>-16.3</i>	<i>-39.6</i>	<i>-5.4</i>	<i>-56.2</i>	<i>-31.3</i>	<i>0.4</i>	<i>0.2</i>	<i>135.3</i>	<i>165.7</i>
L3	3.77	7956	7956	2535	2535	243917	245104	40951	42113	
	<i>% error</i>	<i>-29.9</i>	<i>3.4</i>	<i>-45.6</i>	<i>35.7</i>	<i>-70.5</i>	<i>NA</i>	<i>NA</i>	<i>NA</i>	<i>432.5</i>

Following the decision to focus on the extreme joint and member forces, the two selected analog cases are validated once more against the deflection and force data provided by FPL-1996. The modelling process is additionally refined through these steps. Deflection validation is obtained without issue, and the axial force results are also found to compare within an acceptable range. As expected, the member moment results are generally exaggerated by the Pinned and Rigid, BL insertion point models. Table 2-7 shows these results. As mentioned in Section 1.4.3, the experiments in FPL-1996 took member strain readings on the top chord members and two web members. Member stress and moment data were calculated from surface strain readings. Figure 2-3 shows a diagram of the naming convention for the truss members, with the location of the member labels approximately aligned with the positions of the strain gauges that were applied to the members. Three trusses from FPL-1996; L1, L2, and L3, were deemed comparable to the conventional truss design which the present models attempt to represent. It is important to note that the data for Truss L3 contains apparent inaccuracies as shown by the zero-moment reading on member NW. Excessively large discrepancies in this truss are not considered in this work and are marked “NA” in Table 2-7.

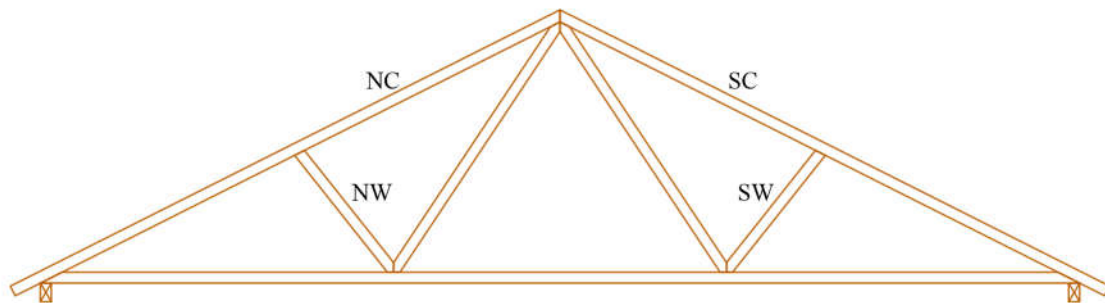


Figure 2-3: 6:12 slope trusses tested in FPL-1996, with members labeled and approximate locations of force data readings shown by location of member labels

The deflection results shown in Table 2-7 are used to further refine the modeling method. Larger sets of data, including joint force readings, would be required for thorough validation, however these data provide the opportunity for refinement of the deflection results and brief discussion of the force estimates. The Rigid and Pinned models behave in the expected way with regards to truss deflection behavior; the Pinned model overestimates

the truss deflection behaviour, while the Rigid model underestimates it. The force results do not provide such clear conclusions due to uncertainties in the force readings, and the focus on member forces rather than joint forces, which were the focus of the previous step. The symmetry of the trusses should also lead to similar force results across the mirrored chord and web members. The differences between the readings taken within each truss raises additional questions regarding the quality of the data.

As previously suggested by the closeness of axial force results in the comparison of all analog cases, the axial force results in Table 2-7 are not sensitive to the joint stiffness. The model axial force results are relatively close to the experimental results. The moment results do not compare closely; however, this is expected based on the comments from Li's (1996) work and the selection of the connectivity analogs to provide extreme - but possible - force results. The web members, and their connections, are expected to be less critical than those of the top and bottom chords and so the discrepancies in these values are not of present concern. Concluding the model development method, the BL insertion point, in combination with the maximum results from the Pinned and Rigid connectivity analogs, are deemed suitable to provide demand values for comparison with the member and joint capacity estimates. Overall, this method facilitates identification of potentially vulnerable elements, and also eliminates members with extremely low D/C ratios that can be considered sufficiently resistant to uplift.

2.2 Model of Truss Under Uplift

Following selection of the appropriate model analogs for a single truss, the first D/C analysis is performed for a realistic hip roof truss under uplift. The present section will use the selected analogs to estimate truss member and joint demand under uniform uplift. In part, this work facilitates development and further refinement of the method for subsequent trusses, now focusing on uplift rather than the gravity loads used in the validation work. The procedures for capacity estimation are then discussed in Section 3.1, to demonstrate the complete D/C analysis method. The results of the same procedure, applied to a comparable section of a stick-frame roof, will be discussed in subsequent chapters.

One of the truss configurations constructed as part of the hip roof tested in Henderson et al. (2013) is selected from the truss drawing package and is used for the first D/C analysis. The envelope modeling method and force results for the selected truss are summarized using the figures in the present section. The second full-length truss in the roof is used for the present modeling. Figure 2-4 shows the configuration of the roof tested in Henderson et al. (2013), and the location of the selected truss, labeled “A2”. This truss is selected for the present analysis because it is the first full-length truss from the outer edge of the roof, aside from the two-ply “A1” truss, and its symmetry simplifies the determination of joint capacities.

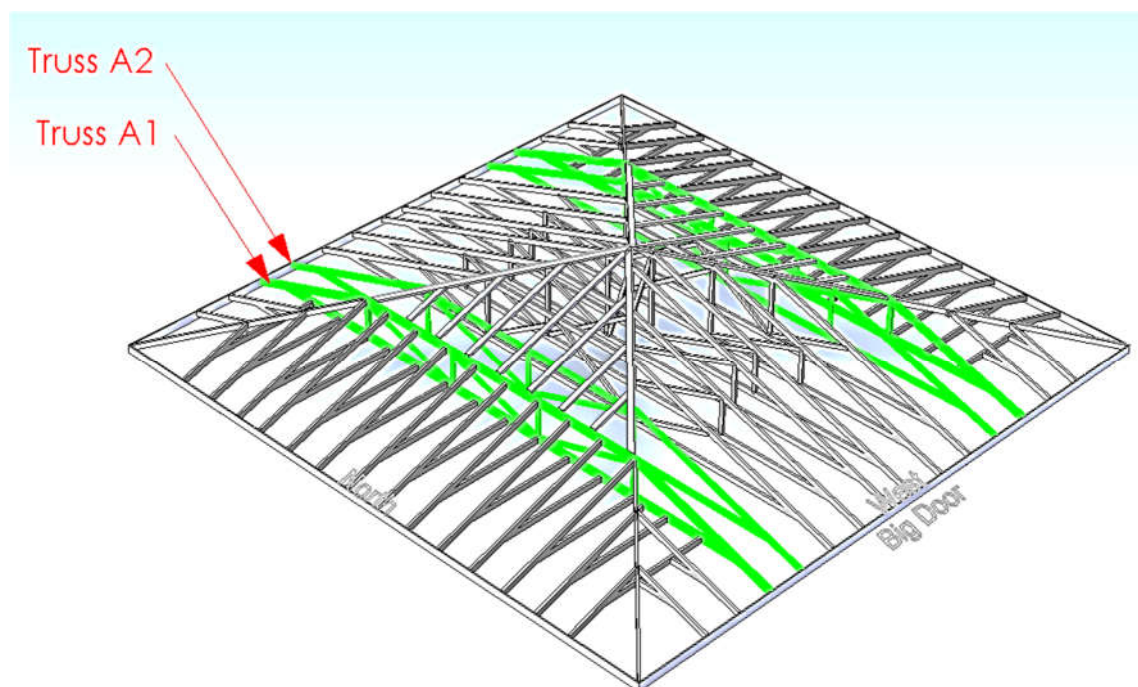


Figure 2-4: Model rendering of full-scale hip roof tested by Henderson et al. (2013)

Figure 2-5 shows a dimensioned drawing of the truss, which is modelled using SAP2000, as shown in Figure 2-6. The metal plate sizes are taken from the drawings prepared by the truss fabricator, but their locations must be estimated by visual inspection. The truss loading is taken as a uniformly distributed load. The uplift force is calculated based on the tributary area loading prescribed by the ASCE 7-10 (2010) Directional Procedure for wind loads on the main wind force resisting system (MWFRS) of a building. The wind speed is

taken initially as 170 km/h (105 mph). This value is the 10 meter, 3-second gust speed specified for design of Occupancy Category 1 buildings in the mainland region of the United States. This design speed corresponds to the peak wind speed, measured at a height of 10 m from the ground. The peak value is taken from an hour of wind speed data, averaged over three-second periods, measured during an event that corresponds to a 15% probability of exceedance in 50 years.

The calculations and selected parameters for determining the roof uplift from this wind speed are shown in Appendix B. The resulting pressure is applied as a uniformly distributed load of 1.22 N/mm acting outwards and normal to the top chord members of the truss. The self-weight of the truss is also included using the mass of SPF No. 2 lumber (Canadian Wood Council/Canadian Standards Association, 2015). For the present modeling, uniform uplift is deemed suitable for identifying the relative weaknesses in the truss; however, it must be noted that this represents a simplified case. Beyond the proof-of-concept stage, other distributions which include higher uplift pressures at the leading edge of the roof should also be studied.

The orthotropic material properties for the truss members are estimated using the tabulated MOE values for SPF 2100F_b-1.8E lumber from the Canadian Wood Design Handbook (2015) and the elastic ratios from Forest Products Laboratory (1999), as shown in Appendix C. Note that this step switches from using the experimental member stiffness data to using average values for the specified species of wood. This results in a perfectly symmetric truss model. The truss is modelled twice; once using the fully rigid connection analog, and once for the pinned case with moment releases at all member ends. The bottom-center insertion point is used for the top and bottom chord members in both models.

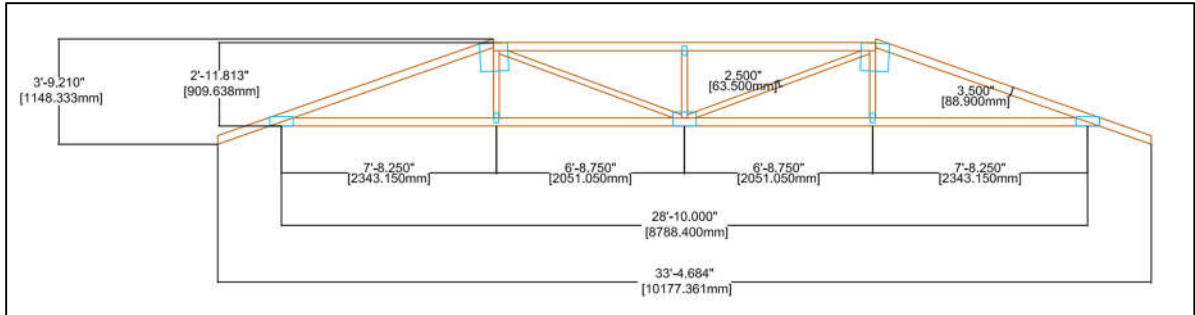


Figure 2-5: Dimensioned drawing of hip roof Truss A2 from the full-scale house tested at the Insurance Research Lab for Better Homes

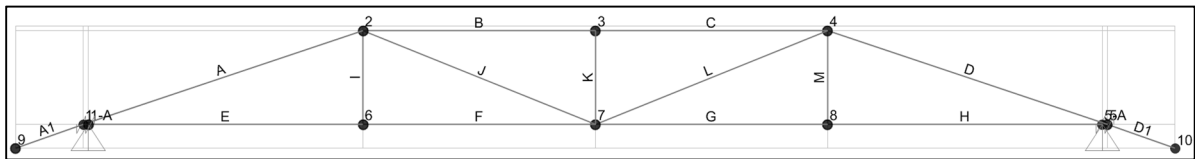


Figure 2-6: SAP2000 model of Truss A2, with numbered joint labels and lettered member labels

Following analysis of each model under the described loads, two tables of results are extracted from each model. The member forces table is used to find the maximum axial force and moments experienced by any chord member and any web member. The locations of the maximum values are also noted to pinpoint regions of vulnerability within the members themselves. Since the chord members and web members each consist of the same types of lumber throughout, only one maximum demand value is required for each to assess whether member failure is likely. Figure 2-7 and Figure 2-8 show the relative axial force and moment distributions, respectively, throughout the truss with the rigid joint assumption. The simulation is also conducted using the Pinned model and results are compared to the Rigid model counterpart. It is important to note that the Pinned analog model maintains joint rigidity in locations where the member is continuous across the joint. For example, the overhanging member at the heel joint is modeled with a rigid connection to prevent instability. The final member and joint demand values are taken as the envelope of maximum forces and moments from the two cases.

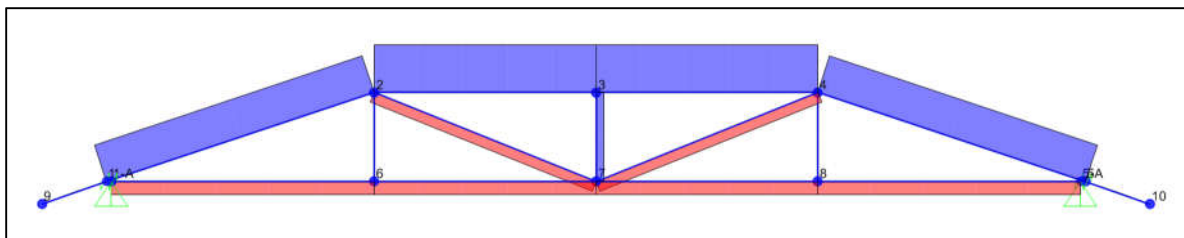


Figure 2-7: Sample of relative axial force results from the rigid SAP2000 model of Truss A2, under 1.22 N/mm uniform uplift. The blue positive results indicate tension and the red results indicate compression

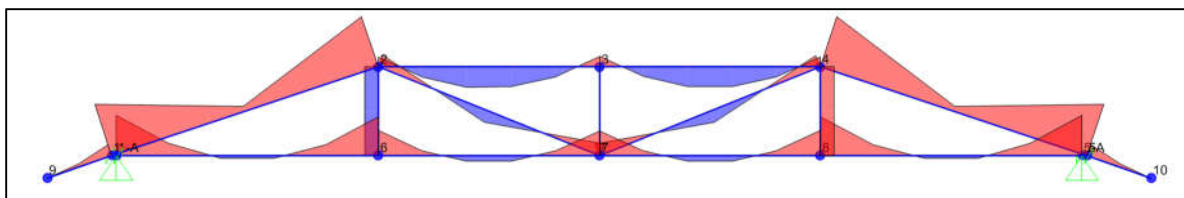


Figure 2-8: Sample of relative member moments from the rigid SAP2000 model of Truss A2, under 1.22 N/mm uniform uplift

The table of joint forces is used to assess each individual joint, considering the effects and orientations of each joined member. The joint forces tables extracted from SAP2000 provide horizontal and vertical forces, as well as the in-plane moments on the joint, due to the actions at the end of each member. As predicted in Section 2.1.3, the joint moments obtained from the model are exaggerated or reduced, when compared to the member end moments. This is due to the aforementioned eccentricity of the axial forces acting through the centroid of the chord members, which are offset from the joint locations due to the BL insertion point. In Figure 2-8, this effect appears to result in an imbalance of the member end moments. In the tensile top chord members, this eccentricity results in larger joint moments, while the compressive axial forces in the bottom chord members reduces the moment in the heel joint and the mid-span joint. These are both acceptable effects. The top chord members are expected to be most vulnerable to uplift failures due to their closeness to the surface of the roof. By using possibly exaggerated moment demand values, the most extreme possible load path scenario can be considered. Alternatively, the bottom chord members are expected to be less vulnerable to moment failures because the contact between members under compression significantly enhances the resistance of the joint.

The axial joint forces are combined and translated into equivalent forces running parallel and perpendicular to the length of the joined member. As applicable, the joint demand values are compared to either the shear or tensile capacity of the joint. These analyses require additional resolution of the joint axial forces to determine the forces in the relevant directions. Additional calculations are required to determine the complete action in locations where a chord member is continuous across the joint. The procedures for calculating the joint capacities, explained in the following chapter, will clarify the need for additional data manipulation. The maximum joint forces under the initial 1.22 N/mm loads are shown in Table A-3 in Appendix D. The present discussion is based on this data; the following D/C analysis uses a reduced uniform load (results shown in Table A-4), as discussed in the following chapter.

2.3 Conclusions

This chapter discusses the development of the modeling method, to be used in the subsequent analyses, for determining the demand on the individual elements of a MPC truss. The literature review identified eight possible model analogs that could be considered practical. The basic modeling procedures in SAP2000 were refined, and the analogs were compared through an initial validation using experimental deflection data. Following this, all eight analogs were tested by comparing the member and joint forces produced by each analog case.

Due to the sensitivity of the force results for certain members to different connectivity conditions or member insertion point analogs, it was discovered that of the eight simplified model analogs, no single method would provide accurate results for both moment and axial forces in all truss elements. This is one reason why the envelope method, taking the maximum force results across all analogs, was considered. While it may be true that it would be more accurate to model the semi-rigidity of the MPC joints, the uncertainties in construction of MPC joints, lack of experimental data, and variability of the parameters that affect joint stiffness make this option practically infeasible. In addition, taking the “worst case scenario” of the load path through the truss under uplift would allow for identification of failures that may not be otherwise noticed and indicate potential gaps in current MPC truss design and construction practice. The maximum results across all

analogs were assessed, and it was found that the bottom-centreline (BL) insertion point, paired with the Pinned and Rigid joint analogs in separate models, will collectively yield the maximum results in nearly all elements.

This chapter provides a validated modeling method that can reliably assess element-level, maximum demand values throughout a trussed structure under uplift. Using the BL insertion point and an envelope of the pinned and rigid connectivity analogs, a realistic hip roof truss was modeled. A uniformly distributed uplift, calculated to correspond to DOD-4 and DOD-6 wind speeds, was applied to the truss model to simulate wind loading and the consequent load effects. Member and joint force results were extracted and processed to provide demand values that can be compared to the capacities estimated in the following chapter.

3 Demand-to-Capacity Model of Hip Roof Trusses under Wind Uplift

Following the development of the modeling method to obtain the demand on the members and joints in a frame under uplift, the analysis must be expanded to include assessment of the element capacities. Then, combining the demand and capacity results will yield D/C ratios. The objective of the overall analysis method is to produce a set of scaled data that can be compared directly to assess the relative vulnerability of the elements throughout the structure. In the present chapter, the D/C analysis for Truss A2 introduced in Section 2.2 is completed, and design and analysis of an equivalent stick-frame section is carried out for comparison. The results of the D/C analysis for the plane truss and the two-dimensional stick-frame case in the following chapter provide evidence and observations related to the likelihood of hip roof framing failures. These observations resulted in preliminary conclusions that can be discussed in relation to the failure images and damage survey observations.

By applying a uniformly distributed uplift which corresponds to a known wind speed, the finite element model estimates the demand throughout the truss. The model analogs selected in Chapter 3 predict the most conservative load effects to represent the maximum probable demand on each truss element under the applied uplift. Capacity values for comparison are determined using code-based resistance calculations (Truss Plate Institute of Canada, 2014; Truss Plate Institute, 2002) and recommended equations from the literature (Lewis, et al., 2006). The objective of this work is to estimate member and connection capacities, apply them to D/C analyses of truss and stick-frame roof sections, and identify important or critical ratios for discussion. To conclude this chapter, the maximum resulting D/C ratios will pinpoint the truss elements that are prone to failure under the given wind speeds, and the modes under which they are most vulnerable. In addition to analyzing the truss elements, D/C ratios for the RTWCs will be included to assess the likelihood of internal framing failure relative to this expected mode of DOD-6. The final chapters of this thesis will discuss the D/C results, for the trussed and stick-frame cases, in comparison with the damage survey data. Predominant vulnerabilities and

potential gaps in the EF-Scale and current residential construction practice will be identified.

3.1 Element Capacity Calculations

The capacity of each truss element is estimated based on code design equations and published, recommended methods. Code equations are considered the most reliable method for the present study because their use has been tested and improved iteratively through many years of use in industry. However, review of common truss design practice has suggested that code-based methods may not capture the entire range of load effects or capacities of every element. To estimate connection strength, Canadian and American design standards for MPC trusses (Truss Plate Institute, 2007; Truss Plate Institute of Canada, 2014) prescribe similar methods for calculating the axial and shear resistance of the plated connections. These calculations have been used for several years and refined with subsequent code releases to provide accurate and practical strength estimates for many configurations of trusses.

The moment capacity of MPC joints has not been addressed historically; prior to the 2002 edition of the American code (Truss Plate Institute, 2007) no design method to account for moment was provided. Recent work has attempted to resolve this gap (Lewis, et al., 2006). Lewis et al.'s (2006) method, which is used in the present study, will be discussed in detail in Section 3.1.2. Member strength values for standard grades of dimensional lumber used in Canada have been obtained through testing and tabulated for design use in the Canadian Wood Design Manual (Canadian Wood Council/Canadian Standards Association, 2015). The values used in the present analysis will be provided in Section 3.1.1.

3.1.1 Member Capacity

The truss fabrication drawings used in the construction of the hip roof tested by Henderson et al. (2013) specify that the truss members were made of a combination of “SPF No.2” and “SPF 2100F_b-1.8E” sawn lumber. To maintain truss symmetry and simplify the comparison of D/C ratios in the analysis, all capacities are calculated based on the “SPF No. 2” material properties. Table 5.3.1A in the Canadian Wood Design Manual (Canadian Wood Council/Canadian Standards Association, 2015) provides specified strength values

for common grades of visually graded lumber. The specified bending, tensile, and compressive strengths for “SPF No. 2” are obtained from this table. These unfactored resistance values are provided in units of stress (MPa). For comparison to the force results from SAP2000, which are extracted in units of Newtons, the resistance values are converted by multiplication with the appropriate section properties of the chord and web members. The chord members consist of standard 2-by-4 inch members, and the webs are 2-by-3’s. The gross areas (A) and section moduli (S) of these sections are calculated and used to determine the strengths listed in Table 3-1 below.

Table 3-1: Material properties and calculated member strengths for truss members using SPF No. 2 sawn lumber

Material Properties SPF No. 2 Visually Graded Lumber				
Specified Resistance [MPa]	Bending at Extreme Fibre, f_b	Tension Parallel to Grain, f_t	Compression Parallel to Grain, f_c	Compression Normal to Grain, f_{cp}
	11.8	5.5	11.5	5.3
Member Properties	Member Moment and Force Capacities			
	$f_b * S$ [N-mm]	$f_t * A$ [N]	$f_c * A$ [N]	$f_{cp} * A$ [N]
Chord Members (38-by-89 mm) $A = 3382 \text{ mm}^2$ $S = 50166 \text{ mm}^3$	592000	18600	38900	17900
Web Members (38-by-64) $A = 2432 \text{ mm}^2$ $S = 25941 \text{ mm}^3$	306000	13400	28000	12900

The calculated member capacities will be compared to the maximum corresponding forces from the truss model by calculating D/C ratios. The maximum moment, tension, and compression results across all chord members are compared to the corresponding chord member capacities, and the maximum web member forces are likewise compared to the web member capacities. The locations of the maximum force results were noted in the previous steps to pinpoint the most vulnerable locations in the members themselves. Comparing the highest member D/C ratios to the highest joint D/C ratios will provide

indication of whether the joints or members are more vulnerable. The original material properties listed in the above table are also used to calculate the joint capacities as explained in the following section.

3.1.2 Connection Capacity

The trusses in Henderson et al.'s (2013) hip roof used the lumber described above, connected by MiTek MII20 truss plates. Plate strength data sheets, prepared by the manufacturer in accordance to Canadian requirements for truss plate testing (Institute for Research in Construction, 2009), were obtained and are used in the present calculations. Relative to the member capacity assessment described previously, joint capacities require significant effort and research to estimate accurately. The Truss Plate Institute of Canada (TPIC) design specifications for MPC trusses (Truss Plate Institute of Canada, 2014) are used for the connection capacity calculations in this study, in addition to the equation proposed in Lewis et al. (2006) for moment capacity. The calculations included determining the capacity of the steel plate, the wood member, and the interaction between the two in the relevant directions. The code equations typically include material resistance factors, which are neglected in the present analysis. The equation from Lewis et al. (2006) does not include resistance factors, but the discussion and test results from their study show that the proposed equation was adjusted to include an inherent factor of safety of 1.5. This means that calculated capacities using this equation are expected to be about 70% of what would be observed from testing or in the field. This factor of safety is removed in this analysis by multiplying the calculated moment resistance by the 1.5 factor. Sample capacity calculations and notes, including relevant code equations and clauses, for all required modes of joint capacity are provided in Appendix E.

For reference, Figure 3-1 shows a diagram of half of the Truss A2, with the joints and members labeled per the construction drawings. The present D/C analysis also follows this convention. Depending on the direction of the axial load acting on each member, different sets of axial and shear capacity calculations are required. The analysis of this truss in the previous chapter shows that the top chord goes into tension and the bottom chord into compression when the truss is under uniform uplift. The diagonal web member, W2, also goes into compression. Wherever a compression member butts up against another member

at the joint, failure under the compressive mode is considered highly unlikely due to contact between the members. Once the plate deforms enough for the members to come into contact, failure becomes dependent on the parallel-to-grain compressive strength of the member, which is relatively high. Compared to the other load effects, axial compression on the members and joints is not considered to be critical. It is therefore neglected from the D/C analysis.

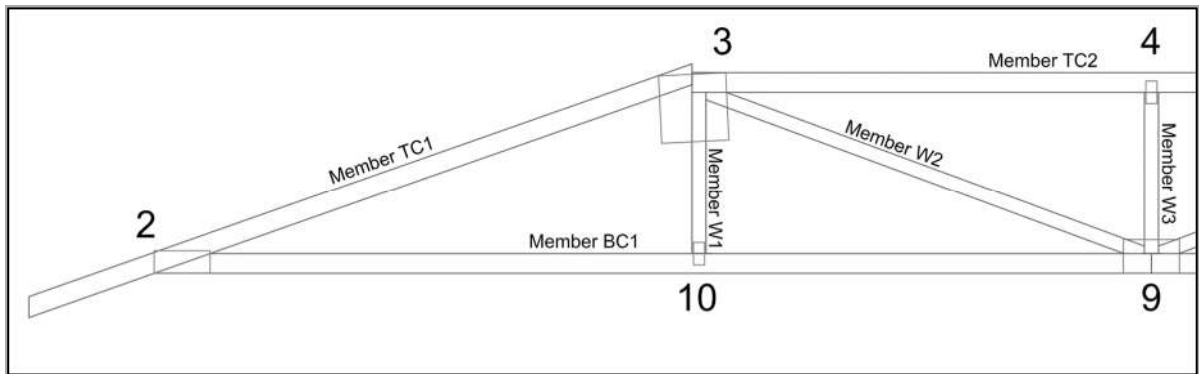


Figure 3-1: Half of modeled hip roof truss with MPC joints and members labeled according to truss manufacturer’s drawing package

Joint tension and shear capacities each require three sets of calculations; the material strength of the plate, the lateral resistance of the plate teeth, and the slip resistance of the plate-to-wood interface must all be checked. In practice, the lowest of these three values is taken as the design strength for the corresponding direction. The TPIC (2014) standard prescribes ultimate limit states design for MPC joints in the clauses under Section 7.3. For members joined along two edges using the same plate, there is also a calculation for assessing the combined shear and tension resistance of the joint, explained in Clause 7.5.4 of the standard. Examples of such joints are shown in Figure 3-1. Joints 3 and 9 both include web members that would require this calculation. The top chord members of Joint 3 would also require similar calculations due to the tensile action at the ends of the members in combination with the shear in the plate parallel to the member length. The other joints only include one possible line of action each in shear and tension.

The moment capacities of the joints are estimated based on the equation developed by Lewis et al. (2006). This equation uses the geometrical parameters of the joint to assess the plate capacity by considering all active areas of the plate and their corresponding moment

arms. The effect of the member axial loads on the moment resistance of the plate is accounted for in Lewis et al.'s (2006) equation through a term that increases the moment resistance of joints which connect compression members, and lessens it for those connecting members in tension. As mentioned, member tension introduces an additional moment couple which worsens the effects of the applied moment on the joint, while compression relieves the plate of some of the tensile effects of the applied moments. Additionally, the deformation - and therefore the failure - of joints under compression will be limited by the members coming into contact with one another.

Axial, shear and moment capacities are calculated for every separate contact area at each joint, meaning that the effects from each joined member are considered separately. This allows for comparison of the SAP2000 results, which are also provided as components of the joint force corresponding to each joined member. Following hand-calculation of capacities for Joints 2 and 3, spreadsheets are developed to perform the remaining calculations and automate the analysis wherever practical. Several manual inputs related to the geometry of each contact area are required. Namely, the specified and estimated plate dimensions from the truss drawings are required, in addition to member geometry. These parameters are used for estimating the length of the seams between joined members and the areas of the surfaces in contact between the members and the plates. Many of these dimensions can be reasonably assumed by visual inspection of the truss drawings since the exact plate placement is not specified. Organization of the capacity calculations is important to ensure that the correct capacity values are being determined according to the direction of loading. The details of the capacity spreadsheets will not be presented in this thesis, but sample calculations for Joint 3 are provided in Appendix E, along with a table of the minimum capacity results for all elements.

3.1.3 Commentary on Current Design Practice

The complexity of capacity estimation for MPC joints presents an unexpected challenge. Undue effort was required to develop an efficient process for assessing joint capacities for many trusses. The procedure for calculating joint capacities for the in-plane actions on the truss requires a high level of organization and does not represent a practical method for efficient use in practice. In practice, MPC trusses are designed by engineers in companies

who specialize in truss design and fabrication. Correspondence with local truss manufacturers (Mr. B. Bunting, pers. comm., 6 February 2017; Mr. C. Cordogiannis, 13 February 2017) has suggested that thorough, code-based calculations are not commonly carried out for trusses. Design is either simplified through prescriptive methods or use of proprietary, “black box” software which is owned by the truss hardware manufacturers. These communications confirm that the nature of truss analysis and design is complex, and that several simplifications must be made even in design software.

From the cited communications, and lack of published information, it is understood that failure modes related to moments in MPC joints are most commonly neglected. Some industry software was even found to neglect joint moments by use of a pinned model analog. Considering the possible vulnerability of joints experiencing moment, which is discussed further in the next section, this practice may neglect an important mode of failure for trusses. Published information to aid with joint capacity estimation includes design equations and plate strength data, both of which are primarily concerned with axial and shear loads. It was not disclosed whether truss manufacturers have access to additional, full joint test data, or whether there are internal, preferred methods for checking the moment resistance of the joints. Prior to the present calculations, information was gathered from all available sources. This work attempts to combine the published methods and go beyond current practice to consider all possible modes of MPC truss joint or member failure.

3.2 Demand-Capacity Analysis

Following calculation of unfactored member and joint capacities, the results from Chapters 2 and 3 are combined to determine D/C ratios for each truss element. Multiple modes of failure are considered for each joint element, according to the number of possible failure modes discussed previously (tension, shear, combined shear/tension, moment, or wood member failure). Member strength values from Table 3-1 are used with the maximum member forces from the truss models to determine member D/C ratios. Table 3-2 shows the highest calculated D/C results and identifies the failure mode corresponding to the critical ratio for each element. D/C ratios are also calculated for RTWCs using toe-nails or the minimum design for hurricane straps. The capacities for these elements are obtained from Morrison and Kopp (2011) and Ellingwood et al. (2004), respectively.

Initially, the D/C analysis is carried out using the demand and capacity results following from the model of Truss A2 under 1.22 N/mm uniform uplift. As mentioned, this load is calculated based on the directional procedure from ASCE 7-10 (2010), using a basic wind speed of 170 km/h. Upon inspection of the initial D/C results, the loading is adjusted to the point at which the most vulnerable element, i.e. the toe-nailed RTWCs, has a D/C ratio equal to one. This is considered to represent the uplift force at which the first element of the truss is expected to fail. By setting the support reactions equal to the capacity of the toe-nailed RTWC, the uplift pressure - and therefore the associated wind speeds - can be back-calculated using the same calculations and parameters as the initial loads. The reduced uplift load, which results in a D/C for the toe-nailed RTWC equal to one, is 0.57 N/mm. This uplift load is found to correspond to a basic wind speed of 115 km/h (72 mph).

The load adjustment is made because in the initial D/C results, which are provided in Appendix F, it is shown that the next highest D/C ratio is produced by the moment capacity of the truss plate at Joint 3. Since the magnitude of the estimated joint moment capacity depends, in part, on the axial forces in the member, the relative D/C ratios do not scale proportionally under changing loads. The updated load allows for better assessment of how close the next-most vulnerable element is to failure. It also enables discussion about whether a framing element is likely to ever fail in advance of the toe-nailed RTWC connection, or alternatively whether it would fail before a RTWC with hurricane straps.

The adjusted wind speed of 115 km/h can be related to the straight-line, basic wind speeds used in ASCE 7-10. It does not represent tornado wind speeds and would require adjustment to allow for direct comparison to DOD-6 for residential structures. However, some observations can be drawn from the literature based on this result. Morrison and Kopp (2011) tested toe-nail connections under realistic wind loading, and similarly related the strength results back to the MWFRS and Components and Cladding design wind speeds used in ACSE 7-05. The adjusted wind speed in the present study is consistent with the wind speed estimates shown in Table 5 of Morrison and Kopp, which neglect load sharing between adjacent connections. This similarity is expected since the present analysis used Morrison and Kopp's mean connection strength as the RTWC capacity. When considering perfect load sharing, the design wind speeds in Morrison and Kopp (2011) increase.

The present adjusted wind speed is much lower than the failure wind speeds estimated by the fragility analyses in Kopp et al. (2016) and Gavanski and Kopp (2017). Both studies considered load sharing and found that at the median probability of failure, the wind speed causing RTWC failure in a hip roof is nearly 250 km/h. As mentioned in Section 1.2.2.1, this wind speed exceeds the range for DOD-6. The basic, 115 km/h wind speed estimate falls below even the lower bound of DOD-6. Beyond the discrepancy due to load sharing, different assumptions regarding internal pressure, roof shape, and wind direction can lead to significant differences in the estimated wind speeds. It is expected that three-dimensional modelling including the effects of sheathing and load sharing will yield much better results that can be easily adjusted for comparison to the EF-Scale. It is important to recall that the present, two-dimensional study focuses on relative vulnerabilities within the hip roof frame, and does not claim to identify the failure wind speeds. The agreement between the adjusted wind speed and Morrison and Kopp's ASCE 7-05 estimates confirms the methodology applied so far.

In Table 3-2, the “vulnerable” elements - those with D/C ratios closest to 1 – are indicated by dark shaded cells. The joints with “N/A” D/C ratios either develop compression in the model results or contain members that are continuous and therefore transfer load through the member rather than the joint. The results from Table 3-2 are shown schematically in Figure 3-2. As can be seen, the D/C ratios for the members and joints vary greatly throughout the truss. The toe-nailed RTWC has the lowest relative strength by a 40% difference, with a D/C ratio of 0.981 compared to the next-highest ratio of 0.695 in Joint 3. This implies that a properly constructed truss will not fail internally, but at the toe-nailed support. This result corresponds with the common understanding of roof failures. As previously mentioned, the original version of the EF-Scale (Wind Science and Engineering Centre, 2006) attributes lower-bound DOD-6 to poor construction. Future work including three-dimensional models can update the failure wind speeds and it is expected that load sharing and the effects of roof sheathing will contribute further to improved resilience of the roof framing.

Table 3-2: Demand-Capacity ratios and governing failure mode for Truss A2 under 0.57 N/mm uplift

Truss Element		Relevant Force Effects and Demand/Capacity (D/C) Ratios					
Joints							
Joint	Member	Axial	Critical Mode	Shear	Critical Mode	Moment	Critical Mode
2	TC1	0.190	Plate Slip	0.117	Plate Capacity	0.209	Member
2	BC1	0.073	Plate Slip	0.046	Lateral	0.207	Member
2	TC1 overhang	N/A		N/A	Combined with TC1	0.188	Member
3	TC1	0.287	Member Tension	0.231	Plate Slip	0.695	Member (Plate D/C 0.34)
3	TC2	0.355	Member Tension	0.013	Lateral	0.695	Member
3	W1	0.004	Member Tension	0.000	Plate Slip	0.023	Member
3	W2	0.074	Member Compression	N/A		0.006	Lateral
4	TC2	0.355	Continuous Member Compression	N/A		0.663	Continuous Member
4	TC2	0.355	Continuous Member Compression	N/A		0.663	Continuous Member
4	W3	0.107	Plate Slip	0.000	Plate Slip	0.093	Lateral
9	BC1	0.054	Member Compression	0.001	Plate Capacity	0.158	Member
9	BC2 right of jt.9	0.054	Member Compression	0.001	Plate Capacity	0.158	Member
9	W2	0.053	Member Compression	N/A		0.015	Lateral
9	W3	0.086	Member Tension	0.000	Plate Slip	0.012	Lateral
9	W4 right of jt.9	0.053	Member Compression	N/A		0.016	Lateral
10	BC1	0.054	Continuous Member Compression	0.005	Lateral	0.175	Continuous Member
10	BC1	0.054	Continuous Member Compression	0.003	Lateral	0.163	Continuous Member
10	W1	0.004	Plate Slip	0.000	Plate Slip	0.039	Lateral
Members							
		Tension	Compression	Shear	Moment		
	Chord Member	0.354	0.054	0.168	0.690	“TC2” mid-panel	
	Web Member	0.087	0.053	0.003	0.026		
Roof-to-Wall Connection							
		Uplift Resistance [N]		Support Reaction [N]		D/C	
	Toe-nail	2800		2746		0.981	
	Hurricane Strap	5840		2746		0.470	

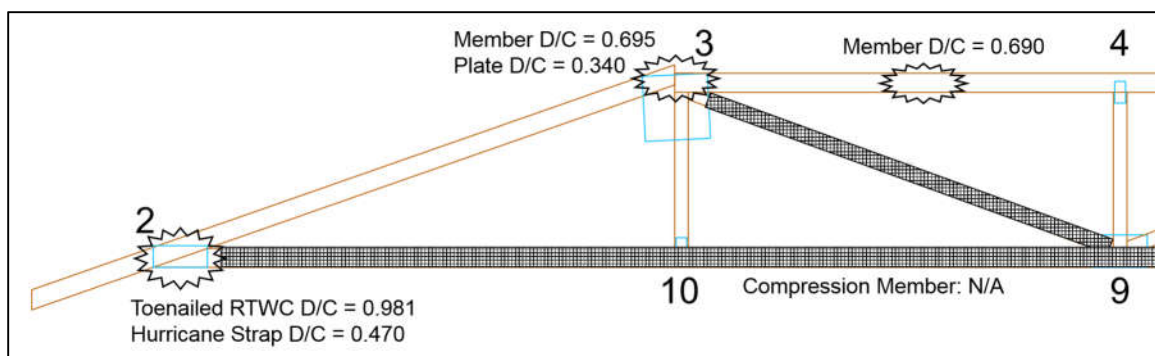


Figure 3-2: Schematic of failure locations in Truss A2 based on estimated D/C ratios from Table 3-2

The initial loading case verifies the failure of the toe-nailed RTWC at lower-bound DOD-6 wind speeds, and both cases provide insight into structures in which hurricane straps are used. As shown in Table 3-2, the framing members and truss joints around Joint 3 are found to be more vulnerable than the RTWC with hurricane straps, having higher D/C ratios. This means that application of hurricane straps could shift failure into the framing components of the truss. The predominant failure mode of Joint 3, based on the relative capacities, is wood member failure, although the possibility of plate failure at this joint should also be noted. The insertion point analog used in this study considers eccentricities that may exist due to poor construction or other geometrical constraints. Adjusting this eccentricity and the plate placement may vary the member forces and joint capacity to the point that the D/C ratio for the plate becomes even higher. This may have implications for regions where hurricane straps are required.

3.3 Conclusions

The preliminary results obtained from analysis of the hip roof truss show that the internal members and connections of a trussed hip roof are unlikely to fail in structures with toe-nailed RTWCs. Weak links are likely to occur, as predicted in previous research, in the RTWC or sheathing. When the toe-nailed RTWC has a D/C ratio of approximately 1, the top chord members are predicted to reach a D/C of 0.70. Possible variations in the load path and element capacities could result in shifts in both of these values; however, since the analysis is based on taking extreme demand values for the framing elements it is

unlikely that deviations in the two D/C ratios will overlap. It is expected that the toe-nailed RTWC will almost always fail first in the plane truss case. This conclusion does not hold true, however, in the case where hurricane straps are employed at the RTWC. In this case, the D/C ratio of the hurricane straps is 0.47, compared again to the 0.70 D/C in the top chord. This means that the connections or wood members in the top chord are the most likely points of failure initiation. The next chapter will study the two-dimensional behaviour of an equivalent stick-frame case.

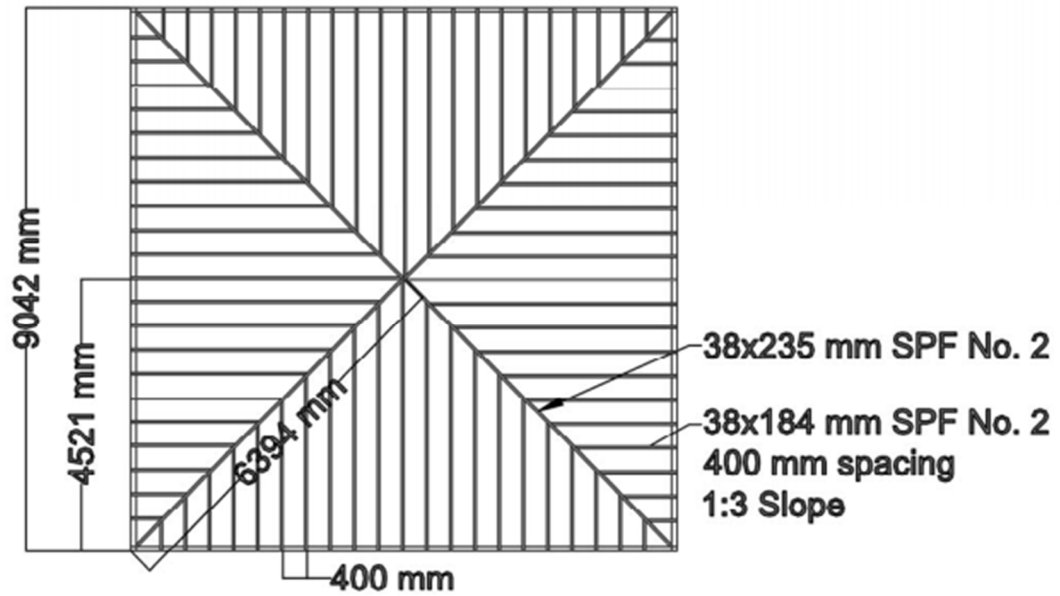
In future work, adjustments to the analysis method should be made prior to modeling three-dimensional roofs. The work can be simplified and redundant calculations can be eliminated based on the results of this analysis and additional, single-truss studies. By identifying patterns in the critical D/C ratios within the first several trusses, it can be determined whether D/C ratios at any locations are sufficiently and consistently low enough to assume that the corresponding elements are “safe”, and need not to be assessed further. In addition, the calculated capacities of similar joints can be compared across several trusses to indicate the sensitivity of the calculations to geometric changes.

4 Demand-to-Capacity Analysis of Stick-Frame Roofs

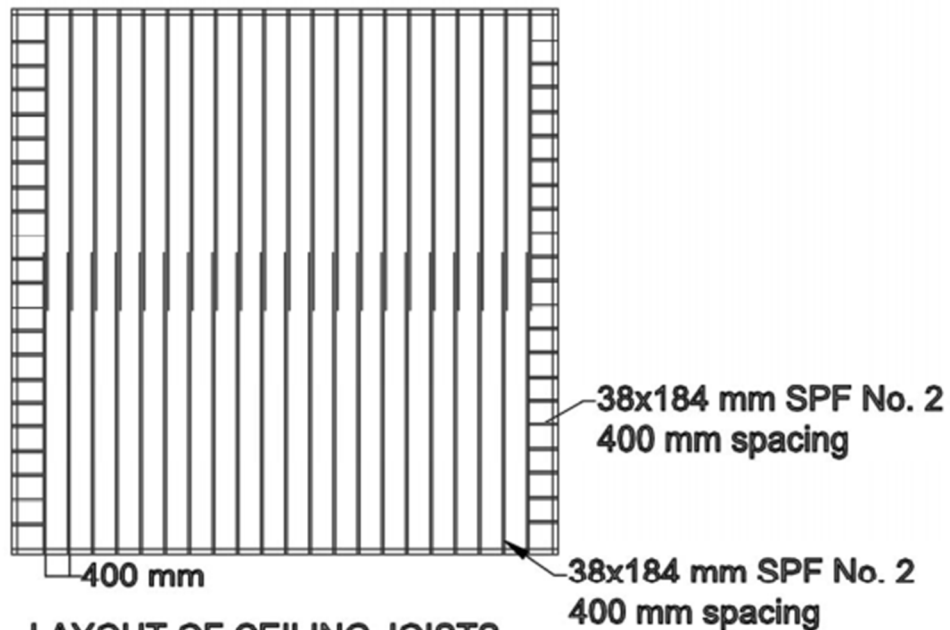
Following analysis of Truss A2, a stick-frame hip roof is designed to match the profile and plan geometry of the trussed-roof from Henderson et al. (2013). This chapter presents the D/C analysis of a two-dimensional section of the designed roof, compares the results to those from the previous chapter, and revisits some of the observed failure from the damage survey data. The present roof is designed according to the prescriptive requirements in Part 9 of the NBCC. The D/C analysis will reveal whether the components of a stick-frame roof with the same shape as that of a trussed structure can be considered more or less vulnerable to uplift failure. The discussion regarding the damage survey observations will also comment on additional factors such as construction quality. Because the evidence of partial roof framing failures predominantly includes stick-frame structures, this discussion is additionally important.

4.1 Design of Stick-Frame Roofs

Section 9.23 of the NBCC (2010) provides prescriptive design requirements for Wood-Frame Construction. The relevant provisions in this section are followed to determine the appropriate member placement and sizing requirements, in addition to the minimum number and direction of nails in each joint. Appendix G includes the design notes for this roof structure, including the relevant Clause and Table numbers. The resulting structure is illustrated in Figure 4-1 with member sizes and spacing labeled. Due to the relatively small footprint of this house, the required jack rafters are shorter in length than the maximum allowable span, which is equal to 5110 mm for the specified 38 x 184 mm lumber. As labeled in Figure 4-1, the longest jack rafter is only 4521 mm in length. This means that intermediate ties or bracing are not required within the cavity of the designed roof structure. Lateral restraint for the jack rafters is provided through nailed connections between the ceiling joists and the rafters at the wall top plate. Under gravity loads, the ceiling joists are expected to go into tension and prevent the rafters from kicking outwards. Under uplift loads, these members are not expected to play a significant role. This should be explored in future work through three-dimensional modeling.



LAYOUT OF JACK AND HIP RAFTERS



LAYOUT OF CEILING JOISTS

Figure 4-1: Plan-view, dimensioned stick-frame member layout drawings

The nailed connections in the stick-frame roof are designed according to tabulated, minimum nailing requirements listed in the NBCC (2010). Four different connection designs are required in the outer roof framing due to the repetitive placement of the members. At the upper end of each the jack rafter where it rests against the hip rafter, two

- 82 mm nails are to be nailed through the hip rafter, into the ends of the jack rafters. Then, at the base of the roof, three connections are required; three - 82 mm toe-nails connect the jack rafter to the wall top plate, two - 82 mm toe-nails connect the ceiling joists to the wall top plate, and seven - 76 mm nails join the jack rafters to the ceiling joists, nailed through their faces on either side. The capacity of each connection will be calculated and discussed in Section 4.2.2. It is interesting to note that the instructions in Section 9.23 of the NBCC do not include the requirement that the hip rafters be joined at the peak of the roof. These members are required only to provide a rigid connection between the structural jack rafters, but they are not considered to be structural themselves.

4.2 D/C Analysis of Stick Frame Members and Joints

To compare the estimated vulnerabilities of the hip roof truss from Section 3.2 to a similar stick-frame case, a two-dimensional D/C analysis of a portion of the designed roof is also carried out. Estimation of the demand and capacity values for a single member is presented in the following sections, before comparing D/C ratios and discussing their significance.

4.2.1 Analysis of Demand on Stick-Frame Member

The member layout of stick-frame roofs induces load sharing between the faces and individual members of the roof. The hip rafter transfers loads between members on adjacent faces of the roof, and the sheathing plays a role in the member-to-member system effects across a single face. Due to this layout, it is not possible to extract a two-dimensional cross-section from the roof for analysis, as was effectively done in the truss analysis. Instead, the present analysis of the stick-frame roof is simplified by studying a single, representative jack rafter. The jack rafter that experiences the highest load effects and support reactions is selected to represent the most vulnerable two-dimensional case. Upon inspection, the rafters nearest to the center of the roof are deemed to be under the highest demand under uniform roof pressures. Because they are the longest structural members within the outer roof frame, the central jack rafters are expected to experience the highest moments and shear internal forces, and their joints will need to resist the largest support reactions. The faces of the roof are identical and so the selected member represents four different jack rafters within the roof.

Analysis of a single rafter can easily be accomplished through hand calculations. For this study, however, SAP2000 is used so that the rafter can be modelled with Pinned and Rigid joint behaviour at the supports, and the maximum force results from both cases can be obtained. Figure 4-2 shows the modeled rafter with applied uplift loads. Like in the truss models, loads are applied as outward pressures, perpendicular to the member, rather than vertically upwards. The magnitude of the applied load is calculated using the same adjusted wind speed as presented in Section 3.2. The pressure corresponding to 115 km/h is multiplied by the tributary area supported by the rafter, resulting in a uniformly distributed load of 0.38 N/mm. From this model, maximum member forces and support reactions are obtained and shown in Table 4-1.

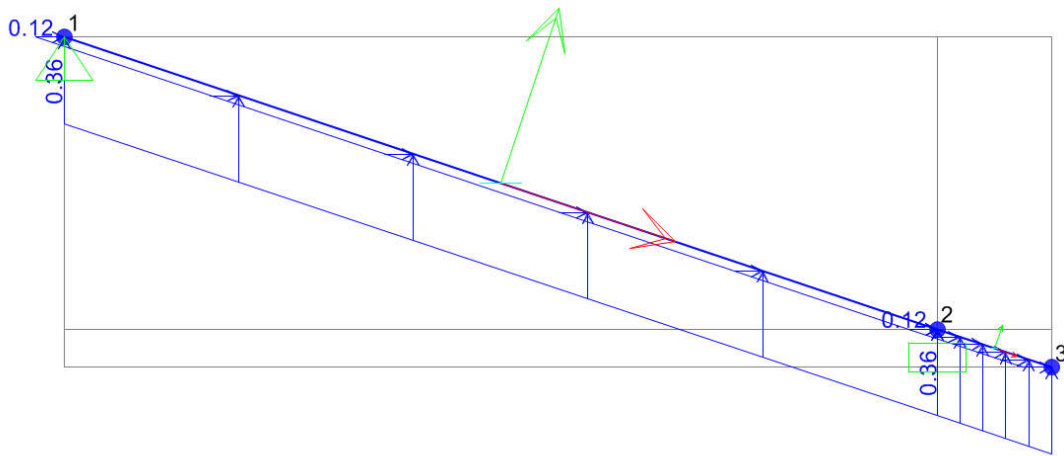


Figure 4-2: SAP2000 model of jack rafter under 0.38 N/mm uniform uplift

Table 4-1: Maximum member and joint demand on jack rafter under 0.38 N/mm uplift. Envelope of results using Pinned and Rigid support conditions

Element	Maximum Demand		
	Horizontal Reaction (N)	Vertical Reaction (N)	
Joint 1	283.83	782.24	
Joint 2	364.48	1006.07	
	Tension (N)	Shear (N)	Bending (N-mm)
Rafter	21.9	850.93	995062

4.2.2 Capacity Estimation for Stick-Frame Elements

For each of the two member supports, the appropriate capacities are estimated based on unfactored design values and equations from the Canadian Wood Design Handbook (Canadian Wood Council/Canadian Standards Association, 2015). Depending on the direction of loading, the required capacity calculations include those for nail withdrawal resistance and lateral resistance.

Joint 1 consists of two nails, end-nailed into the jack rafter in the horizontal direction. This orientation means that the nail withdrawal capacity resists horizontal reactions at Joint 1, and the lateral, or shear, capacity of the nails resists the vertical component. Joint 2 is more complex because there are three different nailing requirements and all of the fasteners can act together, or transfer load to one another, in different directions. Under vertical loads, the jack rafter could either become separated from the ceiling joist and top plate, and fail through combined lateral failure and pullout of the respective connections, or the entire joint could lift off due to withdrawal of the five-total toe-nails that hold the jack rafter and ceiling joist to the top plate. In the horizontal direction, failure of the rafter-to-joist connection is only considered because failure of the toe-nails is additionally resisted by compression in the ceiling joist. Joint moments are not considered. Details of the nailed connection capacities are shown in Appendix H, and the minimum estimated values for each element are shown in Table 4-2 below. Member strengths are calculated using the same calculations as those shown in Table 3-1, however the cross-sectional properties are updated to represent the 38 x 184 mm jack rafter.

Table 4-2: Member and joint capacity estimates for jack rafter under uplift

Element	Estimated Capacity		
	Horizontal Reaction (N)	Vertical Reaction (N)	
Joint 1	532	1184	
Joint 2	4996	891.1	
	Tension (N)	Shear (N)	Bending (N-mm)
Member	38610	10530	2537000

4.2.3 D/C Analysis of Jack Rafter

The demand and capacity values presented in the previous sections are combined in Table 4-3 below to show the D/C results for the modeled elements. Under the same uplift pressure as the trusses, the results show that the jack rafter is also most vulnerable at the toe-nailed RTWC. This analysis does not include the uplift capacity of a RTWC with hurricane straps. Introduction of straps at the RTWC is expected to result in failure at Joint 1, since this location has a relatively high D/C ratio. The next-weakest connection at Joint 2, consists of seven nails joining the rafter to the ceiling joist. It has a much higher capacity of around 5000 N.

Table 4-3: Member and joint D/C ratios for jack rafter under 0.38 N/mm uplift

	D/C Ratio		
Element	Horizontal Reaction		Vertical Reaction
Joint 1	0.534		0.661
Joint 2	0.073		1.129
	Tension	Shear	Bending
Member	0.001	0.081	0.392

The stick-frame results are similar to the results of the truss analysis in two ways. First, they reaffirm the common expectation that a toe-nailed RTWC is likely to be the most vulnerable element of a hip roof at this slope. On the other hand, these results also pinpoint the connection at the ridge of the roof as being the next-most vulnerable element. In both situations, variabilities in the roof behaviour and connection parameters make it possible that other failures may take place. This is especially plausible when construction errors, degrading members, and the outdated design standards to which older stick-frame houses were built are considered. The following section will explore the possibility of construction errors and the effects of roof slope, with discussion based on additional selected hip roof failure photos.

4.3 Additional Discussion of Observed Stick-Frame Failures

The hip roof framing failures introduced in Section 1.2.2.2 describe several different cases and factors that may lead to framing vulnerabilities. Future work will require a range of roof slopes and plan shapes to study roofs such as those shown in Figure 1-4 b) and Figure

4-3 below. The results from the D/C analysis verify that loss of members or faces of a stick-frame hip roof may be likely under relatively low wind speeds, however the progression of failure of large sections of the roof is not well-defined. Other causes such as improper design or construction may have a significant impact as well.



Figure 4-3: Failure of stick-frame roof with irregular roof shapes (Image provided by Dr. David Prevatt)

Upon revisiting the damage survey data and the report from the Moore, OK tornado (Graettinger, et al., 2014), an additional mode of failure related to the stick-frame case is noticed. This mode may point to improper construction of the outer roof frame, or to the potential impact of cascading failures caused by load sharing in stick-frame structures. In Figure 4-4, partial framing failure and removal of large sections of the roof appears to have occurred. Upon closer inspection, however, it becomes apparent that the ceiling joists, and the ceiling beneath them, are intact. Only the jack and hip rafters have been removed or damaged. Based on the results of the D/C analysis for the stick-frame case, this type of failure is unlikely, due to the relatively robust connection between the rafter and the ceiling joist. The RTWC and the connection along the ridge of the roof appears to be much more vulnerable. The pictured failure may have occurred due to improper or missing fasteners between the rafter and the joist at the wall top plate or initiated as failure of the upper rafter joint. Additionally, system effects may have led to progressive, cascading failure of adjacent joints, resulting in removal of entire faces of the roof following initiation at a single point.



Figure 4-4: Partial stick-frame, hip roof failure with ceiling joists intact (Image provided by Dr. David Prevatt)

Figure 4-5 shows another example of a major roof failure which has left the ceiling framing and drywall intact. This failure, and many others like it, would be objectively classified within DOD-6 for residential roofs, however this may be an inaccurate assumption. As mentioned in the previous example, the D/C analysis for the stick frame case did not predict that the rafter-to-wall connection would be vulnerable due to its relatively robust connection to the ceiling joist. Closer inspection of Figure 4-5 suggests that there were some connections at the ends of the intact joists, however from the faces of the members it does not appear that there were more than a few nails. Keeping in mind that these houses were not designed in Canada, exploration of the prescriptive design requirements in the US is required to determine whether these connections are meant to include more nails.



Figure 4-5: Loss of the entire surface of a stick-frame hip roof with intact ceiling joists (Image provided by Dr. David Prevatt)

It is additionally important to note that although these roof failures would fall under the description of DOD-6, it is unlikely, based on the wind speed applied in the D/C analysis, that the wind speeds causing these failures are as high as those resulting in total roof loss through failure of the RTWC. This is an important point for further exploration because it may suggest refinements to the EF-Scale for different residential design methods, or even provide a new DOD for stick-frame structures. Additionally, although removal of the entire outer shell of the stick-framed roof may occur at lower wind speeds than total loss of a trussed roof, these failures are also likely to be far less expensive. In both of the above examples, it appears as though the building envelope is not compromised significantly through the ceiling. In DOD-6 of a trussed structure, entire trusses are typically lost, and the ceiling goes with them due to the bottom chords of the trusses acting as ceiling joists. In the stick-frame structure, a disconnect between the ceiling joist and rafters make the outer structure of the roof more vulnerable to uplift, however it may also protect the interior of the building and its contents by allowing the ceiling joists to stay in place. These effects warrant further exploration.

4.4 Conclusions

The present chapter explores the likelihood of partial framing or connection failures in stick-frame structures. It is found that connection failures may be likely under relatively small wind loads. The RTWC in the stick-frame case was found to have a 10% higher D/C ratio than that of the truss in the previous chapter. This result supports the expectation of poorer performance of stick-frame structures. According to the D/C analysis, the next-most vulnerable element is Joint 1. Introducing hurricane straps would likely result in failure of the connection at the ridge of the roof. Based on the prescriptive design requirements and visual inspection of the damage photos, two possible causes of the vulnerability of stick-frame roofs are long unsupported member lengths, and the typical toe-nailed connections that support the members at each end. Trusses inherently contain far more in- and out-of-plane bracing, and the MPC joints provide high capacity in both tensile and compressive directions.

When paired with the damage survey photo from Chapter 1 and Section 4.3, the variability of partial framing failures becomes apparent. An additional “partial” failure mode is identified where the roof rafters are removed, along with the sheathing, but the ceiling and ceiling joists remain intact. This mode must be explored further to determine the design conditions allowing it to occur, the wind speeds at which it is likely to occur, as well as the potential benefit to having the ceiling remain intact if roof failure must occur. In hurricanes, heavy rainfall would almost certainly destroy the exposed ceiling, however it is not apparent whether tornadoes would have the same effect. Interior inspections of these failures during damage surveys would reveal whether the intact ceiling protects the building contents. It is possible that this failure mode may result in smaller losses and therefore become preferable to the other modes of DOD-6.

5 Conclusions and Recommendations

The focus of this research is to verify the possibility of partial framing failures in hip roofs under wind uplift. Damage survey observations have identified a previously unstudied failure mode for wood-frame residential roofs in which the framing members or their connections fail during tornadoes. These observed failures extend the current understanding that residential roofs are most vulnerable to damage through sheathing loss or failure of the roof-to-wall connection. Statistics of the observed damage in select neighbourhoods following recent tornadoes in Moore, OK, and Joplin, MO, have found that partial framing failures may occur at least as often as the other roof failure modes under EF-1 and EF-2 wind speeds. Further inspection of the damage photos also suggests that this failure occurs predominantly in stick-frame structures.

This work proves the concept of partial framing failures in hip roofs. Hip-roofed homes are commonly understood to be more resistant to wind damage than those with gable roofs. However, when considering the possibility of partial framing failures, it may be revealed that hip roof homes are more vulnerable under this new mode than previously expected. This research contributes to the EF-Scale by exploring the possibility of a new failure type and defining which DOD, and therefore which failure wind speeds, it should be associated with. In addition, through development of the analysis and modeling methods, this thesis explores common residential design and construction practices. Several potential gaps in the building code, current modeling methods, and design practice are identified, with particular regard to designing trusses and stick-frame roofs to resist wind loading.

A numerical modeling and analysis method was developed to investigate the behaviour of common hip roof framing components. The first model was developed to represent the behaviour of MPC trusses under uplift. Both trusses and stick-frame structures were studied to provide a comparative study of the two construction methods. The trussed case was used for model and method development due to the level of complexity in the framing and joint configuration relative to the stick-frame case, and also the amount of published experimental data. The developed method, based on determining demand-to-capacity ratios for all elements of the structure, was then extended to the stick-frame case. The

results of a two-dimensional D/C analysis for the trussed and stick-frame cases have been used to understand the likely locations of vulnerability in the framing structure. When used in conjunction with the damage survey photos, these results provide additional insight into possible code or construction deficiencies leading to the observed failures.

5.1 Key Findings of the Current Work

Observational assessment of the damage survey data, including photos from local events and those provided by Dr. David Prevatt of the University of Florida, proves the occurrence of partial hip roof failures, and the preliminary statistical analysis proves that they may be significantly common. Subjective assessment of the observed damage is completed with the following key findings:

- In the neighbourhoods studied using geo-located damage photos, up to 40% of houses in the EF-1 to EF-3 range of damage suffered partial roof failures as opposed to sheathing loss, RTWC failure, or wall collapse.
- The type of construction may have important implications on the type of roof failure that a house will suffer. The neighbourhood which indicated 40% of residential damage include partial roof failures, the houses appeared to of newer, stick-frame construction with large footprints and steep-sloping roofs. Another region, which showed 15% partial roof failures, contained houses that appeared older, with lower sloping roofs and masonry wall structures. It was also noted that some of the partial failures observed in this section likely involved debris impact.
- Stick-frame roofs appear, based on the survey data, to fail through framing failure more often than trussed roofs do.
- An additional failure mode involving entire or partial removal of the entire outer shell of stick-frame roofs was identified.
 - o These failures suggest that the rafters comprising the sloped portion of stick-frame roofs may lack proper fastening to the ceiling joists or walls beneath them.

- Loss of the outer shell of the roof through this failure mode would be classified as DOD-6 damage upon inspection, however it may occur at lower wind speeds. This requires further study.
 - Because the ceiling remains intact through this failure mode, it is possible that it is preferable to similar DOD-6 level failures of trussed roofs because the seal that protects the building contents from water ingress appears to be maintained. However, this can only be verified by interior inspection of homes damaged through this mode.
- In an earlier stage, this research was presented at an international wind engineering conference. This platform resulted in a discussion with a member of the Wind Engineering community who was present following the Moore, Joplin, and Tuscaloosa tornadoes (Dr. D. Prevatt, pers. comm., 23 May 2017). In this discussion, it was disclosed that the houses shown in the failure photos from the Moore, OK tornado of 2013 were actually constructed in response to a previous, devastating tornado. At that point in time, it was understood that hip roofs perform better than gable roofs in extreme winds, and so reconstruction of the houses following the earlier event involved building extremely large, steep hip roofs, typically using prescriptive stick-framing designs. The performance of these structures, particularly those with steep roofs, in the 2011 and 2013 US tornadoes, raises questions regarding the perceived superior behaviour of hip roofs.

The simplified, load-envelope method of modeling and the D/C analysis has shown the ability to identify locations of vulnerability in both trussed and stick-frame roof sections under wind uplift. Complementing the damage observations, the analysis of the two-dimensional cases for each type of construction resulted in the following conclusions:

- When toe-nailed RTWCs are used, MPC trusses under uniform uplift are most likely to fail through the RTWC, resulting in loss of the entire framing structure and ceiling. When hurricane straps are supplied, however, failure may shift to the truss members and connections (or to the sheathing). The critical modes of failure within the truss structure were found to be associated to member and joint moments

under uplift. The demand due to moment in the top chord members are heightened by the tensile axial forces induced on these members through typical truss behaviour.

- The stick-frame analysis case also found toe-nailed RTWCs to be the most vulnerable point in two-dimensional analysis; however, the upper rafter joint was also found to have a relatively high D/C ratio. Inspection of the damage survey photos suggested that the failed stick-frame roofs may have contained less robust joints than in the designed roof.
- Comparison of the two-dimensional analyses for the truss and stick-frame cases suggests that stick-frame roofs contain more highly vulnerable elements. Under equivalent wind uplift, the D/C of the truss RTWC was 0.98, while the RTWC of the stick-frame jack rafter was 1.12. This was as expected, however the effects of load sharing is an important factor, especially for the stick-frame case, which was not considered in this study.

During the method development and D/C analyses, insight into current engineering and construction practice was gained and a number of unexpected challenges were encountered. These challenges were primarily related to modeling and estimating the realistic performance of wood-framed roofs under wind uplift. In light of these challenges, additional commentary is provided below, and recommendations for future improvement to engineering practice are included later in Section 5.2:

- While there are design standards in place, in Canada and the US, for MPC trusses, these standards seem to miss possibly important load effects, such as moment in the joints, and the effects of MPC joint stiffness. There appears to be a few gaps in the code, and additionally there is a lack of communication among truss design practitioners and structural designers.
- Given the complexity of the design process specified in MPC truss codes, it would not be economical for engineering consultants to design trussed roofs without access to proprietary truss design software. Some of these programs are available

for purchase by other designers, but the detailed design calculations are contained within the “black box” programs. The proprietary nature of truss plate manufacturing processes, and truss design processes in general, do not assist in enabling research to accurately assess these structures.

- Stick-frame roof design is prescribed according to expected snow loads, with specified improvement options for locations with higher expected wind speeds. These improvements include hurricane straps for restraining the roof at the RTWC. However, as seen in the D/C analysis for the stick-frame case, the upper joint is also expected to be vulnerable.
- In addition to the inherent vulnerabilities revealed by this research, improper construction of stick-frame structures is expected to play a significant role.
- There is a lack of experimental research on MPC truss joints, entire trusses, and stick-frame joints. Some data were available for validation of the deflection and force behaviour of the truss models, however the data used were virtually the only sources available. Some research programs have included isolated joint testing or truss testing for specific configurations, however these data were not applicable to the trusses studied in the present work, and no feasible method of estimating the required parameters is available.
- The published experimental data are limited to trusses and wood members under gravity loads. The capacity and nonlinear behaviour of similar members under uplift would be extremely valuable to this work going forward.
- Past wind engineering research has not concerned itself with the structural behaviour of roofs on an element-by-element level. There is a significant body of research concerned with modeling the overall deflection behaviour of trusses, with a few studies that have estimated the reactions at the RTWCs for roofs under uplift. These studies primarily validated their models with the same few sets of experimental data used in this thesis. Although a reasonable method of analysis was developed for the present proof-of-concept, expansion of this work requires more

sophisticated modeling methods. The current push towards performance-based-design of residential structures would also benefit from well-defined modeling methods and additional experimental data.

5.2 Recommendations for Future Work

Further work following from this study should include expanding the modeling method to assess three-dimensional trussed and stick-frame roofs, applying realistic, area- and time-varying uplift pressures, and identifying a representative group of common roof shapes and slopes for assessing the vulnerabilities relevant to each roof shape. The following studies are suggested:

- Three-dimensional analyses of both roof types will be especially important for assessing partial failures in stick-framing roofs since these structures depend largely on load sharing between the members.
- The effect of sheathing on the structural behaviour of both roof types should also be studied through modeling to provide additional bounds for estimating the wind speeds at which partial framing failures are likely to occur. The present study compares partial framing failures to the DOD-6 case of RTWC failure, however without modeling the sheathing they have not been located in relation to DOD-4 damage.
 - o In future three-dimensional analyses using the proposed modeling methods, capacity calculations can be simplified by excluding elements or failure modes with exceptionally and consistently low D/C ratios from two-dimensional truss analyses. Ruling out failures that are almost certain not to occur - and which have not been observed in the damage survey data – will allow for the more vulnerable elements to receive greater consideration and care in the analysis.
- Three dimensional analyses should include a range of roof slopes and different roof plan shapes. The roof used in this study is an excellent starting point because some experimental data is available for validation of the first three-dimensional model

(Henderson, et al., 2013), however the slope of this roof is relatively low compared to the failures shown in the figures.

- Complete statistical analysis of partial failure occurrence, continuing from the work described in Section 1.2.2.3. Completing the statistical assessment of the residential failure modes observed in every neighbourhood included in the survey data will allow for assessment of roof failure occurrences in relation to the location along the path of the tornado (and likelihood of debris damage) and the perceived age of the neighbourhood, and emphasize the importance of understanding all residential failure modes.
- Seek more, detailed experimental data on wood-frame roofs under uplift and the deformation behaviour of metal plate and nailed joints. This work will improve the modeling efforts to include semi-rigid joints and allow for better validation of modeled roofs under uplift.

In a more general context, wind and structural engineering research should focus on improving modeling methods for light-frame wood roofs, improving the base of available data for assessing residential structures under wind uplift, and attempting to understand the discrepancies between the idealized, designed structure and its as-built state. The latter will require an understanding, at the human-level, of decision-making in the construction industry, as well as the willingness of homeowners to accept additional costs for preventative measures, such as hurricane straps, in order to lower their risk of devastating losses in the event of a tornado.

References

- Amini, M. O. & van de Lindt, J. W., 2014. Quantitative insight into rational tornado design wind speeds for residential wood-frame structures using fragility approach. *Journal of Structural Engineering*, 140(7).
- Canada Mortgage and Housing Corporation, 2014. *Canadian Wood-Frame House Construction*. 3rd ed. Canada: Government of Canada.
- Canadian Commission on Building and Fire Codes, 2010. *National Building Code of Canada*. 13th ed. Ottawa: National Research Council of Canada.
- Canadian Wood Council/Canadian Standards Association, 2015. *Wood Design Manual: The complete reference for wood design in Canada*. Ottawa, ON: Canadian Wood Council.
- Changnon, S. A., 2009. Tornado losses in the United States. *Natural Hazards Review*, 10(4), pp. 145-150.
- Dao, T. N. & van de Lindt, J. W., 2008. New nonlinear roof sheathing fastener model for use in finite-element wind load applications. *Journal of Structural Engineering*, 134(10), pp. 1668-1674.
- Ellingwood, B. R., van de Lindt, J. W., Gromala, D. S., Rosowsky, D. V., Gupta, R. & Pryor, S. E., 2006. *Performance-based engineering for light-frame wood construction in the United States: Status and Challenges*. Portland, OR, World Conference on Timber Engineering.
- Ellingwood, B. R., Rosowsky, D. V., Li, Y. & Kim, J. H., 2004. Fragility assessment of light-frame wood construction subjected to wind and earthquake hazards. *Journal of Structural Engineering*, 130(2), pp. 1921-1930.
- Environment Canada, 2013. *Environment and Climate Change Canada: Enhanced Fujita Scale*. [Online] Available at: <https://ec.gc.ca/meteo-weather/default.asp?lang=En&n=41E875DA-1> [Accessed 30 March 2017].

Forest Products Laboratory, 1999. *Wood Handbook: Wood as an Engineering Material (General Technical Report No. FPL-GTR-113)*. Madison, WI: United States Department of Agriculture.

Foschi, R. O., 1977. Analysis of wood diaphragms and trusses. Part II: Truss-plate connections. *Canadian Journal of Civil Engineering*, Volume 4, pp. 353-362.

Fujita, T. T., 1971. *Proposed characterization of tornados and hurricanes by area and intensity. Satellite and Mesometeorology Research Project Report 91*, Chicago, IL: University of Chicago.

Gavanski, E. & Kopp, G. A., 2017. Fragility assessment of roof-to-wall connection failures for wood-frame houses in high winds. *Journal of Risk and Uncertainty in Engineering Systems*, 3(4).

Graettinger, A. J., Ramseyer, C. C. E., Freyne, S., Prevatt, D. O., Myers, L., Dao, T., Floyd, R. W., Holliday, L., Agdas, D., Haan, F. L., Richardson, J., Gupta, R., Emerson, R. N. & Alfano, C., 2014. *Tornado Damage Assessment in the aftermath of the May 20th 2013 Moore Oklahoma Tornado*, Tuscaloosa, AL: The University of Alabama.

Gupta, R. & Limkatanyoo, P., 2008. Practical approach to designing wood roof truss assemblies. *Practice Periodical on Structural Design and Construction*, 13(3), pp. 135-146.

He, M., 2002. *Numerical Modeling of Three-Dimensional Light Wood-Framed Buildings (Doctoral Dissertation)*, Vancouver, BC: The University of British Columbia.

Henderson, D. J., Morrison, M. J. & Kopp, G. A., 2013. Response of toe-nailed, roof-to-wall connections to extreme wind loads in a full-scale, timber-framed, hip roof. *Engineering Structures*, Volume 56, pp. 1474-1483.

Institute for Research in Construction, 2009. *Evaluation Listing CCMC 11996-L: MT-20 and MII-20*. s.l.:National Research Council of Canada.

- Jacklin, R. B., 2013. *Numerical and Experimental Analysis of Retrofit System for Light-Framed Wood Structures Under Wind Loading (Master's Thesis)*, London, ON: The University of Western Ontario.
- King, C. G. & Wheat, D. L., 1987. *Deflection and Member Behaviour of Metal-Plate Connected Parallel-Chord Wood Trusses*, Austin, TX: University of Texas.
- Kopp, G. A., Hong, E., Gavanski, E., Stedman, D. & Sills, D. M.L., 2016. Assessment of wind speeds based on damage observations from the Angus (Ontario) Tornado of 17 June 2014. *Canadian Journal of Civil Engineering*, 44(1), pp. 37-47.
- Kopp, G. A., Morrison, M. J., Gavanski, E., Henderson, D. J. & Hong, H. P., 2010. "Three Little Pigs" project: Hurricane risk mitigation by integrated wind tunnel and full-scale laboratory tests. *ASCE Natural Hazards Review*, 11(4), pp. 151 - 161.
- Kopp, G. A., Morrison, M. J. & Henderson, D. J., 2012. Full-scale testing of low-rise residential buildings with realistic wind loads. *Journal of Wind Engineering and Industrial Aerodynamics*, Volume 104-106, pp. 25 - 39.
- Kumar, N., Dayal, V. & Sarkar, P. P., 2012. Failure of wood-framed low-rise buildings under tornado wind loads. *Engineering Structures*, Volume 39, pp. 79-88.
- Lewis, S. L., Mason, N. R., Cramer, S. M., Wert, D. C., O'Regan, P. J., Petrov, G. & Goclano, D., 2006. *Design of Metal Plate Connected Wood Truss Joints for Moment*. Portland, OR, s.n.
- Limkatanyoo, P., 2003. *System Behaviour of Three-Dimensional Wood Truss Assemblies (Master's Thesis)*, Corvallis, OR: Oregon State University.
- Liu, X., 2013. *Three-Dimensional Modeling of Metal Plate Connected Wood Truss Joints (Doctoral Dissertation)*, Vancouver, BC: The University of British Columbia.
- Li, Z., 1996. *A Practical Approach to Model the Behaviour of a Metal-Plate-Connected Wood Truss System (Master's Thesis)*, Corvallis, OR: Oregon State University.

- Li, Z., Gupta, R. & Miller, T. H., 1998. Practical approach to modeling of wood truss roof assemblies. *Practice Periodical on Structural Design and Construction*, Volume 3(3), pp. 119-124.
- Mackerle, J., 2005. Finite element analyses in wood research: A bibliography. *Wood Science and Technology*, Volume 39, pp. 579-600.
- Maraghechi, K. & Itani, R. Y., 1982. Influence of truss plate connectors on the analysis of light frame structures. *Wood and Fiber Science*, 16(3), pp. 306-322.
- Martin, G. K., 2010. *Evaluation of System Effects and Structural Load Paths in a Wood-Framed Structure (Master's Thesis)*, Corvallis, OR: Oregon State University.
- Meecham, D., 1992. The improved performance of hip roofs in extreme winds - A case study. *Journal of Wind Engineering and Industrial Aerodynamics*, Volume 43, pp. 1717-1726.
- Meecham, D., Surry, D. & Davenport, A. G., 1991. The magnitude and distribution of wind-induced pressures on hip and gable roofs. *Journal of Wind Engineering and Industrial Aerodynamics*, Volume 38, pp. 257-272.
- Morrison, M. J. & Kopp, G. A., 2011. Performance of toe-nail connections under realistic wind loading. *Engineering Structures*, 33(1), pp. 69-76.
- Morrison, M. J., Kopp, G. A., Gavanski, E., Miller, C. & Ashton, A., 2014. Assessment of damage to residential construction from the tornadoes in Vaughan, Ontario, on August 2009. *The Canadian Journal of Civil Engineering*, Volume 41, pp. 550-558.
- National Research Council of Canada, 2017. *Model code adoption across Canada*. [Online] Available at: http://www.nrc-cnrc.gc.ca/eng/solutions/advisory/codes_centre/code_adoption.html [Accessed 30 06 2017].
- Pan, F., Cai, C. S., Zhang, W. & Kong, B., 2014. Refined damage prediction of low-rise building envelope under high wind load. *Wind and Structures*, 18(6), pp. 669-691.

- Pfretzschner, K. S., 2012. *Practical Modeling for Load Paths in a Realistic, Light-Frame Wood House (Master's Thesis)*, Corvallis, OR: Oregon State University.
- Prevatt, D. O., Coulbourne, W., Graettinger, A. J., Pei, S., Gupta, R. & Grau, D., 2013. *Joplin, Missouri, Tornado of May 22, 2011: Structural Damage Survey and Case for Tornado-Resilient Building Codes*. Reston, VA: American Society of Civil Engineers.
- Prevatt, D. O., van de Lindt, J. W., Graettinger, A. J., Coulbourne, W., Gupta, R., Pei, S., Hensen, S. & Grau, D., 2011. *Damage Study and Future Direction for Structural Design Following the Tuscaloosa Tornado of 2011*, Gainesville, FL: University of Florida.
- Reed, T. D., Rosowsky, D. V. & Schiff, S. D., 1997. Uplift capacity of light-frame rafter to top plate connections. *Journal of Architectural Engineering*, 3(4), pp. 156-163.
- Riley, G. J., 1998. *Analytical Model of Metal-Plate-Connected Wood Truss Joint Stiffness (Doctoral Dissertation)*, Ithaca, NY: Cornell University.
- Rosowsky, D., Reed, T. & Tyner, K., 1998. Establishing uplift design values for metal connectors in light-frame construction. *Journal of Testing and Evaluation*, 26(5), pp. 426-433.
- Shanmugam, B., Nielson, B. G. & Prevatt, D. O., 2009. Statistical and analytical models for roof components in existing light-framed wood structures. *Engineering Structures*, Volume 31, pp. 2607-2616.
- Sills, D. M., McCarthy, P. J. & Kopp, G. A., 2014. *Implementation and application of the EF-scale in Canada*. Madison, WI, American Meteorological Society.
- Simmons, K. M., Kovacs, P. & Kopp, G. A., 2015. Tornado damage mitigation: benefit-cost analysis of enhanced building codes in Oklahoma. *Weather, Climate, and Society*, 7(2), pp. 169-178.
- Sparks, P. R., Schiff, S. D. & Reinhold, T. A., 1994. Wind damage to envelopes of houses and consequent insurance losses. *Journal of Wind Engineering and Industrial Aerodynamics*, Volume 5, pp. 145-155.

- Standohar-Alfano, C. D. & van de Lindt, J. W., 2016. Tornado risk analysis for residential wood-frame roof damage across the United States. *Journal of Structural Engineering*, 142(1).
- Structural Engineering Institute, 2010. *ASCE 7-10 Minimum Design Loads for Buildings and Other Structures*. Reston, VA: American Society of Civil Engineers.
- Truss Plate Institute of Canada, 2014. *Truss Design Procedures and Specifications for Light Metal Plate Connected Wood Trusses*, Bradford, ON: TPIC.
- Truss Plate Institute, 2007. *National Design Standard for Metal Plate Connected Wood Truss Construction*. Alexandria, VA: American National Standards Institute (ANSI).
- van de Lindt, J. W., Pei, S., Dao, T., Graettinger, A., Prevatt, D. O., Gupta, R. & Coulbourne, W., 2013. Dual-objective-based tornado design philosophy. *Journal of Structural Engineering*, 139(2), pp. 251-263.
- van de Lindt, J. W. & Dao, T. N., 2009. Performance-based wind engineering for wood-frame buildings. *Journal of Structural Engineering*, 135(2), pp. 169-177.
- van de Lindt, J. W., Graettinger, A., Gupta, R., Skaggs, T., Pryor, S. & Fridley, K. J., 2007. Performance of wood-frame structures during Hurricane Katrina. *Journal of Performance of Constructed Facilities*, 21(2), pp. 108-116.
- Vatovec, M., 1996. *Analytical and Experimental Investigation of the Behaviour of Metal-Plate-Connected Wood Truss Joints (Doctoral Dissertation)*, Corvallis, OR: Oregon State University.
- Vatovec, M., Miller, T. H., Gupta, R. & Lewis, S., 1997. Modeling of metal-plate-connected wood truss joints: Part II - Application to overall truss model. *Transactions of the American Society of Agricultural Engineers*, Volume 40(6), pp. 1667-1675.
- Weston, J. & Zhang, W., 2017. *Finite element modeling of nailed connections in low-rise residential home structures*. Denver, CO, Structure Congress 2017.

Wind Science and Engineering Centre, 2006. *A Recommendation for an Enhanced Fujita Scale*, Lubbock, TX: Texas Tech University.

Wolfe, R. W. & LaBissoniere, T., 1991. *Structural Performance of Light-Frame Roof Assemblies - II: Conventional Truss Assemblies*, Madison, WI: Forest Products Laboratory, FPL-RP-499.

Wolfe, R. W. & McCarthy, M., 1989. *Structural Performance of Light-Frame Roof Assemblies - I: Truss Assemblies with Truss Stiffness Variability*, Madison, WI: Forest Products Laboratory, FPL-RP-492.

Wolfe, R. W., Percival, D. H. & Moody, R. C., 1986. *Strength and Stiffness of Light-Frame Sloped Trusses*, Madison, WI: Forest Products Laboratory, FPL-RP-471.

Wolfe, R. W., Stahl, D. & Cramer, S., 1996. *Experimental Assessment of Wood Trusses With Square-End Webs*, Madison, WI: Forest Products Laboratory, FPL-RP-544.

Wood Truss Council of America (WTCA), 2002. *Metal Plate Connected Wood Truss Handbook: A comprehensive guide to the design and use of metal plate connected wood trusses in construction today*. 3rd ed. Madison, WI: WTCA.

Appendix A: Semi-Rigid Joint Stiffness Inputs

These data are applied as partial member end releases in SAP2000:

- “P” values represent the translational stiffness
- “M3” values represent the in-plane rotational stiffness
- The “I” and “J” terms specify whether these values are applied to the member’s start joint or end joint, respectively. The location of these values are described in the table.

The joint stiffness data is applied selectively based on the data in Maraghechi and Itani (1982), Vatovec (1996), and Liu (2013).

Table A-1: Joint stiffness assignment for Semi-Rigid analog

TABLE: Frame Release Assignments - Partial Fixity				
Frame	PI	M3I	PJ	M3J
Text	N/mm	N-mm/rad	N/mm	N-mm/rad
BC1-1	29246	249244330		
BC1-2			61645	245176879
BC2-1	61645	245176879		
BC2-2			29246	249244330
TC1-1	29246	249244330		
TC1-2				245176879
TC2-1		245176879		233200497
TC3-1		233200497		245176879
TC4-1		245176879		
TC4-2			29246	249244330

Appendix B: Initial and Adjusted Wind Load Calculations

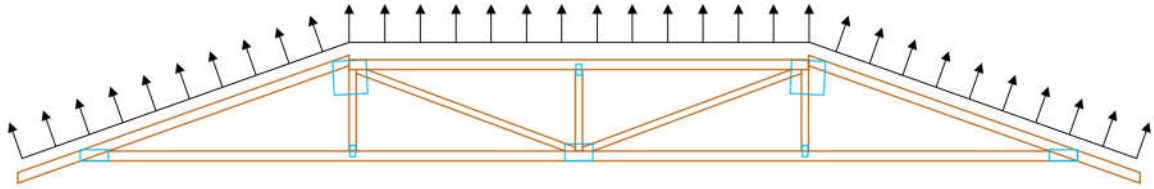


Figure A-1: Diagram of Truss A2 under uplift pressure

Tributary width of truss = 24" = 609.6 mm

Structure height = 8 m at eaves

$h = 8.76 \text{ m}$

Plan width, $L = 9 \text{ m}$

Calculations carried out according to Directional Procedure for MWFRS, Chapter 27 of ASCE 7 – 10.

Exposure category C

Basic wind speed, $V = 105 \text{ mph}$ (Fig 26.5 – 1C)

Directionality factor, $K_d = 1.0$ (no load combination)

Topographic factor, $K_{zt} = 1.0$

Gust – effect factor, $G = 0.85$ (rigid building)

Internal pressure coefficient, $G C_{pi} = \pm 0.55$ (partially enclosed)

Velocity pressure exposure coefficient, $K_h = 0.97$ (Table 27.3 – 1)

$$\text{Velocity pressure, } q_z = 0.00256K_hK_{zt}K_dV^2 = 27.3773 \frac{lb}{ft^2}$$

External pressure coefficients for hip roof (Table 27.4 – 1)

$$\frac{h}{L} = \frac{8.76}{9} = 0.97$$

$$\theta = 18^\circ$$

Table A-2: External pressure coefficients from Table 27.4-1 in ASCE 7-10

External Pressure Coefficients from Table 27.4-1 (values taken by interpolation)		Windward Face	Leeward Face
Wind Direction	Normal to Ridge	-0.18, -0.778	-0.6
	Parallel to Ridge	-1.17	NA

$$\text{Extreme combination: } C_p = -1.17, GC_{pi} = 0.55$$

$$p = qGC_p - q_i(GC_{pi})$$

where $q_i = q_h$ at $h = 7.6$ (to avoid interpolation), $K_h = 0.94$

$$\therefore p = (27.3773 * 0.85 * (-1.17)) - (26.531 * 0.55) = -41.82 \frac{lb}{ft^2}$$

$$-41.82 \frac{lb}{ft^2} = -2002.29 Pa$$

$$\text{Truss uplift, } w = p * \text{trib. width} = -2002.29 * 0.6096 = 1215.2 \frac{N}{m}$$

$$w = 1.22 \frac{N}{mm} \text{ uplift}$$

Adjusted Wind Load Calculations:

Desired support reaction – RTWC Capacity = 2800 N

$$\therefore \text{Total uplift} = 2800 * 2 = 5600 \text{ N}$$

$$\frac{\text{Initial Reaction}}{\text{Initial Load}} = \frac{12093.94}{1.22} = \frac{\text{Updated Reaction}}{\text{Updated Load}} = \frac{5600}{\text{Updated Load}}$$

$$\text{Updated Load} = 0.57 \text{ N/mm}$$

Working backwards through Directional Procedure for MWFRS:

$$\frac{570 \frac{\text{N}}{\text{m}}}{0.6096 \text{ m}} = 935.04 \text{ Pa}$$

$$935.04 \text{ Pa} = 19.529 \frac{\text{Lb}}{\text{ft}^2}$$

$$\begin{aligned} p &= qGC_p - q_i(GC_{pi}) \\ &= (0.00256 * 0.97 * V^2)(G * C_p) - (0.00256 * 0.94 * V^2)(GC_{pi}) \end{aligned}$$

$$p = -0.00247V^2 - 0.001324V^2 = 19.529$$

$$\therefore V = 71.753 \text{ mph}$$

Appendix C: Calculation of Orthotropic Moduli of Elasticity for Truss A2 Members

Longitudinal Modulus of Elasticity (MOE) taken from Table 5.3.2 in the Canadian Wood Design Manual (Canadian Wood Council/Canadian Standards Association, 2015), for SPF 2100 F_b – 1.8E:

$$E = 12400 \text{ MPa}$$

Orthotropic properties calculated using the Elastic ratios shown in Table 1-2:

$$E1 \text{ (longitudinal)} = 12400 \text{ MPa}$$

$$E2 \text{ (tangential)} = 12400 * 0.055 = 682 \text{ MPa}$$

$$E3 \text{ (radial)} = 12400 * 0.102 = 1264.8 \text{ MPa}$$

$$G12 = 12400 * 0.06 = 744 \text{ MPa}$$

$$G13 = 12400 * 0.071 = 880 \text{ MPa}$$

$$G23 = 12400 * 0.012 = 140 \text{ MPa}$$

The above values were used in Truss A2 and the stick-frame rafter model. Note that the preceding validation models, based on the FPL studies, used averages of the MOE values listed in the individual FPL reports (Wolfe, et al., 1986; Wolfe & LaBissoniere, 1991; Wolfe, et al., 1996)

Appendix D: Truss A2 Joint Demand under Initial and Updated Uplift

See Tables C and D on following pages.

Table A-3: Truss A2 joint demand under initial uplift loading

Joint Demand Under Initial 1.22 N/mm Load											
Frame	Joint	Raw Results (continuous members omitted)						Member Force Direction	Joint Demand		
		F1	F3	P (along member)	V (normal to member)	Angle	M2		Shear	Tension	Moment
Text	Text			N	N		N-mm	T/C			
1	Jt. 2	10536.2	5340.8	11812.5	14919.5	0.5	257656.5	T	12572.3	14919.5	257656.5
5	Jt. 2	4564.4	10.4	4564.4	4282.5	0.0	268776.4	C	4282.5	N/A	268776.4
1	Jt. 3	11581.8	2375.4	11822.9	13115.4	0.2	910426.0	T	13115.4	11822.9	910426.0
2	Jt. 3	14565.3	1233.5	14617.4	1233.5	0.1	910426.0	T	1233.5	14617.4	910426.0
9	Jt. 3	2.5	59.3	59.3	2.5	1.6	18553.4	T	2.5	59.3	18553.4
2	Jt. 4	14565.3	1252.2	14617.2	1252.2	-0.1	868945.8	T	1252.2	14617.2	868945.8
3	Jt. 4	14565.3	1249.5	14616.9	1249.5	0.1	868945.8	T	1249.5	14616.9	868945.8
11	Jt. 4	0.0	2501.7	2501.7	0.0	1.6	452.9	T	0.0	2501.7	452.9
6	Jt. 9	4564.4	18.0	4564.5	18.0	0.0	211609.4	C	18.0	N/A	211609.4
7	Jt. 9	4564.4	18.0	4564.5	18.0	0.0	211888.8	C	18.0	N/A	211888.8
11	Jt. 9	0.0	2493.6	2493.6	0.0	1.6	439.5	T	0.0	2493.6	439.5
5	Jt. 10	4564.4	40.7	4564.6	40.7	0.0	236411.4	C	40.7	N/A	236411.4
6	Jt. 10	4564.4	12.2	4564.4	12.2	0.0	215840.8	C	12.2	N/A	215840.8
9	Jt. 10	2.5	51.1	51.1	2.5	1.6	20570.5	T	2.5	51.1	20570.5

Table A-4: Truss A2 joint demand under adjusted uplift loading

Joint Demand Under Adjusted 0.57 N/mm Load											
Frame	Joint	Raw Results (continuous members omitted)						Member Force Direction	Joint Demand		
		F1	F3	P (along member)	V (normal to member)	Angle	M2				
Number	Text			N	N		N-mm	T/C	Shear	Tension	Moment
1	Jt. 2	-4750.4	-2428.7	-5335.2	-6746.1	0.5	123437.4	T	-5687.2	-6746.1	123437.4
5	Jt. 2	2096.1	13.9	2096.1	1975.3	0.0	122476.3	C	1975.3	2096.1	122476.3
1	Jt. 3	5240.8	1057.0	5346.4	5918.0	0.2	411560.6	T	5918.0	5346.4	411560.6
2	Jt. 3	-6582.5	-571.1	-6607.3	-571.1	0.1	-411560.6	T	-571.1	-6607.3	411560.6
9	Jt. 3	-1.2	48.5	48.5	1.2	1.6	-7026.7	T	1.2	48.5	7026.7
2	Jt. 4	6582.5	-579.6	6607.1	-579.6	-0.1	392526.5	T	-579.6	6607.1	392526.5
3	Jt. 4	-6582.5	-578.4	-6607.0	-578.4	0.1	-392526.5	T	-578.4	-6607.0	392526.5
11	Jt. 4	0.0	1158.0	1158.0	0.0	1.6	212.6	T	0.0	1158.0	212.6
6	Jt. 9	-2096.1	15.7	-2096.1	15.7	0.0	-93563.9	C	15.7	-2096.1	93563.9
7	Jt. 9	2096.1	15.7	2096.1	15.7	0.0	93691.6	C	15.7	2096.1	93691.6
11	Jt. 9	0.0	-1149.8	-1149.8	0.0	1.6	-206.6	T	0.0	-1149.8	206.6
5	Jt. 10	-2096.1	27.6	-2096.2	27.6	0.0	-103484.4	C	27.6	-2096.2	103484.4
6	Jt. 10	2096.1	13.3	2096.1	13.3	0.0	96303.1	C	13.3	2096.1	96303.1
9	Jt. 10	1.2	-40.4	-40.4	1.2	1.6	7985.4	T	1.2	-40.4	7985.4

Appendix E: Truss Joint Capacity Calculations and Minimum Joint Capacities for Truss 2A

The following sample calculations are based on the Member TC1 capacities from Joint 3. The TC1 contact area is shown in the following diagram.

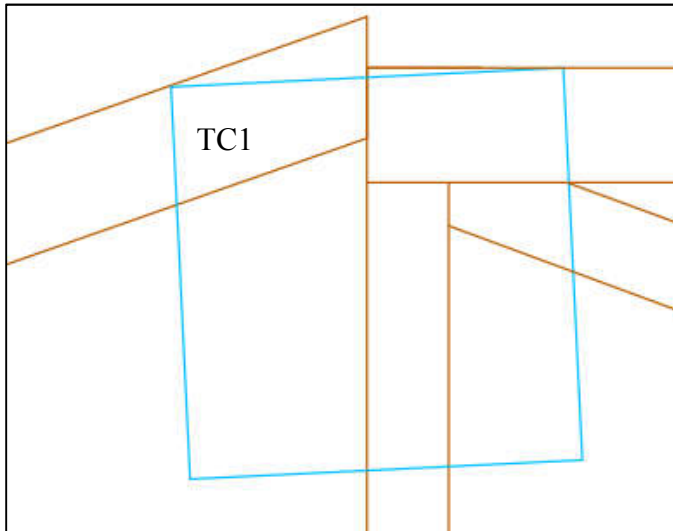


Figure A-2: Truss A2 Joint 3 diagram with member TC1 contact area shown

Capacity calculations for Member TC1 contact area:

Tensile and shear capacities calculated based on standard design equations from Chapter 7 of TPIC (2014).

Tensile Capacity:

1. Lateral Tooth Resistance

Lateral resistance n_r , is calculated from interpolation of n_u and n'_u :

$$n_u = \frac{p_u q_u}{p_u \sin^2 \theta + q_u \cos^2 \theta} \quad (TPIC \ 7.3.3.3)$$

$$n'_u = \frac{p'_u q'_u}{(p'_u \sin^2 \theta + q'_u \cos^2 \theta)}$$

p_u, q_u, p'_u, q'_u provided by truss plate manufacturer;

$$p_u = 2.13 \frac{\text{MPa}}{\text{plate}}, q_u = 1.22 \frac{\text{MPa}}{\text{plate}}, p'_u = 1.71 \frac{\text{MPa}}{\text{plate}}, q'_u = 1.47 \frac{\text{MPa}}{\text{plate}}$$

n_u corresponds to loading parallel to plate axis,
and n'_u corresponds to perpendicular loading.

Interpolation is required for loads at angles between $\rho = 0^\circ$ and 90° .

θ represents load direction relative to member length.

Here, $\theta = 0^\circ$, and $\rho = 19^\circ$

$$n_u = \frac{2.13 * 1.22}{1.22} = 2.13 \frac{\text{MPa}}{\text{plate}}$$

$$n'_u = 1.71 \frac{\text{MPa}}{\text{plate}}$$

$$\text{Interpolate: } n_r = 2.13 - \left(\left(\frac{2.13 - 1.71}{0 - 90} \right) * (0 - 19) \right) = 2.04 \frac{\text{MPa}}{\text{plate}}$$

Capacity = n_r * contact area * no. of plates

$$N_r = 2.04 * 10449.72 * 2 = 42662.72 \text{ N}$$

* Contact areas estimated by inspection of truss drawings

2. Tooth Slip Resistance

Slip resistance n_s , is calculated from interpolation of n_s and n'_s :

$$n_s = \frac{p_s q_s}{p_s \sin^2 \theta + q_s \cos^2 \theta} \quad (\text{TPIC 7.3.3.3})$$

$$n'_s = \frac{p'_s q'_s}{(p'_s \sin^2 \theta + q'_s \cos^2 \theta)}$$

p_s, q_s, p'_s, q'_s provided by truss plate manufacturer;

$$p_s = 2.1 \frac{\text{MPa}}{\text{plate}}, q_s = 1.25 \frac{\text{MPa}}{\text{plate}}, p'_s = 1.97 \frac{\text{MPa}}{\text{plate}}, q'_s = 1.22 \frac{\text{MPa}}{\text{plate}}$$

Again, $\theta = 0^\circ$, and $\rho = 19^\circ$

$$n_s = 2.10 \frac{\text{MPa}}{\text{plate}}$$

$$n'_s = 1.97 \frac{\text{MPa}}{\text{plate}}$$

$$\text{Interpolate: } n_s = 2.07 \frac{\text{MPa}}{\text{plate}}$$

Capacity = n_s * contact area * no. of plates

$$N_s = 2.07 * 10449.72 * 2 = 43315.25 \text{ N}$$

3. Plate Strength

$$\text{plate strength from supplier, } t_p = \frac{200 \frac{\text{N}}{\text{mm}}}{\text{plate}}$$

Seam length, $L = 300\text{mm}$

$$T_r = 200 * 300 * 2 = 120000 \text{ N}$$

\therefore minimum tensile resistance of joint at TC1 = 42662 N

Shear Capacity

1. Lateral Tooth Resistance

Lateral shear resistance calculated in same way as lateral tensile resistance, however

Here, $\theta = 90^\circ$, and $\rho = 71^\circ$

$$N_r = 1.43 * 10449.72 * 2 = 29886.2 \text{ N}$$

2. Tooth Slip Resistance

Slip shear resistance calculated in same way as slip tensile resistance, however

Here, $\theta = 90^\circ$, and $\rho = 71^\circ$

$$N_s = 1.226 * 10449.72 * 2 = 25622.7 \text{ N}$$

3. Plate Strength

$$\text{plate strength from supplier, } v_p = \frac{112 \frac{N}{mm}}{\text{plate}}$$

$$V_r = 112 * 300 * 2 = 67200 \text{ N}$$

$$\therefore \text{minimum shear resistance of joint at TC1} = 25622.7 \text{ N}$$

Combined Shear & Tension Plate Strength

$$C_{rST} = (ST_{rL1} * L_1 + ST_{rL2} * L_2) \quad (TPIC 7.5.4)$$

$$ST_{rL1} = V_{rL1} + \left(\frac{\theta}{90}\right) * (T_{rL1} - V_{rL1})$$

$$ST_{rL2} = T_{rL2} + \left(\frac{\theta}{90}\right) * (V_{rL2} - T_{rL2})$$

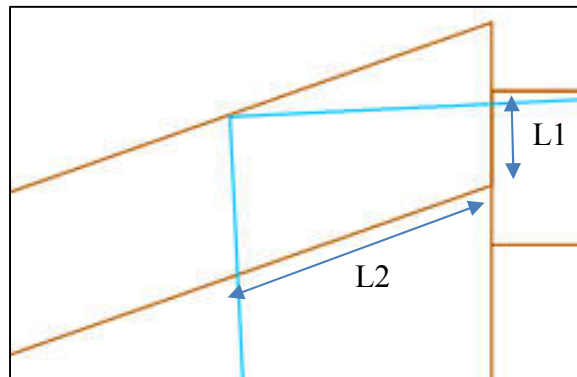


Figure A-3: Joint 3 with shear and tension lengths labeled

$$L1 = 47.104 \text{ mm}, L2 = 156.40 \text{ mm}$$

In this case, the force perpendicular to the member causes compression, so only the direction parallel to TC1 is considered.

T_{rL1} : Interpolate plate tensile resistance values

$$T_{rL1} = 200 - \left(\left(\frac{200 - 145}{0 - 90} \right) * (0 - 19) \right) = \frac{188.4 \frac{N}{mm}}{plate}$$

$$V_{rL2} = 102 - \left(\left(\frac{102 - 84}{0 - 30} \right) * (0 - 19) \right) = \frac{90.6 \frac{N}{mm}}{plate}$$

$$C_{rST} = 188.4 * 47.104 * 2 + 90.6 * 156.4 * 2 = 46088.47 N$$

Plate Moment Capacity

Moment Capacity of plate calculated according to Lewis et al. (2006). Additional information on the required geometric and material parameters provided in Section 8.7 of TPI (2007).

Moment Resistance, M_a

$$M_a = C_m * \frac{T_1(W_p + y + z - d'_1) + \frac{T_2(4W_p + 2y + 4z + 3d'_1)}{3} + C_s(d'_1 - z - y) + C_w(d'_1 - y)}{5}$$

$$y = \frac{t_1 * R_t * \left(F_y * (1.8z + W_p) + (F_u * (W_p + z)) \right) - 2 * P_t}{d_2 * C + t_1 * R_t * (1.8F_y + F_u)}$$

$$C = F_{cp} * (1.7F_{c*}) / (F_{cp} \sin^2 \theta + 1.7F_{c*} \cos^2 \theta)$$

$$T_1 = 2 * t_1 * R_t * F_y * (W_p - y + z)$$

$$T_2 = t_1 * R_t * (F_u - F_y) * (W_p - y + z)$$

$$C_s = 0.8t_1 * R_t * F_y * (y - z)$$

$$C_w = y * d_2 * C$$

* See explanation of variables in TPI(2007)

$$C_m = 1 \text{ (panel joint)}$$

$$W_p = d - d_{le} + 1.5 = 3.5 - 1.85 + 1.5 = 3.15''$$

$$d'_1 = 3.5''$$

$$d_2 = 1.5''$$

$$t_1 = 0.03583''$$

$$R_t = 0.5$$

$$z = 1''$$

$$F_u = 399 \text{ MPa} = 58000 \text{ psi}$$

$$F_y = 36000 \text{ psi}$$

$$P_t = 11893.53 \text{ N} = 2673.774 \text{ lbs}$$

* Note that P_t is tension in the member based on the initial $1.22 \frac{\text{N}}{\text{mm}}$ loads.

$$\theta = 71^\circ$$

$$F_{cp} = 6.5 \text{ MPa} = 942.75 \text{ psi}$$

$$F_{c*} = 19.9 \text{ MPa} = 2886.25 \text{ psi}$$

∴

$$C = 942.75 * \frac{1.7 * 2886.25}{942.75 * \sin^2 19 + 2886.25 * \cos^2 19} = 3394.03 \text{ psi}$$

$$y = \dots = 0.29585$$

$$T_1 = 2 * 0.03583 * 0.5 * 36000 * (3.15 - 0.29585 + 1) = 4971.39$$

$$T_2 = 0.03583 * 0.5 * (58000 - 36000) * (3.15 - 0.29585 + 1) = 1519.04$$

$$C_s = 0.8 * 0.03583 * 0.5 * 36000 * (0.29585 - 1) = -364.32$$

$$C_w = 0.29585 * 1.5 * 3394.03 = 1506.19$$

$$M_a = \left(\frac{1}{5} \right) * \left(4971.39 * (3.15 + 0.29585 + 1 - 3.5) \right. \\ \left. + \frac{1519.04 * (4(3.15) + 2(0.29585) + 4 - 3(3.5))}{3} \right. \\ \left. - (364.32 * (3.5 - 1 - 0.29585)) + (1506.19 * (3.5 - 0.29585)) \right) \\ = 2422.71 \frac{lbs - in}{plate} = 273730.1 \frac{N * mm}{plate}$$

$$\therefore M_r = 2 * 273730.1 = 547460.2 N * mm$$

Lateral Moment Capacity taken by rearranging 7.5.8.4.4. These calculations not shown because rearrangement results directly in D/C ratio.

The table on the following page lists the minimum capacity results for all joints, not including the lateral moment resistance values, which are incorporated at the time that the D/C ratios are determined. The tabulated values include member strength values where the members themselves provide the minimum capacity.

Table A-5: Truss A2 minimum joint capacities

Minimum Truss Joint Capacities - Truss A2									
Frame	Joint	Member Force Direction (T/C)	Shear Capacity (N)	Tension (N)	Member Tension/Compression Capacity (N)	Minimum Axial Capacity (N)	Ma (Factor of Safety Removed)	Member Bending	Minimum Moment Capacity (N-mm)
1	Jt. 2	T	48707.0	35414.0	18601	18601	2113628	591963	591963
5	Jt. 2	C	43118.1	28899.7	38893	28900	1826866	591963	591963
14	Jt. 2	C			38893	38893	1434710	591963	591963
1	Jt. 3	T	25631.1	42642.8	18601	18601	1211483	591963	591963
2	Jt. 3	T	45035.1	55306.3	18601	18601	1971392	591963	591963
9	Jt. 3	T	34417.2	48240.4	13376	13376	591886	306107	306107
10	Jt. 3	C	18475.9	19833.4	27968	19833	505030	306107	306107
2	Jt. 4	T	NA	*Continuous Member Strength	18601	18601		591963	591963
3	Jt. 4	T	NA	*Continuous Member Strength	18601	18601		591963	591963
11	Jt. 4	T	6296.8	10838.7	13376	10839	658371	306107	306107
6	Jt. 9	C	19913.6	35560.0	38893	35560	1088799	591963	591963
7	Jt. 9	C	19913.6	35560.0	38893	35560	1088799	591963	591963
10	Jt. 9	C	9838.7	13790.3	27968	13790	509535	306107	306107
11	Jt. 9	T	12063.4	19760.6	13376	13376	535656	306107	306107
12	Jt. 9	C	9838.7	13790.3	27968	13790	509567	306107	306107
5	Jt. 10	C	NA	*Compressive Member Strength	38893	38893		591963	591963
6	Jt. 10	C	NA	*Compressive Member Strength	38893	38893		591963	591963
9	Jt. 10	T	6296.8	10838.7	13376	10839	442019	306107	306107

Appendix F: Results of D/C Analysis of Truss A2 with Initial Loading Applied

Table A-6: D/C results for Truss A2 under initial uplift loading

Truss Element		Relevant Force Effects and Demand/Capacity Ratios					
Joints							
Joint	Member	Tension	Critical Mode	Shear	Critical Mode	Moment	Critical Mode
2	TC1	0.42	Plate Slip	0.68	Member Tension	0.44	Member
2	BC1	N/A		0.10	Lateral	0.17	Lateral
2	TC1 overhang	N/A		N/A	Combined with TC1	0.41	Member
3							
3	TC2	0.79	Member	0.03	Lateral	1.54	Member
3	W1	0.00	Member	0.00	Plate Slip	0.06	
3	W2	N/A		N/A		0.02	
4	TC2	0.79	Continuous Member	N/A		N/A	Continuous Member
4	TC2	0.79	Continuous Member	N/A		N/A	Continuous Member
4	W3	0.25	Plate Capacity	0.00	Plate Slip	0.20	Lateral
9	BC1	N/A		0.00	Plate Capacity	0.17	Plate
9	BC2 right of jt.9	N/A		0.00	Plate Capacity	0.36	Member
9							
9	W3	0.19	Member	0.00	Plate Slip	0.03	Lateral
9	W4 right of jt.9	N/A		N/A		0.03	Lateral
10							
10	BC1	N/A	Continuous Member	0.00	Member	N/A	Continuous Member
10	W1	0.00	Member	0.00	Plate Slip	0.10	Lateral
Members							
		Tension		Compression		Moment	
Chord Member		0.783	“TC2”	0.117		1.502	“TC2” around mid-panel
Web Member		0.187		0.117		0.063	
Roof-to-Wall Connection							
		Uplift Resistance [N]		Support Reaction [N]		C/D	
Toe-nail [1]		2800		6046.97		2.160	
Hurricane Strap		5840		6046.97		1.035	

Appendix G: Design Notes for Stick-Frame Hip Roof

Stick frame roof designed in accordance with Part 9 of the NBCC (2010)

Section 9.23:

Member Requirements

- Hip rafters must be 50 mm greater in depth than the jack rafters and at least 38 mm wide.
- Ceiling joists and collar ties of > 38 x 89 mm are permitted to reduce the span for rafters and joists where roof slope is 1:3 or greater (N/A due to sufficient maximum span)
- Prescribed Member Sizes:
 - o Wood species SPF No.2, assumed snow load 1.5 kPa
 - o Jack Rafters: 38 x 184 mm (2-by-8 lumber) at 400 mm spacing, Maximum span = 5.11 m (Table A-6)
 - o Hip Rafters: 38 x 235 mm (2-by-10 lumber)
 - o Ceiling Joists: 38 x 184 mm at 400 mm spacing

Joint Requirements

- All nails should be long enough so that not less than half of the required length penetrates into the second member
- Table 9.23.3.4, “Nailing for Framing” prescribes the following nail lengths and quantities:
 - o Ceiling Joist to Wall Top Plate: 2 – 82 mm nails, toe-nailed
 - o Roof/Jack Rafter to Wall Top Plate: 3 – 82 mm nails, toe-nailed
 - o Roof/Jack Rafter to Ceiling Joist: 7 – 76 mm nails, perpendicular to member faces
 - o Roof/Jack Rafter to Hip Rafter: 2 – 82 mm nails, toe-nailed or end-nailed through Hip Rafter

Appendix H: Nailed Connection Capacity Calculations

Nailed connection capacities calculated as unfactored resistances based on the Canadian Wood Design Manual (Canadian Wood Council/Canadian Standards Association, 2015).

Jack Rafter to Hip Rafter:

Consider both lateral resistance of nails and withdrawal capacity to withstand vertical and horizontal reactions, respectively.

Lateral Resistance:

$$N_r = N'_r * n_s * n_F * K * J_F \quad (CSA 086 - 7.2)$$

$$J_F = 0.67 \text{ (assume end - nailed)}$$

$$K = 1$$

$$n_s = 1 \text{ (no. of shear planes)}$$

$$n_F = 2 \text{ (no. of nails)}$$

Assuming maximum penetration of nail:

$$N'_r = 0.707 \text{ kN (Nail Selection Table, 76 mm nail, pp. 242)}$$

$$\text{Removing resistance factor } \phi = 0.8, N'_r = \frac{0.707}{0.8} = 0.88375 \text{ kN}$$

$$N_r = 0.88375 * 1 * 2 * 1 * 0.67 = 1.184 \text{ kN}$$

Nail Withdrawal:

$$P_{rw} = Y_w * L_p * n_f$$

$$\phi Y_w = 4.2 \frac{N}{mm}$$

$$Y_w = \frac{4.2}{0.6} = 7 \frac{N}{mm}$$

Assume $L_p = 76 \text{ mm} - 38 \text{ mm}$ (max. penetration)

$$P_{rw} = 7 * 38 * 2 = 532 \text{ N}$$

Jack Rafter to Ceiling Joist

Lateral resistance of 7 – 76 mm nails:

Minimum Penetration = 18 mm

$$N'_r = 0.571 \text{ kN}$$

$$N_r = \left(\frac{1}{0.8}\right)(0.571)(7) = 4.996 \text{ kN}$$

Jack Rafter to Wall Top Plate (toe-nail)

Withdrawal resistance – only consider vertical resistance because it can be assumed that the ceiling joist will withstand the horizontal reaction.

$$P_{rw} = \left(\frac{1}{0.6}\right)(4.2 * 38 * 3 * 0.67) = 534.66 \text{ N}$$

Also note that the withdrawal resistance of the Rafter-to-Plate toe-nail will need to be combined with that of the Joist-to-plate toe-nail to be calculated next, since this joint is expected to fail as a unit rather than through the 7-nail connection between the members.

Ceiling Joist to Wall Top Plate (toe-nail)

$$Prw = \left(\frac{1}{0.6}\right)(4.2 * 38 * 2 * .67) = 356.44 \text{ N}$$

Combined RTWC Capacity

$$P_{rw} = 534.66 + 356.44 = 891.1 \text{ N}$$

Curriculum Vitae

Name: Sarah Stevenson

Post-secondary Education and Degrees: University of Manitoba
Winnipeg, Manitoba, Canada
Bachelor of Science – Civil Engineering
2010-2015

University of Western Ontario
London, Ontario, Canada
Master of Engineering Science – Wind Engineering
2015-2017

Honours and Awards: Queen Elizabeth II Graduate Scholarship in Science and Technology (OGS)
2016-2017, 2017-2018

Second-Place Teaching Assistance Excellence Award
Fall 2016

Catherine Lalonde Memorial Scholarship for Wood-Related Research
2016

University of Manitoba President's Scholar
2010-2015

Related Work Experience: Teaching Assistant
University of Western Ontario
2015-2017

Publications:

Stevenson, S. A., Kopp, G. A., El Ansary, A. M., “Numerical assessment of partial hip roof failures during tornadoes.” Proceedings of the 13th Americas Conference on Wind Engineering, May 21-24, 2017, Gainesville, USA.

Stevenson, S., Hong, E., Jaffe, A. (2017) Technical Report to Environment Canada on the findings of the Forensic Damage Survey following the Tornados in Windsor and La Salle, Ontario on August 24, 2016.

Stevenson, S., Mohammad K., Svecova, D., Thomson, D. “Study of acoustic emission signals for detection of impending failure of FRP bars.” Proceedings of the 7th International Conference on Fiber Reinforced Polymer Composites in Civil Engineering, August 20-22, 2014, Vancouver, Canada.